

Air Force Institute of Technology

**AFIT Scholar**

---

Theses and Dissertations

Student Graduate Works

---

3-2-2006

## **Analysis of Photoconductive Properties in Ge<sub>2</sub>Sb<sub>2</sub>Te<sub>5</sub> (GST) Chalcogenide Films for Applications in Novel Electronics**

John R. V. Chezem

Follow this and additional works at: <https://scholar.afit.edu/etd>



Part of the [Electrical and Electronics Commons](#), and the [Semiconductor and Optical Materials Commons](#)

---

### **Recommended Citation**

Chezem, John R. V., "Analysis of Photoconductive Properties in Ge<sub>2</sub>Sb<sub>2</sub>Te<sub>5</sub> (GST) Chalcogenide Films for Applications in Novel Electronics" (2006). *Theses and Dissertations*. 3314.  
<https://scholar.afit.edu/etd/3314>

This Thesis is brought to you for free and open access by the Student Graduate Works at AFIT Scholar. It has been accepted for inclusion in Theses and Dissertations by an authorized administrator of AFIT Scholar. For more information, please contact [richard.mansfield@afit.edu](mailto:richard.mansfield@afit.edu).



ANALYSIS OF PHOTOCONDUCTIVE PROPERTIES IN  $\text{Ge}_2\text{Sb}_2\text{Te}_5$  (GST)  
CHALCOGENIDE FILMS FOR APPLICATIONS IN NOVEL ELECTRONICS

THESIS

John Roy Vogus Chezem  
Second Lieutenant, USAF

AFIT/GE/ENG/06-14

DEPARTMENT OF THE AIR FORCE  
AIR UNIVERSITY

***AIR FORCE INSTITUTE OF TECHNOLOGY***

---

---

Wright-Patterson Air Force Base, Ohio

APPROVED FOR PUBLIC RELEASE; DISTRIBUTION UNLIMITED.

The views expressed in this thesis are those of the author and do not reflect the official policy or position of the United States Air Force, Department of Defense, or the United States Government.

ANALYSIS OF PHOTOCONDUCTIVE PROPERTIES IN  $\text{Ge}_2\text{Sb}_2\text{Te}_5$  (GST)  
CHALCOGENIDE FILMS FOR APPLICATIONS IN NOVEL ELECTRONICS

THESIS

Presented to the Faculty  
Department of Electrical and Computer Engineering  
Graduate School of Engineering and Management  
Air Force Institute of Technology  
Air University  
Air Education and Training Command  
In Partial Fulfillment of the Requirements for the  
Degree of Master of Science in Electrical Engineering

John Roy Vogus Chezem, BSEE  
Second Lieutenant, USAF

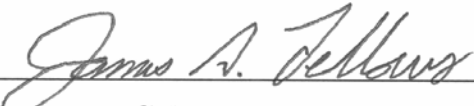
March 2006

APPROVED FOR PUBLIC RELEASE; DISTRIBUTION UNLIMITED.

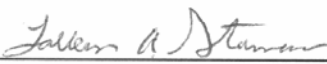
ANALYSIS OF PHOTOCONDUCTIVE PROPERTIES IN  $\text{Ge}_2\text{Sb}_2\text{Te}_5$  (GST)  
CHALCOGENIDE FILMS FOR APPLICATIONS IN NOVEL ELECTRONICS

John Roy Vogus Chezem, BSEE  
Second Lieutenant, USAF


Approved:

  
\_\_\_\_\_  
Lieutenant Colonel James A. Fellows (Chairman)

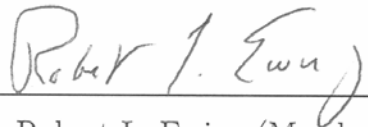
2 MAR 06  
Date

  
\_\_\_\_\_  
Major LaVern A. Starman (Member)

2 Mar 06  
Date

  
\_\_\_\_\_  
Dr Michael A. Marciniak (Member)

2 Mar 06  
Date

  
\_\_\_\_\_  
Dr. Robert L. Ewing (Member)

2 MAR 06  
Date

## ***Abstract***

This thesis investigated the thermal phase-change properties in  $\text{Ge}_2\text{Sb}_2\text{Te}_5$  (GST) chalcogenide-based films and determined the feasibility of coupling the GST with photosensitive DNA material for novel optical device applications. Modeling and testing of GST was researched with the approach that GST would react as a resistive mechanism through thermal manipulation. Test structures were fabricated in the PolyMUMPs MEMS fabrication process. GST material was deposited (by RF sputtering) on the surface of the test structures. The GST was analyzed primarily in the amorphous to crystalline transition states due to more distinct changes in the resistance between partial states. Using both filtered light (via a monochromator) and non-filtered white light was incident on the GST for photo response testing. A biased voltage was applied to the device and the current change was measured. The GST was tested electrically, applying a current sweep across the device and measuring change in resistance as the GST changed states. Data recorded on the thermal properties of GST leading to resistive changes from both optical and electrical sources was analyzed.

The results of this research indicate how future optical and electrical testing of the GST can be improved. The data measured by testing the GST electrically was compared to other research data (following similar testing procedures), revealing that optimal designs need sub-micro layers of GST with electrodes placed above and below the GST. It was concluded that higher power light sources will be needed to continue exploring the optical reaction of GST in future research.

*To my Wife,  
Father and Mother,  
Family and close friends,  
Those who loved me.  
To those who inspired me,  
Taught me to never give up,  
Always strive for excellence,  
And make a difference.*

## *Acknowledgments*

First, I would like to thank my thesis committee, Dr. Marciniak, Maj Starman, and Dr. Ewing, for their direction and advice in helping improve the quality of my thesis. I would like to extend special thanks for the support Maj Starman provided during difficult times, and to Dr. Ewing, Dr. Schuermeyer, and Ms. Rubeiz for their time and expertise in assisting with my experiment in the AFRL laboratory. I would also like to give a very sincere thank you to my advisor, Lt Col Fellows. The leadership and counsel he provided were essential to the success of reaching my goal in completing this huge task. Finally, I would like to thank Heng Li for all her time and help in growing the GST for this research.

Most importantly, I would like to thank my wife and family. My wife picked up all the responsibilities around the house while I attended AFIT. While I was studying and getting little sleep, she was managing the house, making my meals, pregnant and having our first son; and giving me the support I needed. Her support was invaluable to the success and completion of my degree. Finally, to my parents, my mother and father, thank you for raising me with love and the expectation to excel and to do my best, for showing me how to pick myself up when I fall and being there to celebrate my accomplishments, and teaching me to do what is right even if it is the most difficult.

John R.V. Chezem



## *Table of Contents*

Heading	Page
Abstract .....	iv
Dedication .....	v
Acknowledgments.....	vi
Table of Contents.....	vii
List of Figures .....	x
List of Tables .....	xii
List of Equations .....	xiii
1. Introduction .....	1
1.1 Motivation.....	1
1.2 Problem Statement .....	3
1.3 Scope.....	4
1.4 Thesis Outline.....	6
1.5 Summary.....	7
2. Literature Review.....	8
2.1 Introduction .....	8
2.1.1 Brief History of Photoconductors .....	9
2.2 Comparison of Photodetectors and their Significance .....	9
2.3 Chalcogenide Materials .....	13
2.3.1 Fundamental Characteristics and Physical Properties.....	14
2.3.1.1 Defect Theory.....	18
2.3.1.2 Energy Band and Density of States Properties.....	22
2.3.2 Unique Properties Due to Direct Electrical and Photonic Interaction.....	26
2.3.2.1 Electrical Phase-change Crystallization Behavior.....	27
2.3.2.2 Photoinduced Phenomena .....	30
2.3.3 Summary of Chalcogenide Material Properties.....	34
2.4 Summary of Applications Using Chalcogenide Materials .....	35
3. Theory and Modeling .....	38
3.1 Introduction .....	38

3.2	Marine DNA – Large Capacity Multistate Optoelectronic Memories.....	38
3.3	Chalcogenide: Multistate Interface Design .....	40
3.3.1	Heat Transfer Model.....	43
3.3.2	Scalability .....	52
3.4	Summary .....	53
4.	Design and Fabrication .....	55
4.1	Introduction .....	55
4.2	Design Objectives.....	55
4.3	Resources, Cost, and Availability.....	56
4.4	L-Edit Design Layout.....	57
4.5	Fabrication Process .....	59
4.5.1	MEMSCAP PolyMUMPs Fabrication Process .....	61
4.5.2	Safety Procedure and Post Processing.....	63
4.6	Deposition of Chalcogenide (University of Utah).....	64
4.7	Summary.....	69
5.	Experiment and Setup.....	70
5.1	Introduction .....	70
5.2	Lab Equipment and Test Setup.....	71
5.3	Experiment.....	73
5.3.1	Resistance vs. Intensity .....	74
5.3.2	Responsivity vs. Wavelength.....	75
5.3.3	Scalability .....	76
5.4	Electrical Testing .....	77
5.5	Summary .....	77
6.	Results and Analysis .....	78
6.1	Introduction .....	78
6.2	Photo Analysis .....	79
6.3	Electrical Analysis.....	88
6.3.1	Phase-change Results Comparison to Other Research.....	94
6.3.2	Scalability Analysis .....	96
6.4	Summary.....	97
7.	Conclusion and Future Recommendations .....	100

7.1	Research Summary.....	100
7.2	GST for Multistate and Hybrid Applications.....	101
7.2.1	Optical Manipulation of GST.....	101
7.2.2	Electrical Manipulation of GST.....	103
7.2.3	Reliability.....	105
7.2.4	Design and Fabrication.....	106
7.2.5	Summary of Conclusions.....	107
7.3	Lessons Learned.....	108
7.3.1	Test Equipment.....	108
7.3.2	Design.....	109
7.3.3	Experience.....	109
7.4	Recommendations for Future Research.....	109
	Appendix A – FEMLAB Procedures.....	112
	Appendix B – GST SEM Images.....	120
	Appendix C – Test Matrix Data.....	121
	References.....	122
	Vita.....	126

## *List of Figures*

Figure	Page
2-1 Quantum well structure of a photoconductive device.....	12
2-2 Schematic bonding topology of $\text{Se}_{1-x-y}\text{As}_x\text{Ge}_y$ [18].....	16
2-4 Atomic structure of GST in crystalline and amorphous form [10].....	17
2-5 Different bonding configurations of elemental chalcogens [6].....	21
2-6 Energy band structure of crystalline and amorphous GST [10].....	23
2-7 CFO energy band model for GST [6].....	24
2-8 Sketch of TCB and VAP in the chalcogenide structure [18].....	25
2-9 Phase diagram of GST along the pseudobinary line [20].....	28
2-10 I-V plot for GST characteristics during transitions [21, 22].....	29
2-11 Absorption edge of chalcogenide, under illumination and thermal annealing [6]..	31
2-12 Kinetics in $\text{As}_{50}\text{Se}_{50}$ with polarization and unpolarized light [6].....	33
2-13 VAP photoinduced anisotropy in chalcogenide materials [6].....	34
3-1 Resistance characteristics of GST during phase-change [33].....	42
3-2 Thermal timing diagram of GST between amorphous and crystalline states [34]...	43
3-3 Heat flux model of GST test structure.....	44
3-4 Representation of different states in GST test structure.....	45
3-5 FEMLAB's model simulation geometry and design parameters.....	48
3-6 FEMLAB simulation of GST at different energies for steady state analysis.....	50
3-7 FEMLAB simulation of GST at different energies for transient analysis.....	51

3-8	Linear scaling theory of GST.....	53
4-1	Top view of chalcogenide test chip designed in L-Edit.....	58
4-2	Cross section view of the three-layer PolyMUMPs process [38].....	60
4-3	SEM top view of electrode pair with 4.5- $\mu\text{m}$ trench.....	62
4-4	Absorption vs. photon energy for GST at different oxygen impurities [41].....	66
4-5	SEM image of test chip array with GST 4- $\mu\text{m}$ , low oxygen impurity level.....	67
4-6	Electrode pair before and after deposition 4- $\mu\text{m}$ of GST.....	67
4-7	Amorphous GST images from first batch of samples received in December.....	68
5-1	Experiment equipment configuration.....	73
6-1	I-V plot of photo testing data, 6 $\text{\AA}$ /s Low Oxygen GST 14- $\mu\text{m}$ gap.....	79
6-2	Test Chip, growth of GST at 9 $\text{\AA}$ /s to 4- $\mu\text{m}$ thick (no usable devices).....	86
6-3	Material structure of GST from batch one and two 6 $\text{\AA}$ /s, grown to 4- $\mu\text{m}$ .....	88
6-4	Current sweep test of GST with electrode gap of 2- $\mu\text{m}$ .....	90
6-5	Current sweep test of GST with electrode gap of 6- $\mu\text{m}$ .....	91
6-6	Current sweep test of GST with electrode gap of 10- $\mu\text{m}$ .....	92
6-7	SEM of GST before and after current sweep 0 to 100 mA, electrode gap of 6- $\mu\text{m}$ ..	96

*List of Tables*

Table	Page
3-1 GST Material Properties.....	48
5-1 Test Matrix.....	70
C-1 GST Test Matrix Data.....	121

## *List of Equations*

Equation	Page
(2-1) Chalcogenide deviant electron configuration reaction equation.....	20
(3-1) Energy flux equation for thermal absorption.....	46
(3-2) Heat transfer equation.....	47
(3-3) Density of GST equation using Vegard's Law.....	47
(3-4) Energy relationship equation between irradiance and thermal flux in GST.....	52
(3-5) Equivalent relationship for thermal and irradiance energies on scaled GST.....	53
(5-1) Irradiance equation.....	74
(5-2) General form for Responsivity equation.....	75
(5-3) Responsivity equation for microbolometers.....	76

# *ANALYSIS OF PHOTOCONDUCTIVE PROPERTIES IN Ge<sub>2</sub>Sb<sub>2</sub>Te<sub>5</sub> (GST) CHALCOGENIDE FILMS FOR APPLICATIONS IN NOVEL ELECTRONICS*

## *1. Introduction*

### *1.1 Motivation*

As silicon devices begin to reach their performance limit due to physical constraints, to keep up with demands and continue to accelerate the capabilities of technology, new and creative measures need to be taken. Currently, many are investigating ways in which electronic and computer technology can be modeled more like the human brain, a powerful multi-parallel processing unit that consumes very little power while operating at great efficiency [1] where the same circuitry can be used for logic and memory. One recent example demonstrating how current research is progressing towards technology that operates more like the human brain is a joint venture between IBM, Sony, and Toshiba, the development of the Cell Microprocessor, a multi-core CPU, designed for parallel physics and artificial intelligence processing. In another example, major computer microprocessor manufacturers to include Intel and Advanced Micro Devices have stopped competing for faster clock frequencies and have begun the battle of multi-integrated CPUs [1].

Currently, the majority of integrated circuit devices suffer from a common design characteristic; they all are designed in a way that limits their layout to two dimensions.



One specific area that researching  $\text{Ge}_2\text{Sb}_2\text{Te}_5$  (Germanium-Antimony-Tellurium or GST) attempts to overcome is this two-dimensional limitation in current device fabrication methods due to photolithography techniques by providing a connection between current devices and more novel three-dimensional devices, incrementally aiding the advancement in technologies that can operate more like the human brain. Because GST and other chalcogenide materials have unique phase-change properties that allow for multiple states in the material itself [2], this enables the development of devices using these properties that can operate in a pseudo-analog realm with multiple states rather than just two, as used in binary computing.

Researching the optical phase-change properties for multiple-state electronics in GST is important. First, this material shows promising capabilities to perform as a multiple-state electronic device [2]. Second, the interface mechanism between current technologies and a three-dimensional volumetric memory array currently being investigated by the Air Force Research Laboratory requires this multiple-state electronic property. Not only could GST be used for this specific application as a multiple-state opto-electronic device, but it shows promising abilities in phase-change memories [3], opto-mechanical MEMS [4], organic, bio and chemical semiconductor hybrid circuits, as well.

The Air Force Research Laboratory's goal is to determine if this material's properties are usable for a photodetector communication device to interface with 3-dimensional memories for use in space applications. There are many applications in

which chalcogenide detectors could be used to support the Air Force mission, to include optical sensors and advanced memory logic devices. The most important thing to look at is that chalcogenide bulk properties are being used rather than devices that use semiconductor hole and electron properties; this allows the chalcogenide devices to be much more resistant to radiation effects, which is highly desirable in space applications. Another important aspect to look at is that current technological research indicates that future electronic applications are shifting from electrical to photonic circuitry. This research will further the development of cutting edge technologies and give the Air Force more tools to develop high-tech equipment supporting the Air Force's goal to maintain air superiority through advanced technologies.

## ***1.2 Problem Statement***

The evaluation of photoconductive characteristics in  $\text{Ge}_2\text{Sb}_2\text{Te}_5$  chalcogenide films is needed to determine feasibility for its implementation as a photodetector communication device to interface with current integrated circuit technologies and three-dimensional optical memory arrays currently being developed by the Air Force Research Laboratory. Specifically, the feasibility of multiple states within the material through radiative stimulation needs to be determined; optimally, it would be desirable if the GST exhibits at least seven distinct states due to the material the Air Force Research Laboratory is developing out of Japanese salmon sperm DNA for three-dimensional memory having seven distinct states. Currently, both electrical and optical characterizations of this material have already been completed, electrically for phase

change memories and optically for its opto-mechanical effects [4-9]. What is novel about this research project is the type of photoconductive analysis being investigated on the chalcogenide material, analyzing its optical response as a resistive measurement in an electrical circuit, which has not been performed before, as far as current journal research indicates.

### **1.3 Scope**

The optical and electrical characteristics of this material will be researched in regards to how it responds as a photoconductive detector using a common bolometer photodetector model. The two questions that this research plans to answer are: based on the responsivity as a function of wavelength of light and resistivity as a function of intensity of light, can there be a way the GST will support changes in its resistance due to light and maintain that resistance change at steady state with electrical signals passing through the GST? And second, will the GST scale accordingly in its two-dimensional area and respond linearly to the scaling of the design as predicted to what basic radiometric calculations show?

Most of the research will be experimental in addition to some theoretical modeling, to include expertise within the Air Force Institute of Technologies (AFIT): microelectronics clean room lab and the adjacent MEMS test lab. The research will be done by designing a two-dimensional array of various rectangular geometrical gaps between surface micromachined electrode sets using the PolyMUMPs fabrication process.

Following the fabrication of the electrode array test structure; chalcogenide deposition was performed in collaboration with the University of Utah.

Before the actual experiment is done, a model of the material in FEMLAB finite element analysis software will be investigated to predict the results of the experiment. After the chalcogenide material is deposited between the electrodes, its resistive response will be analyzed while light is incident on the material, using a second set of identical electrode pairs with chalcogenide between them with no incident light acting as a noise canceling circuit. Various wavelengths (from ultraviolet to infrared), intensities, and step responses of light will be analyzed. The experiments will be conducted at the Air Force Research Laboratory facilities. These facilities will be used to perform and record the actual experimental results due to the current optical equipment setup which has all the equipment needed for the experiment and the assisting contractor familiar with this equipment, as well as the automated testing software the contractor has designed. The collected data will be analyzed to develop theories and models for feasible chalcogenide photodetecting devices.

Some variables that will not be considered in this experiment are the electrical and quantum effects due to the junction between the chalcogenide material and both the polysilicon and gold used as the electrodes. Other variables omitted include the quality of the GST being used and factoring in any effects of the doping levels both in the PolyMUMPs process and the chalcogenide deposition process.

## 1.4 *Thesis Outline*

Following the introduction in this chapter, chapter two includes a comprehensive look at the applicable properties currently known about chalcogenides that will need to be considered in modeling the results in FEMLAB software from this experiment. This chapter also includes a brief history of photodetectors, to include a description of the current types to help present the benefits and disadvantages of each type being used today. Chapter two concludes with an overview of current research and applications being applied to chalcogenides.

Chapter three presents the theory behind the experimental methods being applied in this research and the finite element modeling results from FEMLAB of the experiment. This chapter describes the specific modeling of the GST's thermal phase-change properties that will be analyzed in this experiment, not only describing the step by step process, but also presents and explains the equations and numerical calculation modeling of the actual experiment, forecasting how the experiments should work and the expected results based on scalability. Chapter four details the design and fabrication methods used, describing the fabrication processes used and the logic behind the design layout, to include explaining why these design and fabrication options were chosen over other possible choices.

Chapter five will cover the experimental procedures describing the facilities, equipment, actual setup used to record the results and other lab procedures. Chapter six will present the results and give an analysis of the data regarding the feasibility of the

material as a multistate photoconductive device, looking at factors that play a beneficial role in the material performance and what possible factors could be hindering its performance or be causing unexpected results. Finally, chapter seven provides a summary of the results, presents a conclusion to the analysis in chapter six, and outlines the factors being overlooked and what areas of research should follow considering the results found here.

### **1.5 Summary**

It has been assumed that the chalcogenide film will exhibit a resistive response due to its phase-change properties in thermal excitation from the light source similar to documented phase-change properties in the GST from thermally excited electrical sources [2, 3, 10, 11]. Therefore, the GST is being analyzed for its thermal phase-change properties, first through optical manipulation, and if unsuccessful, then by similar procedures done in other research the GST, will be tested electrically. The GST as grown from the University of Utah will be analyzed. Optical evaluation will be accomplished by illuminating the surface of the GST at different intensities and applying a bias voltage to read the change in resistance via the measured current. Electrical evaluation will be accomplished by applying a current sweeping from 0 to 100 mA and determining how the GST changes state through measured. Currently, the test structure layout has been fabricated on a 2-mm x 2-mm MEMS chip with a precision on the order of 2- $\mu$ m. The GST material will be deposited on the surface of the test structures and the devices will be analyzed.

## *2. Literature Review*

### *2.1 Introduction*

In the past two centuries, the ability to record light through various devices has progressed, leading not only to developments in photography, but also to photodetecting devices that go beyond photography applications: communications, infrared detection, photonic circuitry, and many other applications ranging across the known visible spectrum and far into the known radiation spectra. To further the development of devices that detect these radiative waves to provide advancements in optical processing circuitry and more robust devices in harsh environments such as space, areas such as analog devices and radiation hardened materials are being investigated. Research found on the material properties of chalcogenide materials are showing promising capability to be developed in both the ability to operate in a pseudo-analog realm and be resilient to radiation environments, since the chalcogenide device operations take advantage of the bulk material properties. In the last century, more than 25 years of research and analysis went into the development and advancement of photodetecting devices, as well as the study of chalcogenide materials. This chapter summarizes the work done in these fields, including a brief history of and a comparison of current photodetectors, the properties of chalcogenide materials, and an overview of the areas where chalcogenides have been used thus far.

### ***2.1.1 Brief History of Photoconductors***

For thousands of years, mankind has recorded his own history. Evidence of this reaches back to cave paintings, and spans to present time where mankind continues to make a record of his existence by recording information, electronically, as digital bits. To that end, the development of tools for historical record, art, scientific discovery, and more have been achieved. More recent developments in photographic tools detect photons. These developments can be traced back to the early 1830s [12]. Although originating from photography, these tools have begun to take on many other applications, such as radar, infrared night vision, spectroscopic analysis, photonic computing, and communications. Only recently with the advances in semiconductor devices has this process changed from one of producing permanent images by means of a chemical reaction that occurs when light hits a photosensitive film or material, to one that records images digitally through advanced semiconductor devices. These devices, known as photodetectors, have not only been used for photograph recording in the visual spectrum; there have been a wide range of designs to include many bandwidths of radiative energy, including infrared, visible, ultraviolet, and more. Photodetectors, most commonly semiconductor devices, convert optical signals into electrical signals.

### ***2.2 Comparison of Photodetectors and their Significance***

Photodetectors have allowed not only the simple process of recording radiative energy digitally and storing it quickly into various digital media, they have also allowed for the ability to rapidly apply advanced processing routines and algorithms on detection



and recognition applications, where raw data would not present such clear analysis and useful information. Photodetectors have a broad range of applications (both commercial and military), including infrared sensors, fiber-optic communications interfaces, and digital imaging.

Currently, there has been interest for optical devices to bridge the gap and replace electrical devices in integrated circuit technologies, creating photonic circuitry. To date, silicon has been the primary material used to build microelectronics. Silicon electronics are cheap to manufacture because silicon has unique properties that allow devices to be made easily and reliably in mass quantities. While the advance in photodetecting devices has been phenomenal, technological development naturally continues. Currently, photodetectors are divided into two types, thermal and photonic [13]. Thermal detectors are more classical. More recent are photon detectors which harness the theory of quantum physics. Looking at current technology, both thermal and quantum photodetectors, will give some insight why other materials are of interest and may have advantages.

Bolometers, thermocouples, and pyroelectric devices are specifically thermal photodetectors. Thermal photodetectors rely on the bulk properties of the material and its coefficient of thermal response: resistance change for bolometers, voltage change for thermocouples, and capacitance change for pyroelectrics. Thermal photodetectors respond to the total radiation energy incident on the detector in a two step process. First, the radiation must change the temperature of the detector, and second, the

temperature parameter must change, e.g., resistance [14]. This process is slower than generation of electron-hole pairs in a photon detector. These detectors are advantageous because their response is much broader, on the order of 10 to 100 times that of photon detectors bandwidth, typically visible to 40- $\mu\text{m}$  in wavelength. Operating temperature for infrared wavelength is room temperature as opposed to cryogenic for photonic detectors. Thermal detectors are generally less expensive than photonic detectors [14].

Photonic photodetectors, on the other hand, have a faster response time and rely on the detection of electron-hole pair generation. They have a much more precise measurement of the radiant energy incident on the detector. The operation of these photodetectors involves three steps: electron-hole pair generation by incident light through photon absorption, carrier transport by induced electrical current and/or multiplication by whatever current gain device may be present, and collection of photocurrent in an external circuit to provide the output signal. There are three different mechanisms by which photodetectors operate on the principle of photocarrier detection: photoemissive, photoconductive, and photovoltaic detectors. Photoemissive detectors operate when a photon impinges on a solid surface, which is called the photocathode, of an evacuated or gas-filled tube containing both a photocathode and one or more anodes. This process, where the cathode releases a photoelectron which is collected by an electrode at positive electric potential, the anode, is known as the external photoelectric effect [15]. A photoconductive detector operates by applying an electric potential across the photo-absorbing region which causes an increase in current

flow in proportion to the irradiance of the photon energy that exceeds the energy gap between the valence and the conduction band [15]; this additional current is known as the photocurrent.

Although photoconductive and photovoltaic detectors operate in very similar ways, photovoltaic detectors have the ability to generate a voltage potential and a photocurrent without applying a biased voltage across the device. This ability is unique to photodiodes, where, when an optical signal is incident on the photodiode, the depletion region serves as a boundary between the photogenerated electron-hole pairs and the electric current flows in the external circuit [16]. Other photodetectors include those that operate by manipulating quantum physics. These are quantum well and quantum dot photodetectors. They are unique photonic excited photodetectors, because rather than operating through normal bulk properties in the material from radiation affecting the space charge region, quantum well and dot devices operate on the principle of quantum potentials as depicted in Figure 2-1.

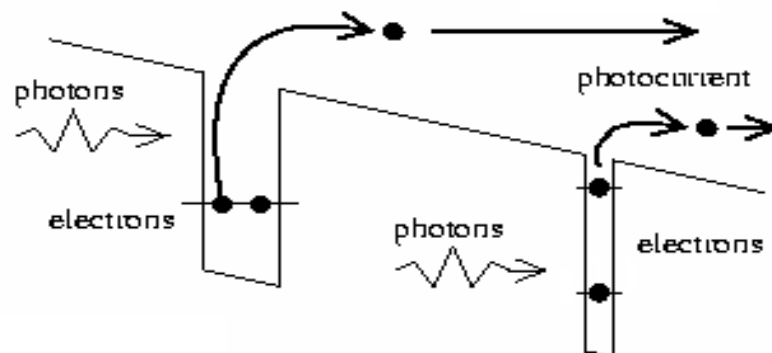


Figure 2-1 Shows how as quantum well of structure decreases, less energy is needed to detect the photocurrent.

Unfortunately most photodetectors suffer from a common weakness, that is, they operate in real time capturing the signal only when it is present. Chalcogenides, on the other hand, have properties that allow for a permanent storage of the image, where when a image is placed on the chalcogenide, a image can be permanently burned into the material. Particularly chalcogenides phase change properties and threshold states caused by their interaction with light allow for this capability. These effects will be discussed in detail further in this chapter.

### ***2.3 Chalcogenide Materials***

Chalcogenides are material compounds containing one or more elements from Group VI of the periodic table. Oxygen, sulfur, selenium, and tellurium are part of this group, but oxygen is generally treated separately when dealing with chalcogenides for traditional reasons [6]. Amorphous chalcogenides are commonly known for their glassy material composition, and were used in ancient Egypt for making small sculptures [7]. In the early 1950s, researchers working with these materials discovered something new: these glassy compounds contained semiconducting properties. This opened a new field of research in semiconductor physics dealing with amorphous semiconductors and noncrystalline solids, of which chalcogenides are only a part [7, 14].

At first, chalcogenides, like other amorphous semiconductor materials, attracted a lot of attention due to their amorphous state and semiconductor properties. However, researchers quickly lost interest in chalcogenides, and for many years, they were thought to have very little technological use. Originally, chalcogenides exhibited only basic

intrinsic properties of common semiconductors, and because of their amorphous state, they have a much lower mobility than crystalline semiconductors. Up through the late 1960s, these materials continued to be seen as uninteresting and thought to have few or no valuable properties. Then, by 1968, two amorphous semiconducting devices were successfully developed using chalcogenide materials, demonstrating a novel phase change property [10, 17, 18].

### *2.3.1 Fundamental Characteristics and Physical Properties*

Contrary to initial thoughts, chalcogenides materials have some unique properties. Unlike common semiconductors (such as silicon and gallium-arsenide) which are crystalline, amorphous semiconductors have a very limited long-range periodic order. This unique property allows for these amorphous semiconductors to have electrical and optical phenomena that are quite unlike those of crystalline semiconductors [17]. There are four main factors that play a role in these unique phenomena. First, chalcogen atoms are two-fold coordinated, thereby allowing for a considerable degree of localized structural flexibility. The second is that the electron states at the top edge of the valence band and the bottom edge of the conduction band are spatially isolated due to the disorder and defects inherent in amorphous materials. The third is that the top of the valence band is composed of chalcogen-derived lone-pair,  $p-\pi$  electron states described by the small polaron theory, also known as weak bonds. Finally, homopolar, similar or like-atom bonds can exist, particularly in non-stoichiometric compositions [5].

To further explain each of these factors, non-radiative electron-hole recombination is due to optically-induced electron-hole pair excitation which is aided through the trapping of the photo-excited charge carriers in the localized band-tail states, leading to a range of local conformational or bond-breaking changes. Excitation of the chalcogen  $p$ - $\pi$  states at the top of the valence band can lead to local structural conformation changes centered on the structurally flexible chalcogen atoms, e.g., ‘bond-twisting’ displacements of chalcogen atoms. Optically-induced excitation of weak, homopolar bonds in the structure can lead to bond-breaking and self-trapping excitons [5]. Not only do these theories give rise to the unique properties in chalcogenide and other amorphous materials, they also have been noted as the probable causes for the limited electrical conduction in these materials, as well. Chalcogenide materials have a wide variety of electrical and photonic properties depending on the exact molecular combination of elements [17]. Figure 2-2 shows a representation of a common chalcogenide material structure clearly depicting the limited long-range periodic order found in these compounds.

Understanding the structure of the material is important, and is necessary for effectively engineering the material in applications such as microelectromechanical systems devices. Although there are established methods of investigating crystalline semiconductor materials, a more in-depth understanding of the materials are needed when investigating amorphous materials. For example, when using x-ray diffraction on an amorphous semiconductor material, instead of clearly resolving peaks found when

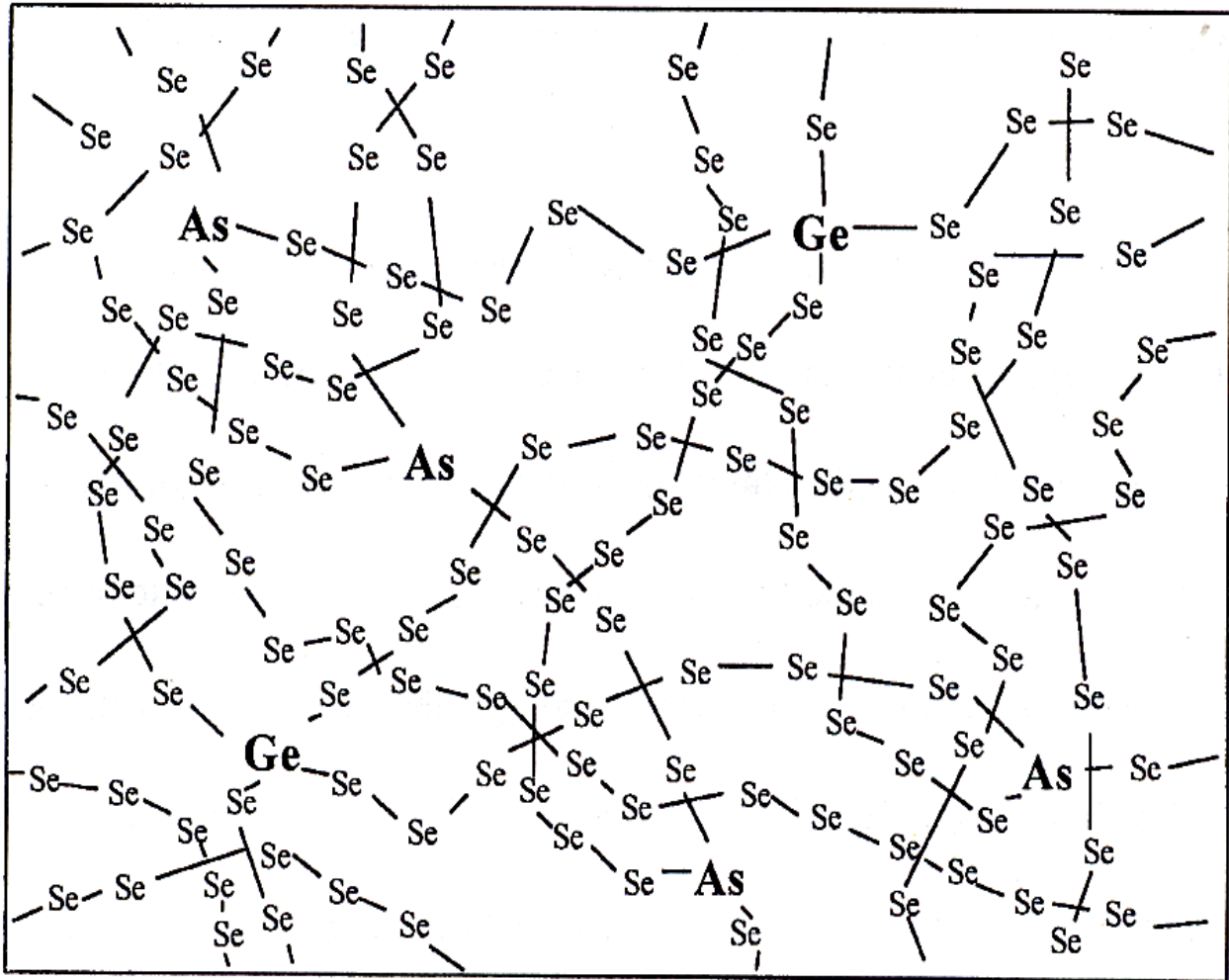


Figure 2-2 Schematic bonding topology of  $\text{Se}_{1-x-y}\text{As}_x\text{Ge}_y$  outlining the limited long-range periodic order common in these compounds [17].

analyzing crystalline materials, the results will be halos needing additional insight and assumptions on their interpretations. Using techniques that are common for characterizing crystalline materials does not provide vague information in the case of amorphous materials; rather, with a clearer understanding of certain theories of the materials, useful data can be extracted [6].

In the case of GST chalcogenide compound, the atomic formation was found to have two possible structures: a stable hexagonal structure and a metastable face centered cubic (FCC) lattice. “Since the metastable phase crystallizes faster, in fast phase-change operation, the crystalline GST is always in the FCC phase” [10]. Figure 2-3 depicts the lattice structure for both crystalline and amorphous phases, where the dashed line represents an example of covalent bonds between tellurium atoms.

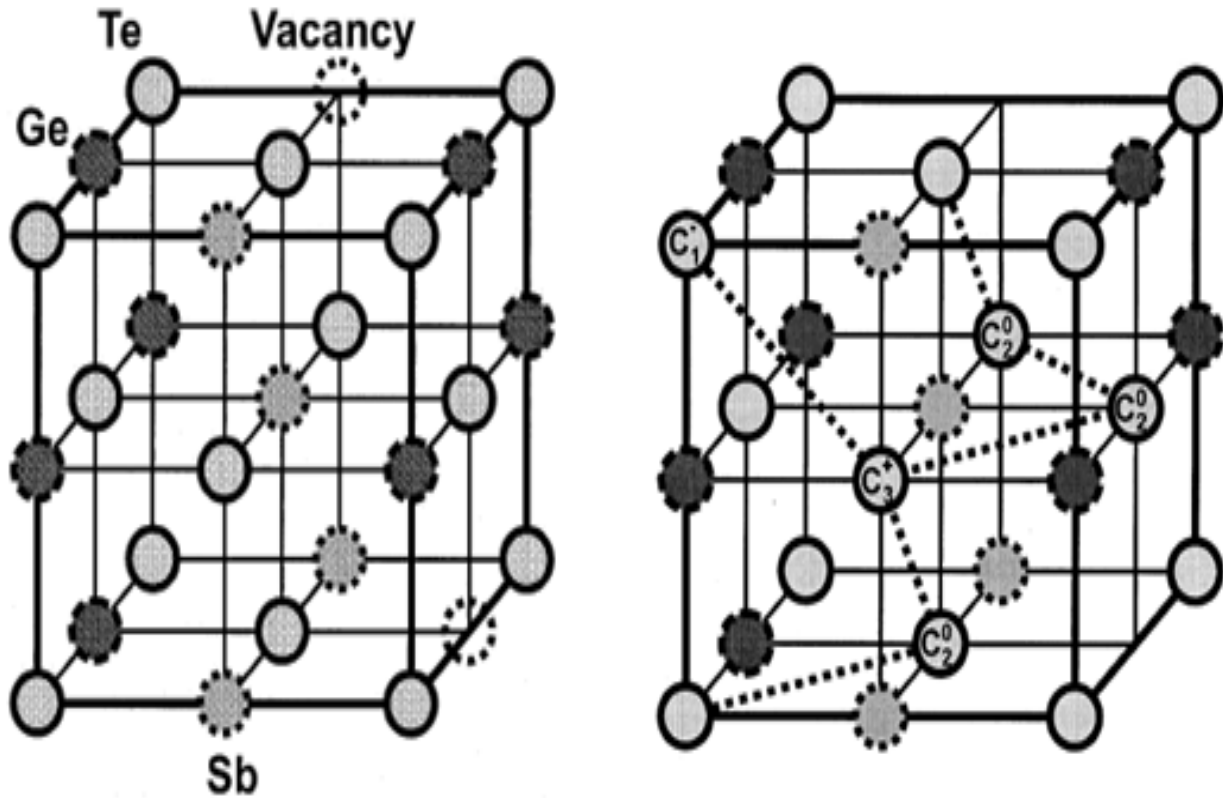


Figure 2-3 (left) Atomic structure of the FCC crystalline GST. (right) Atomic configuration of the amorphous GST, where the cubic geometry has been retained for reference [10].



Note that the chalcogenide atoms can lie in the fundamental state ( $C_2^0$ ) or in differently coordinated defect centers ( $C_3^+$  and  $C_1^-$ ), where the subscript number indicates the number of connecting atoms and the superscript charge indicates the ionic charge of that particular atom; these are known as valence alteration pairs (VAP) which will be discussed later. Also note that the stoichiometric compound,  $\text{Ge}_2\text{Sb}_2\text{Te}_5$ , presents about 20% of structural vacancies in the Ge-Sb sublattice [10].

In reality, the chalcogenide structure is slightly distorted.

“All the atoms have a six-fold coordination, with a sublattice randomly occupied by germanium and antimony and the other by tellurium atoms. The two-fold Tellurium atoms are linked in chains (dashed lines), while germanium connects the tellurium chains to the antimony planes. At finite temperature all glasses contain defects. In semiconductors with lone-pairs the most likely defects are VAP. Depending on the stoichiometry, structural vacancies can be observed in the Ge–Sb sublattice. Also in GST about 20% of the Ge–Sb atomic sites are indeed vacant [10].”

The theories provided below should offer a better understanding about how chalcogenide and other amorphous materials operate in order to make a good analysis of the data that will be recorded in this experiment and help to offer some insight on any unusual data that may be discovered.

### ***2.3.1.1 Defect Theory***

To establish a better understanding of defects in amorphous semiconductors, the 8-N Rule [6] needs to be explained in describing a nondefective ideal glass. A glass

compound in which all atoms satisfy their valence requirements can be called an ideal glass. To achieve this, the atoms need to obey the 8-N rule in the case of  $N \geq 4$ , where N is the number of valence electrons and the coordinate number is given by 8-N. For example, in the case of  $\text{Ge}_2\text{Sb}_2\text{Te}_5$  (GST), this means that all the gallium and antimony atoms are two-fold coordinated and tellurium atoms are five-fold coordinated. In addition, to attain a short range of order, stoichiometry should be maintained; in an ideal glass, all of the outer shell electrons of a particular atom are involved with chemical bonds to the nearest-neighbor atoms and no ‘wrong’ homopolar bonds such as Ge-Ge or Te-Te should exist [6, 17].

In chalcogenides, the bonds are often flexible because the glass-forming regions are quite large and the material deviates from stoichiometry. This means that the presence of homopolar bonds are inevitable. There are some types of defects which describe the compositions within chalcogenide materials: negative-u defects, coordination defects, wrong bonds, and some other alternative theories that are not as agreed upon and accepted [6, 18]. Out of these different types of defects, the defect theory most focused on for chalcogenides is the coordination defect theory. This theory seems to give a reasonable explanation for the structural defects, known as lone-pair compounds, which are found in chalcogenides. Chalcogenides are known as lone-pair compounds because of the four outer electrons, p-orbital or  $\pi$ -orbital, characteristic of the chalcogenide used for bonding. Known as the valence alternation model, the formation of over-coordinated defects through interaction of lone-pair electrons is explained by an empty orbital of a

positively-charged dangling bond that has been argued to interact with lone-pair electrons of the neighboring chain, forming a three-fold coordination defect [6]. “The gain in energy due to the formation of an extra bond was considered to be the driving force for compensating the energy cost for creation of the doubly occupied site at the negatively charged dangling bond [6].”

In the VAP model, defects form according to the following reaction:



where C stands for a chalcogen molecule, the subscripts describe the coordination, and the superscripts correspond to the ionization charge. The positive sites are three-fold coordinated and the negative sites are singly coordinated. Regarding the stability of natural species, the triply coordinated center was concluded [6] to be more stable than a singly coordinated one (a simple dangling bond). Energy levels of the various defects configurations are schematically shown in Figure 2-4. The circles indicate the different electron orbitals in both s and p states and the lines in the middle of them represent unbonded valence electron charge(s). Most important to note for this research are dangling bonds (lines in Figure 2-4), which can be effected by radiative energy leading to faster absorption times improving its efficiency [5].

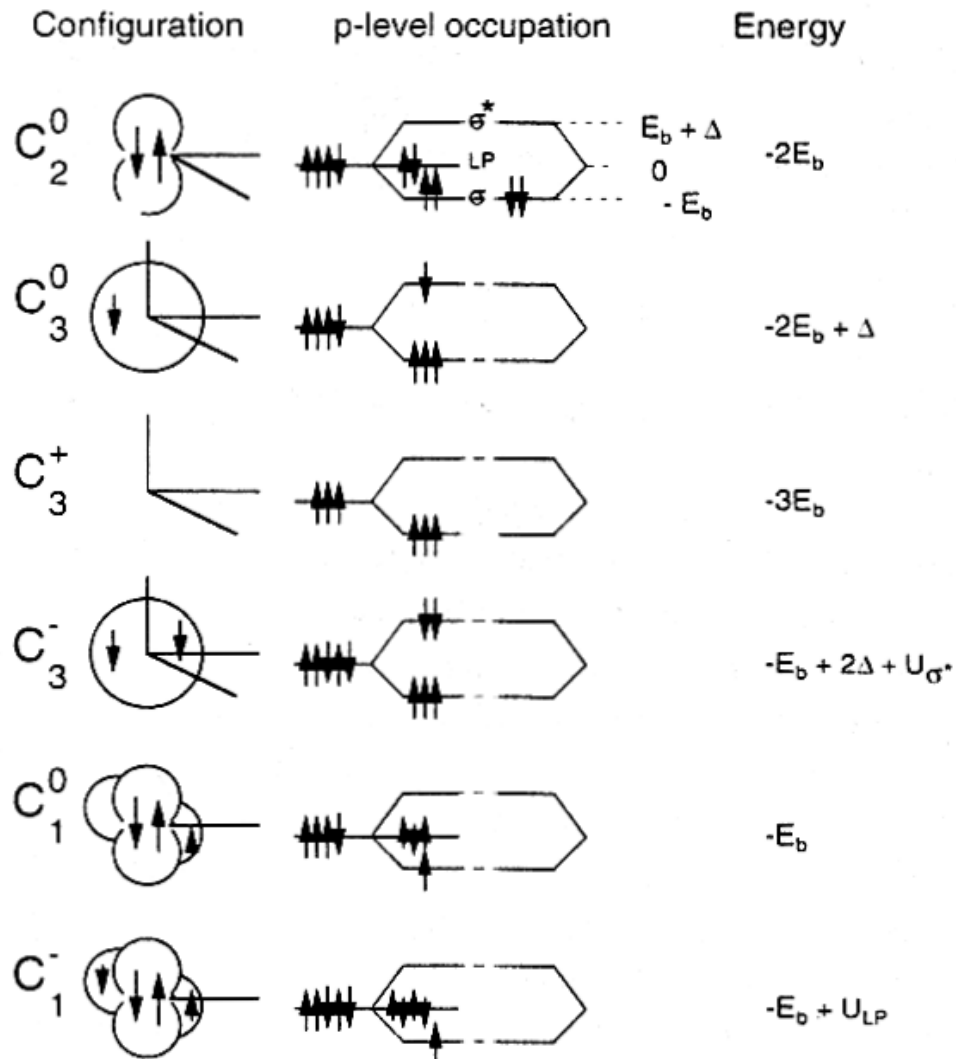


Figure 2-4 Structure and energy for different bonding configurations of elemental chalcogens [6].

The VAP model was developed before being applied to chalcogenides, so when applied to chalcogenides, the conclusions of the VAP model are based on highly simplified molecular orbital diagrams and are considered “somewhat speculative” [6]. Defects in amorphous chalcogenides were generally found to have both positive correlation energy and a simple dangling bond (the most stable natural defects). These

two conclusions differ from that of the original VAP model [6]. The reaction given in Figure 2-4 is exothermic, and therefore, the creation of the VAP  $C_3^+$  and  $C_1^-$  is preferred over the neutral  $C_2^0$  since it lowers the energy of the system. In addition to the valence alteration pairs, there has also been some recent evidence for states shallower than the valence alteration pairs. These shallower states, called three-center bonds, are formed from other structural deviations [17].

### *2.3.1.2 Energy Band and Density of States Properties*

Originally, quantum theory in semiconductors was based completely on the presence of long-range order and on the periodicity of the crystalline structures. Furthermore, it was believed that since amorphous solids do not have long range periodic order, they cannot be described by energy band diagrams nor do they behave like standard semiconductors. However, around the mid 1950s, it was discovered that the key in understanding the properties of solids is not their periodic structure but the chemical nature of their molecular combination [10]. Sometime after this discovery, chalcogenide glasses were found to act as semiconductors with an energy gap as well [11]. The covalent interatomic bonds produce the usual bonding in the valence band and create anti-bonding in the conduction band. However, since each chalcogenide atom has lone-pairs, band-tailing and non-bonding in the density of states appears near the top of the valence band-edge. Because these states are very localized, their carrier mobility is correspondingly very low [10].

Further investigation of amorphous semiconductors has shown that the density of states drops off sharply at the edge of the energy bands. The energy band structure of the material directly relates to its mobility. Observing the rapid reduction in the density of states at the energy band edge indicates how the electrons will be able to propagate through the material within the bands and will not propagate within the band gap [17]. In Figure 2-5, the energy versus density of states diagram depicts these two relationships. Also note there are states in the band gap from particular defects that can effect the mobility and other material parameters.

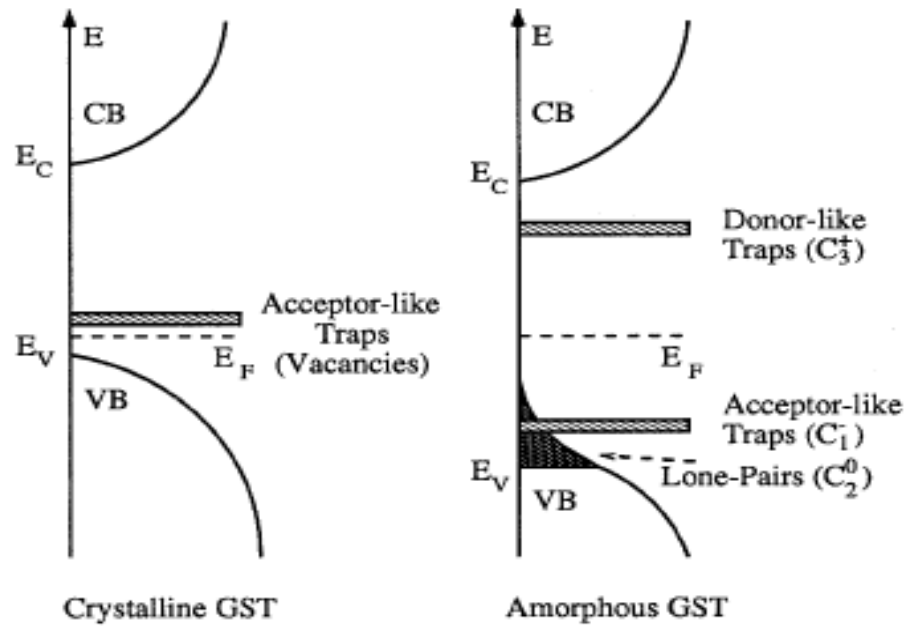


Figure 2-5 Schematic band structure of crystalline and amorphous GST [10].

Another model, commonly known as the Cohen-Fretzsche-Ovinsky (CFO) model [6], presents the main theory for the density of states in amorphous semiconductors

showing how the overlapping band tails from lone pairs effect both the conduction band and the valence band, which is depicted in Figure 2-6 [10].

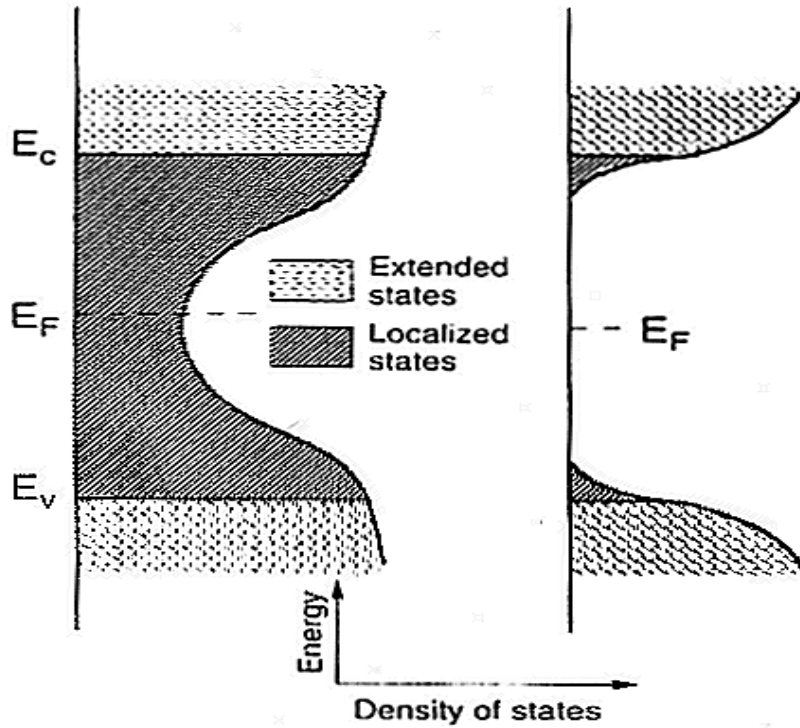


Figure 2-6 Overlapping band tails in amorphous semiconductors, CFO model (left), rather weak tails protruding into the gap due to VAP (right) [6].

The states within the gap are due to the large number of traps in the material created by dangling bonds and other nonperiodic bonding defects within the material, also known as deviant electron configurations. Neutral dangling bonds containing unpaired electrons form a positive and a negative trap according to theories [17]. It is also important to note that slight deviations in the bond lengths and angles, as well as other structural imperfections, occur when widening of the band edge takes place,

making the band-tailing less abrupt than crystalline materials which helps to explain the CFO model in Figure 2-6.

VAP and three center bond traps form additional states between the band gap in the energy band structure of the material. Figure 2-7 is a visual representation of these VAP and three center bond traps.

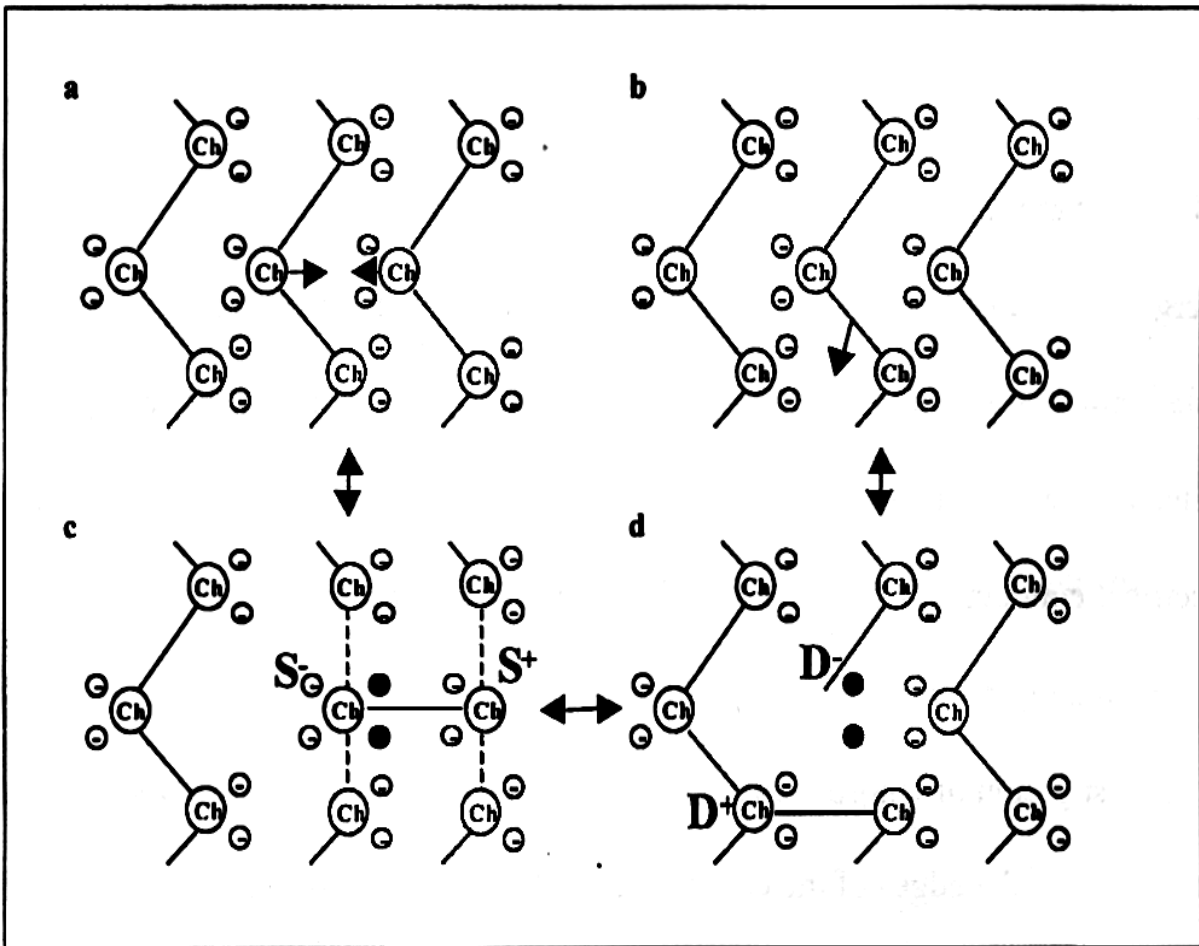


Figure 2-7 Sketch of three center bonds (TCB) and VAP where Ch circles designate chalcogenide atoms, (a and b) indicate the chalcogenide in a periodic form and the arrows indicate the possible transitions which are affected by VAP resulting in (c) with TCB and solid empty circles mark lone-pair non-bonding TCB electrons, straight dotted lines indicate covalent TCB, and the solid lines where the D indicates positive and negative dangling bonds (d) [17].



The energy gap in the CFO model indicates trapped electrons and holes by ionic attraction within the band gap causing the lifetimes of carriers in chalcogenide materials to be dramatically reduced in comparison to crystalline materials. To control the electronic properties of the material, such as mobility, impurities need to be added that either add or remove states in the energy band gap. These impurities, documented by Dr. Ovshinsky in the mid 1980s, either increase the mobility of the material by preventing dangling bonds from forming or decrease the mobility by causing more bonding deviations to form [17].

### *2.3.2 Unique Properties Due to Direct Electrical and Photonic Interaction*

The development of chalcogenide materials and their research began somewhat slowly, but as discoveries were made about the unique physical properties within chalcogenides, this fostered other areas of research and exploration that continued to lead to new and very unique findings about these materials. The literature suggests two main applications identified as being heavily researched and sought after concerning unique chalcogenide properties. The first, which is being looked at very extensively for new memory applications, is the phase-change properties in chalcogenides, allowing them to shift between amorphous and crystalline structures through a thermal mechanism using electrical pulses to change the states of the material. The second application uses the same thermal mechanism, but through optical manipulation, where the bulk materials (as a thin layer) are used for their phase-change properties as higher (crystalline) or lower (amorphous) reflectivity in DVD-RAM media [19]. However, little research has

been done that combines the two areas, looking at phase-changing the material optically for electrical circuit implementation as a variable resistor. A brief look at these two properties will give a better understanding of chalcogenides.

### ***2.3.2.1 Electrical Phase-change Crystallization Behavior***

In the 1960s, researchers began to investigate the chemical and metallurgic properties of amorphous semiconductors and discovered some distinguishing characteristics of the chalcogenide materials: two types of reversible switching phenomena between an amorphous and poly-crystalline state [11]. The first transformation, called ovonic threshold switching, is an electrical field-assisted and reversible transition, which makes an amorphous semiconductor switch from a highly resistive to a conductive state. Once the amorphous resistivity drops, a second transformation, called ovonic memory switching, occurs in which a reversible phase-change from the amorphous to the crystalline state is induced by heating due to current flow through the material [10].

The phase-change behavior in this type of chalcogenide material, known as bistable material, is accompanied by a change in the atomic structure. While the structural change within the material is not completely understood, the shifting has been hypothesized to involve a combination of electrical and thermal processes. Given a bistable chalcogenide with an amorphous structure, thermal energy supplied to the material will allow for bond breaking between neighboring atoms in the material. In an unbonded state, the structure of the material is free to align in any form. The atoms will

tend to form a poly-crystalline structure due to the fact that this arrangement has a lower energy than an amorphous one. Finally, the amount of the structure that is crystalline formed in the bistable structure is directly proportional to the amount of time the energy is applied. It has been documented that given the correct crosslinking of atoms in particular compositions of chalcogenides such as GST, the structure of the material can be switched between the pseudobinary line depicted in Figure 2-8 [17, 20].

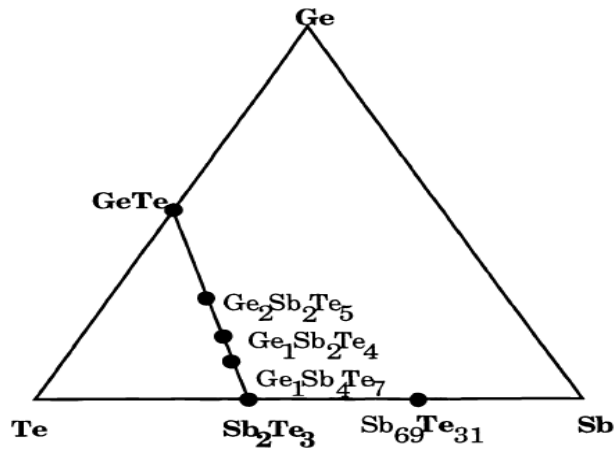


Figure 2-8 Phase diagram of the Ge-Sb-Te ternary alloy system indicating how reversible changes can occur between the atomic structure of ordered and disordered phases along the pseudobinary line [20].

Within the class of GST materials, the compounds along the pseudobinary GeTe-Sb<sub>2</sub>Te<sub>3</sub> tie-line, as shown in Figure 2-8, have fast crystallization properties.

Crystallization times down to 20 ns and user data rates up to 35 Mb/s have been documented in optical disk media for phase change optical recording [20].

Furthermore, from a poly-crystalline state, the bistable material can be transitioned back into an amorphous structure through a similar process of applying

thermal energy. Thus, the material has more of a tristable capability between crystalline, polycrystalline, and amorphous states. By applying enough thermal energy to break the atomic bonds and rapidly removing the energy, this process, known as ‘quenching’, locks in the random arrangement in the bonds of the material when returning the melted material back to a solid [17]. Research into this phenomenon has shown that when an applied current sweep across the GST material is performed, the resultant current versus voltage curve is as depicted in Figure 2-9, where when the GST is in amorphous form the voltage increased rapidly as current is increase due to GST being highly resistive in amorphous form, and then as the material begins to melt and form a more crystalline structure, the resistance in the GST drops as indicated in Figure 2-9 by the voltage drop during the current sweep. Once the GST is crystalline, the current sweep is indicated by the (full set) curve in Figure 2-9.

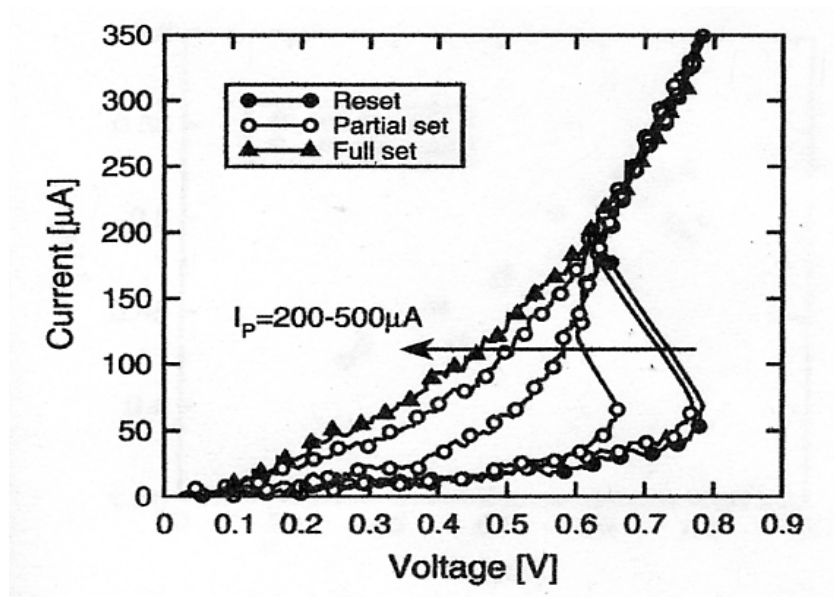


Figure 2-9 Current versus voltage plot for GST characteristics during material transitions between amorphous and crystalline states [21, 22].

### *2.3.2.2 Photoinduced Phenomena*

As well as electrically modifying the structure and properties of an amorphous solid through releasing energy during nonradiative recombination, these amorphous semiconductors exhibit a large variety of photoinduced metastable phenomena, as well. Reversible photoinduced structural changes are a phenomenon unique to glassy amorphous chalcogenides and are not observed either in amorphous Group IV semiconductors or in innate crystalline chalcogenides. This is a metastable state because, as the chalcogenide expands in one direction and contracts in the other, there is a limiting amount of radiated energy the chalcogenide can absorb before it begins to soften. There are specific reasons for this uniqueness being restricted to vitreous, or glassy, chalcogenides, but first, an understanding of photodarkening is needed for these reasons to become clear [6].

Photodarkening is an effect, occurring when the chalcogenide is illuminated, when the absorption edge shifts to lower energies, meaning the energy gap decreases corresponding to longer wavelengths. Later annealing near the glassy-transition temperature leads to a recovery, however, never complete, of the initial parameters of the film. The curve in Figure 2-10 corresponding to the annealed state occupies an intermediate position between the curves describing the current evaporated and illuminated states. Should the annealed film be illuminated, one would have a completely reversible behavior during the illuminated process and annealed states. Similar changes can be observed in most Ge- and As- based chalcogenides [6]. This is

important to note, because while this experiment is not going to anneal the GST, the initial change in the material should be different than any following test on the material due to transforming the material from amorphous to crystalline and back to amorphous, which has similar effects on the material as annealing.

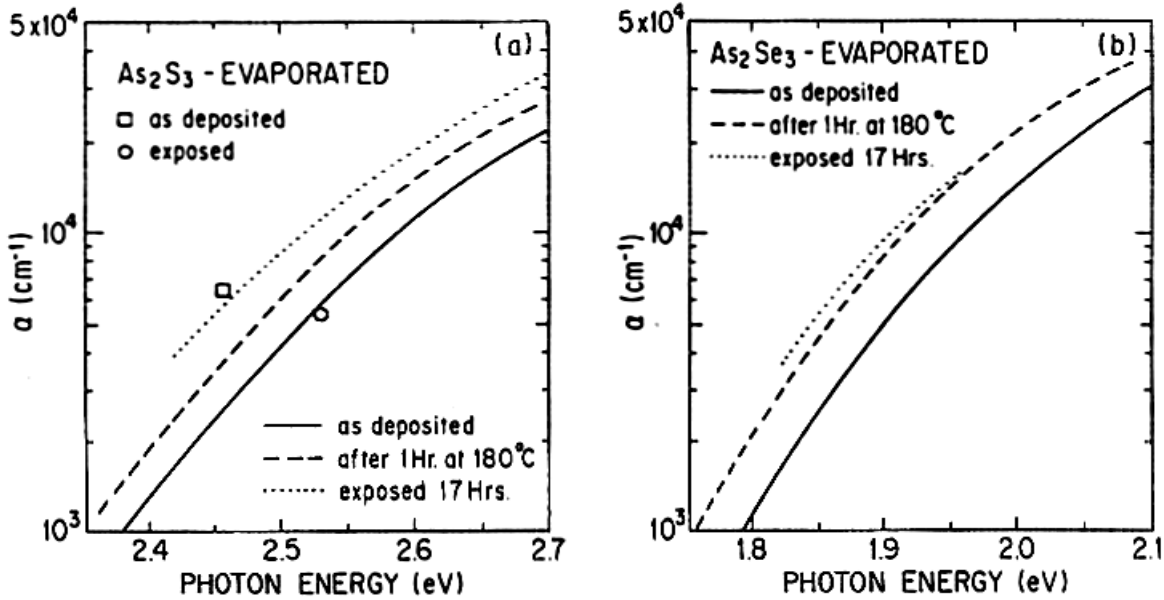


Figure 2-10 Reversible shift of the absorption edge of typical chalcogenide glasses,  $\text{As}_2\text{S}_3$  and  $\text{As}_2\text{Se}_3$ , under photoillumination and thermal annealing [6].

The reason for reversible photostructural changes being restricted to glassy chalcogenides is described as follows. “The top of the valence band in chalcogenides is formed by chalcogen lone-pair electrons and it is believed that the change in the interaction of lone-pair electrons resulting from the structural change is responsible for the photodarkening. The importance of the chalcogen lone-pair electrons is further

emphasized by the fact that photodarkening disappears in metal-doped chalcogenides [6].”

Another important factor found in the photoinduced phenomena of chalcogenide materials besides photodarkening is photoanisotropy. Although this experiment does not consider different aspects of polarized light and its effect on the phase-change transitions for an optical-analogue memory, this is something to consider for future experimental testing, because it has not been applied to this type of an experiment and seems to have a significant impact on the material.

If chalcogenide glasses are illuminated by linearly polarized light, along with photodarkening, light-induced anisotropic effects will occur, such as photoinduced dichroism, “the property of absorbing one of two or more plane-polarized components of transmitted light more strongly than the another,” [6] and birefringence. A comprehensive study of photoinduced vectoral effects found that photodarkening and photodichroism appear with different kinetics in amorphous materials. Photodichroism reached saturation much earlier than did photodarkening in these experiments. Photoinduced dichroism can be reorientated by changing the polarization of the light, in which case, the existing dichroism is reduced at a much faster rate than that of its creation. In the case of circularly polarized or nonpolarized light, the dichroism in each and every direction would cancel out the others [6]. Figure 2-11 shows the time dependence of the quantity of  $2(I_{\parallel} - I_{\perp}) / (I_{\parallel} + I_{\perp})$ , where  $I_{\parallel}$  and  $I_{\perp}$  are intensities of light

in arbitrary units transmitted through the sample with the electric vector parallel or perpendicular, respectively, to that of the inducing light [6].

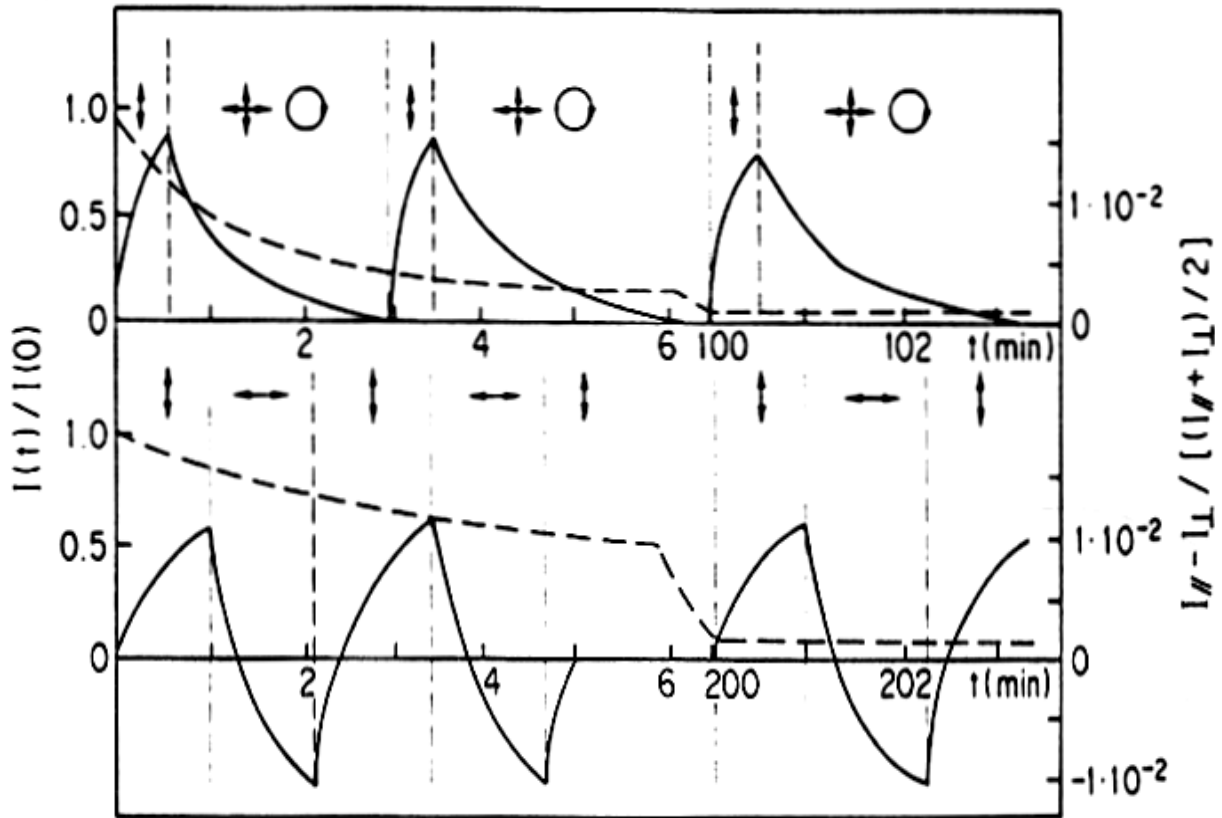


Figure 2-11 Kinetics of photodarkening (dashed line) and photoinduced dichroism (solid line) in an  $\text{As}_{50}\text{Se}_{50}$  film: (arrow) light polarization; (circle) unpolarized (or circularly polarized) light [6].

One group of models which explain photoinduced anisotropy rather well suggests that the anisotropy will be a result of bond flipping at the intimate VAP sites. The authors of this model argue that the concentration of native defects present in amorphous chalcogenides is adequate to explain these defects. In the case of linearly



polarized light, the light induced reversible anisotropic dilatation and contraction, and it was argued that these formations of dynamic interlinked bonds were “followed by the redistribution of special orientation of bonding and nonbonding electrons” [6]. Figure 2-12 schematically illustrates this anisotropy due to bond flipping at intimate valence alteration pairs.

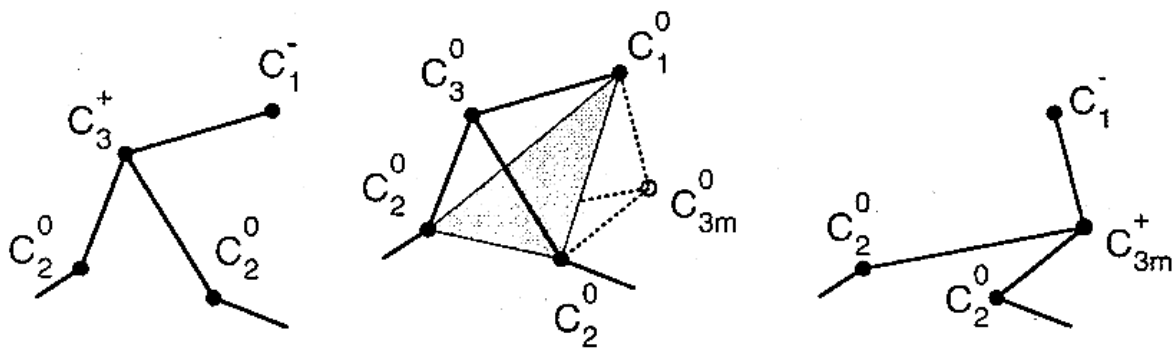


Figure 2-12 A flip of the valence alteration pairs pyramid from left to right showing the effects of photoinduced anisotropy in chalcogenide materials [6].

### 2.3.3 Summary of Chalcogenide Material Properties

It is important to note that not all the different properties of chalcogenides have been presented here. In this chapter, the material presented outlines the main area of chalcogenide material properties that are believed to be most relevant in this thesis work. The investigation into what these materials hold for both electrical and photonic properties will provide the needed background for further discussions. A close look into the physical and electrical properties of chalcogenide materials has shown that, through

added impurities the density of states can be controlled and ultimately affect the ability to phase change between amorphous and crystalline states [3, 10, 17]. Even though doping was investigated for electrical phase switching applications, this could play an important role in photoinduced reaction in the chalcogenide material, as well. More importantly for this research are the photoexcited properties. Photostructural changes result from bond switching via the formation of dynamic bonds of unpaired electrons from the nonbonding orbitals. A crucial role played by lone-pair electrons in the formation of dynamic bonds provides an explanation of why photoinduced structural changes are limited to amorphous chalcogenides [6]. Much effort is being given to understanding the nature of photoinduced anisotropy. Despite considerable progress, a complete understanding of its mechanisms is not clear [6].

#### ***2.4 Summary of Applications Using Chalcogenide Materials***

Chalcogenide materials continue to show promising capabilities in a variety of applications and are gaining a lot of interest in many fields of semiconductor applications, quite ironic to how they were initially perceived. Just as unique as the properties in chalcogenide materials are the applications being investigated and utilized by them. Chalcogenides were originally developed for applications and testing in amorphous semiconductor devices as early as the 1950s [6, 17, 18, 23], but following the discoveries of their more unique properties, they began to be used in many optics applications from various wave guides [24] such as Bragg reflectors [25], thin films used in solar cells, and infrared applications [26, 27]. Another note to mention about

chalcogenide glasses is that the presence of homopolar bonds, as discussed earlier, plays a decisive role in some applications such as photoresists and electron beam resists. These types of resist allow for the ability of submicron-level lithography processing [6]. Due to their density of states and energy bandgap, chalcogenide materials are ideal for mid-infrared applications both in absorbing and emitting in these wavelengths [6, 13, 27]. Because chalcogenides are easily pressed into various shapes, they are also found in applications for moldable lenses for use in optics, infrared, and microlenses for microelectromechanical systems [6, 24, 28, 29].

One of the most recent areas being pursued with great enthusiasm is chalcogenides' ability to shift phases reversibly with low hysteresis from both amorphous and crystalline states for applications in nonvolatile memories, such as flash technologies. In just the past few, years flash memory applications have exploded, most widespread as the 'digital film' for digital camera memory. Other applications include portable flash drives, hard drive components in space equipment such as the recent missions to Mars, and media storage in every aspect of electronic equipment: MP3 players, cell phones, BIOS chips, PDAs, etc. Chalcogenides show promising results in this area because of their nonvolatile ability to maintain different logic states based on their phase change properties and high speed program rate of less than 100 ps [10, 17, 21, 30]. Other research with chalcogenide materials, where applying the unique photoinduced anisotropy effects to thin film layers of chalcogenide on microelectromechanical systems cantilevers,

creating an opto-mechanical reaction based on polarized light incident, is being investigated. These devices allow for a completely optically actuated device [5].

Current searches in the electronic journals reveal new and frequent research in unique applications of chalcogenide materials. More than 700 articles in IEEE and over 800 in ScienceDirect the first half of this year have been published referencing chalcogenides. With all the new research occurring so quickly, it is hard to make the claim that the research in this thesis has not already been done, but to the best efforts given in this literature search, the research of chalcogenide materials, specifically for  $\text{Ge}_2\text{Sb}_2\text{Te}_5$ , applications dealing with photodetection using the threshold phase change properties outline earlier, appears novel.

### ***3. Theory and Modeling***

#### ***3.1 Introduction***

Although this research is focused heavily on understanding GST through experimental research, accurate modeling can help to provide insight into how the experiment should be approached and the types of procedures used. Modeling can also provide a better understanding when unexpected results occur. The design and modeling in this chapter follow the actual design described in chapter four which is used in the experiment. This design was optimized for optical testing of the GST, where the surface area of the GST was important for both optical excitation and the ability to couple the GST with marine DNA for future application research into novel volumetric memories. The idea was to create a surface test area that could both allow for optical testing and the ability to place thin layers of the marine DNA for device and material coupling.

#### ***3.2 Marine DNA – Large Capacity Multistate Optoelectronic Memories***

Salmon and their eggs are a popular cuisine in Japan. Currently, Japan harvests thousands of tons of salmon per year, with one of the waste products being salmon sperm. Although the salmon and their eggs are highly desired, the sperm are disposed of as waste, estimated at 10,000 tons per year [31]. The amount of waste was even considered an environmental pollutant because of the sheer volume by which it is disposed.

Recently scientists were interested in finding usefulness in this natural resource. Since DNA can be crystallized [32], it could be explored for semiconducting properties and possibly provide a new material for integrated circuit technologies. One researcher, Dr. Naoya Ogate of the Chitose Institute of Science and Technology in Hokkaido, Japan, began looking at the salmon sperm DNA and found it to have some interesting properties reacting with light, and the ability to hold multiple states within the material structure due to optically-induced phenomenon [31].

This material shows promising capabilities, not only in optical applications and optoelectronics, but as cellular membranes, as well. The Air Force Research Laboratory sees this material as a resource to support research in biochromophores and nonlinear optical polymers [31]. The Information Directorate (AFRL/IF) is interested in this material as an avenue to develop novel three-dimensional or volumetric memory technologies with an end goal to develop cognitive optical computing. Cognitive computing is where the computer memory and logic are one and the same, enabling dynamic data storage and restructuring of logic processing and enabling the computer to learn, similar to the human brain. Coupling the DNA with a multistate semiconducting material such as GST would allow the DNA material to operate with current integrated circuit (IC) technologies using the GST as an interface, bridging the gap between today's technologies and those of the future.

### *3.3 Chalcogenide: Multistate Interface Design*

Since chalcogenide materials have been researched extensively for both their electrical and optical properties and exhibit multistate capabilities as an amorphous semiconductor, they appeared to be an ideal material to interface current technologies with the marine DNA polymer. The driving interest in this chalcogenide, GST, is the capability to change states [10, 21, 30], (amorphous, semi-crystalline, and crystalline) through thermal interaction [4, 9]. This would allow researchers to develop new multistate devices, coupling the DNA with GST to record and maintain the varying states of the polymer within the GST.

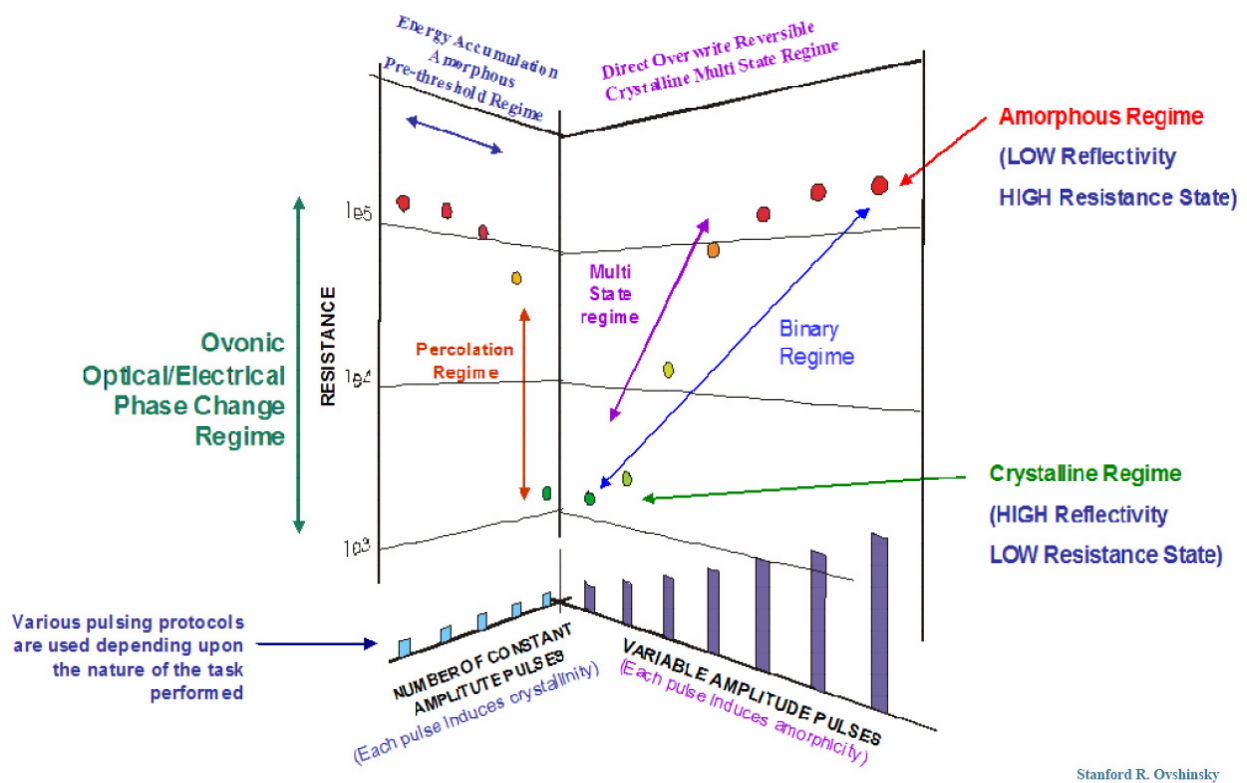
There are three steps this research is interested in modeling in order to determine the capability of GST as an interface material for the DNA and current IC technologies, two in modeling the GST to accurately predict and understand how it will interface with the polymer and a third to understand how the GST can be modeled for finite element analysis such as in a SPICE program. The first two models are to determine the required irradiance to sufficiently change the GST between states and identify the scaling factor of irradiance to surface area of GST for different surface area sizes. The third model is to analyze the GST's photoresponse as a function of wavelength; by using the transfer function from that data to equate the device characteristics to a finite element, large scale SPICE modeling can be achieved. Simple transfer functions are characterized as low-pass, band-pass, or high-pass filters. For example, a frequency response from a device that had good frequency response in lower frequency but greatly attenuates higher

frequencies would be considered a low-pass filter. Using Laplace transforms, the frequency response data can be characterized by an equation called a transfer function, not only for simple models but more complex ones, as well. A two port finite element circuit (using simple elements, capacitors, resistors, and inductors) can be derived from the GST's frequency response transfer function as an equivalent model of the GST test circuit, allowing for large scale integrated circuit analysis in a SPICE program. Although there is interest in this third model, due to time constraints, this research will only model the first two and discuss the third model in chapter seven under future recommendations.

Some research in this area has already been done. Research from ECD Ovonic [33] presents an overview of the properties of GST, but with little to no quantitative results and analysis. The modeling and analysis in this research are not only to determine the feasibility of implementing a coupled chalcogenide and marine DNA polymer device, but to present some findings similar to Dr. Ovshinsky's, of ECD Ovonic, with quantitative results. Thus, the basis for the modeling in this research follows the properties Dr. Ovshinsky describes [33] as a process of manipulating the chalcogenide GST between amorphous and crystalline states. This is done through pulses of energy, where the material stores the amount of energy placed into it, and when enough energy is absorbed, the material shifts to a new structural phase as indicated in Figure 2-8 along the pseudobinary line between GeTe and Sb<sub>2</sub>Te<sub>3</sub>. Similarly, the reverse process can be achieved using variable amplitude pulses of energy where each pulse



induces a higher degree of amorphous structure in the material. Figure 3-1 presents a general overview indicating how the resistance changes relative to the current state of the material, and shows how energy applied to the device relates to each phase shift.



Stanford R. Ovshinsky

Figure 3-1 Resistance characteristics of a GST chalcogenide device, (left) multistate phase shifts from amorphous to crystalline states, (right) multistate phase shifts from crystalline to amorphous states [33].

To accurately model how the GST transitions between amorphous and crystalline states, a more quantitative understanding in the difference of how the chalcogenide shifts between crystalline and amorphous states is needed. Although structural changes can be induced from different types of energy (electrical, optical, etc.), the method to change the material is the same: by heating, melting, and then cooling the material. As shown in

Figure 3-2, shifting the material from an amorphous to crystalline state occurs when the material is heated between the glass transition temperature, around 300°C, and the melting point, around 600°C, and is held at this temperature long enough for the supplied energy to crystallize the material. Alternatively, when the crystallized material is heated above the melting point, and then quickly quenched, an effective reset of the material to an amorphous state occurs [21, 30, 34].

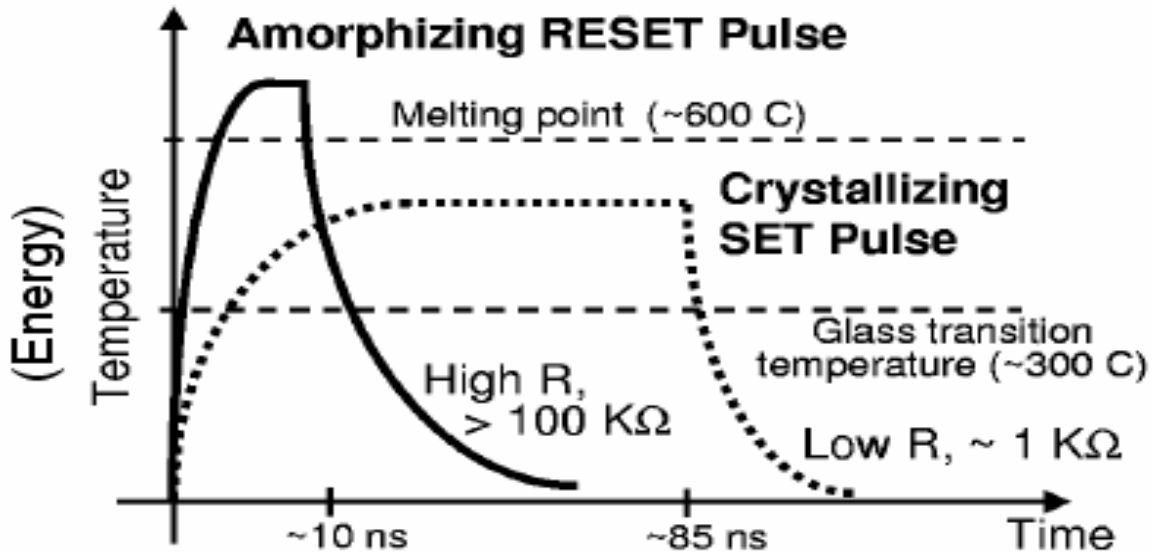


Figure 3-2 General diagram indicating pulse length and intensity of required energy to set and reset chalcogenide material for phase-change between amorphous and crystalline states [34].

### 3.3.1 Heat Transfer Model

An important step in any experiment is building a model to correctly predict the results; this will both give insight in which directions the experiment should be investigated and possibly predict any possible problems that could be avoided. The

desired approach in modeling this experiment is to find an accurate model that will predict the amount of irradiance ( $\text{W}/\text{m}^2$ ) needed to shift the material between each state: amorphous, varying pseudo-amorphous states, and crystalline. Another important factor to consider for developing a test model is to incorporate a design that can be easily fabricated. This design needs to allow one surface of the GST to be exposed, where the light source can directly irradiate the material. The design for the experiment also needs to incorporate a way to test the GST electrically by an external circuit to verify the phase changes in the material via measured current-voltage relationships. Figure 3-3 represents a simple model meeting these desired requirements.

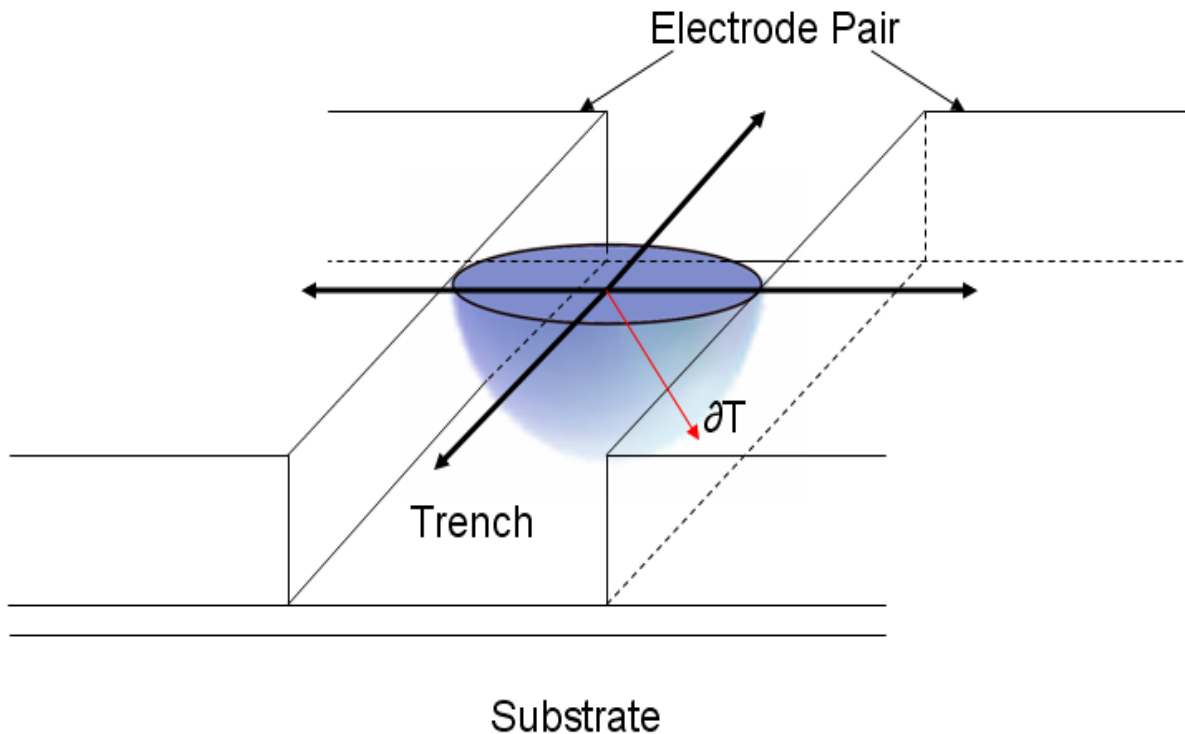


Figure 3-3 Heat flux model: GST-filled trench between electrodes is irradiated with light such that the surface is heated creating a gradient of heat through the GST.

The first parameter needed is determining the irradiance that will raise the surface temperature of the material above the glass transition temperature of 300°C but below the melting point of 600°C. This condition will cause a rapid growth of large crystals (in the material), shifting the material from an amorphous to a crystalline state. GST does not actually contain pseudo-crystalline states; rather, the cause for this appearance in the materials is due to part of the material shifting to crystalline and part of the material remaining in a amorphous state. Both [21] and [34] have identified similar results. An example of this is represented in Figure 3-4. As the GST within the trench is

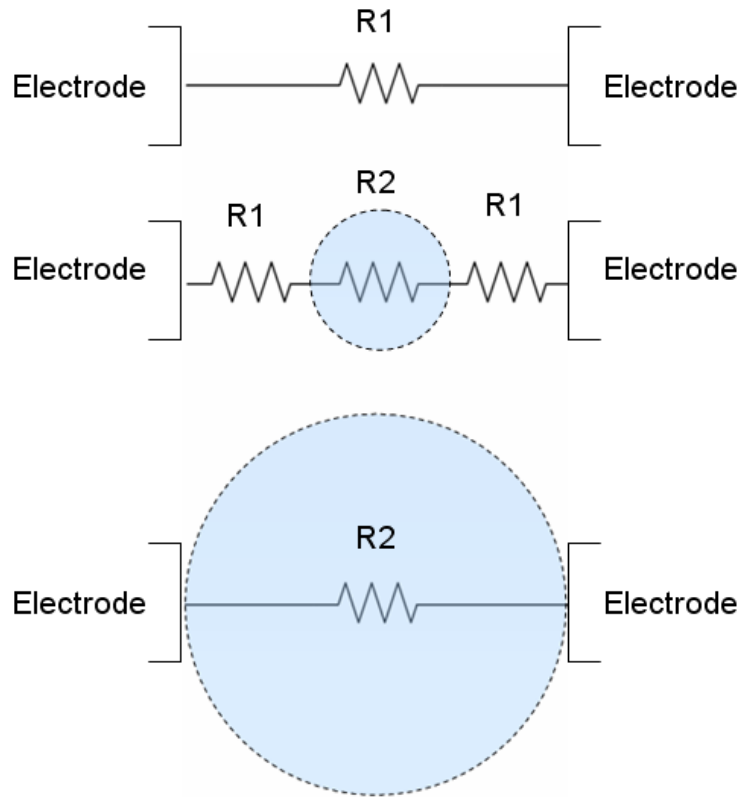


Figure 3-4 GST representation in different states, (top) amorphous state (middle) pseudo-crystalline state (bottom) crystalline state, where R1 is high resistance amorphous GST and R2 is low resistance crystalline GST.

transformed from amorphous to crystalline, the ratio of crystalline to amorphous material between the electrodes allows for multiple resistance values relating to multiple states for the device. Crystallization occurs either by nucleation of critically sized particles or by growth of crystallites at the amorphous region boundary [22]. Although this is a more accurate model, the model that will be used here will assume a more general understanding of pseudo-crystalline states, looking at the material properties externally through its resistance change and not differentiate between nucleation or growth of the crystallization.

Modeling the GST to determine the irradiant energy required to make state changes from amorphous to crystalline is done given a specific flux of energy on the surface of the chalcogenide. When this energy is absorbed, assuming 100% absorption, the temperature will increase due to photon absorption in the material, creating phonons, or quantized lattice vibrations. Once the surface temperature can be determined, based on the intensity of irradiating light, the desired irradiant energy to heat the GST above the glass transition temperature but below the melting point to change the state from amorphous to crystalline can be determined. The temperature on the surface of the GST can be determined by:

$$\hat{n} \cdot (k\nabla T) = q_0 + h(T_{\text{inf}} - T) \quad (3-1)$$

where  $\hat{n}$  denotes the outward pointing normal vector,  $q_0$  is the inward heat flux in W/m<sup>2</sup>,  $h$  is the heat transfer coefficient,  $T_{\text{inf}}$  is the external temperature,  $T$  is the

temperature at the given point in the material, and  $k$  is thermal conductivity.

Assuming that the absorption is 100% and only at the surface, the irradiant energy on the surface is equal to the inward heat flux,  $q_0$ , and the heat transfer coefficient can be approximated as the thermal conductivity of the material. Using the heat transfer equation for conduction from Fourier's Law [35], and assuming no convection, one obtains:

$$\nabla \cdot (-k\nabla T) = q_{gen} - \rho C \left( \frac{dT}{dt} \right) \quad (3-2)$$

where  $C$  is the specific heat,  $\rho$  is the density of the material and  $q_{gen}$  is the power generated per unit volume. All the material properties are listed in Table 3-1, where thermal conductivity,  $k$ , specific heat,  $C$ , and electrical resistivity,  $P$ , were taken from [22], and the density of the material was calculated by linear interpolation using Vegard's Law from the densities of Ge, Sb, and Te present:

$$\rho[Ge_2Sb_2Te_5] = \frac{2}{9}\rho[Ge] + \frac{2}{9}\rho[Sb] + \frac{5}{9}\rho[Te] \quad (3-3)$$

Using the calculated density and the specific heat value of GST from [22], the heat capacity was then calculated. Using the values in Table 3-1 and Equations (3-1) and (3-2), an accurate model for determining the ratio of energy required to transform the chalcogenide to different states can be developed.

Table 3-1 GST Material Properties

Material	Thermal Conductivity $k$ [W/m-K]	Density $\rho$ [kg/m <sup>3</sup> ]	Specific Heat $C$ [J/m <sup>3</sup> -K]	Heat Capacity $C_p$ [J/kg-K]	Electrical Resistivity $P$ [ $\Omega$ -m]
Crystalline GST	0.5	6138	$1.2 \times 10^6$	195.5	$6 \times 10^{-5}$
Amorphous GST	0.5	6138	$1.2 \times 10^6$	195.5	$1 \times 10^{-9}$

FEMLAB, now known as COMSOL Multiphysics, a finite element analysis simulation program, is used to model and simulate the heat transfer equations and the given properties of GST with different values of irradiance, and provides the amount of irradiance energy required to raise the temperature into the crystallization region. The model design simulated in FEMLAB is depicted in Figure 3-5.

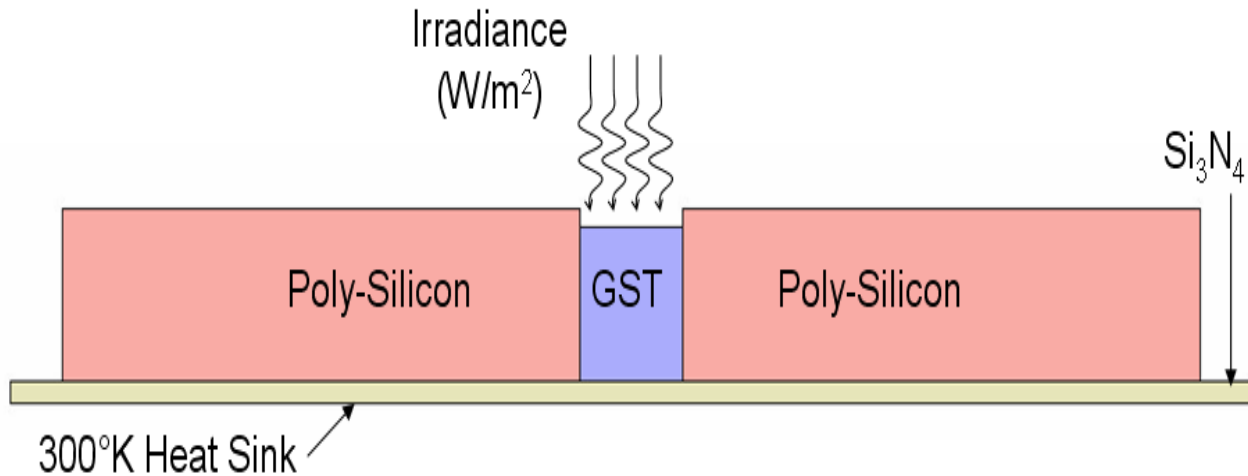


Figure 3-5 FEMLAB's model simulation geometry and design parameters.

The FEMLAB model was simulated with irradiance values of 0.2, 0.65, 1.1, and 1.55 mW/mm<sup>2</sup>. A more ideal simulation would be to model a transient analysis for periods of around 3 sec, 30 sec and maybe 5 min. These times could be accomplished in the actual experiment. Figure 3-6 presents the results from these simulations. Note the temperature values are in Kelvin and the required temperature range to transform the amorphous GST would be between 700K and 800K, which is indicated in Figure 3-7 by colors of white and light yellow. Pulsing the GST with irradiance above 1.6 mW/mm<sup>2</sup> would be ideal for a fast melting and subsequent quenching to “reset” the GST back to an amorphous state as indicated in Figure 3-2. The first simulation was done at steady state with a constant flux of energy, which indicates that at least 1.1 mW/mm<sup>2</sup> for long periods of time is required to transform the material to crystalline. Therefore, lower energies, such as 0.2 and 0.65 mW/mm<sup>2</sup> (which were simulated), would not work. Because longer pulse times not only heat up the GST, but also the surrounding device structure, preventing an adequate source for a heatsink when resetting the GST back to an amorphous state, only very short times will be acceptable (less than a minute) for a reset to amorphous state. Observing the result from longer times, such as a couple of minutes, may provide useful data for transitioning the GST to a crystalline form.



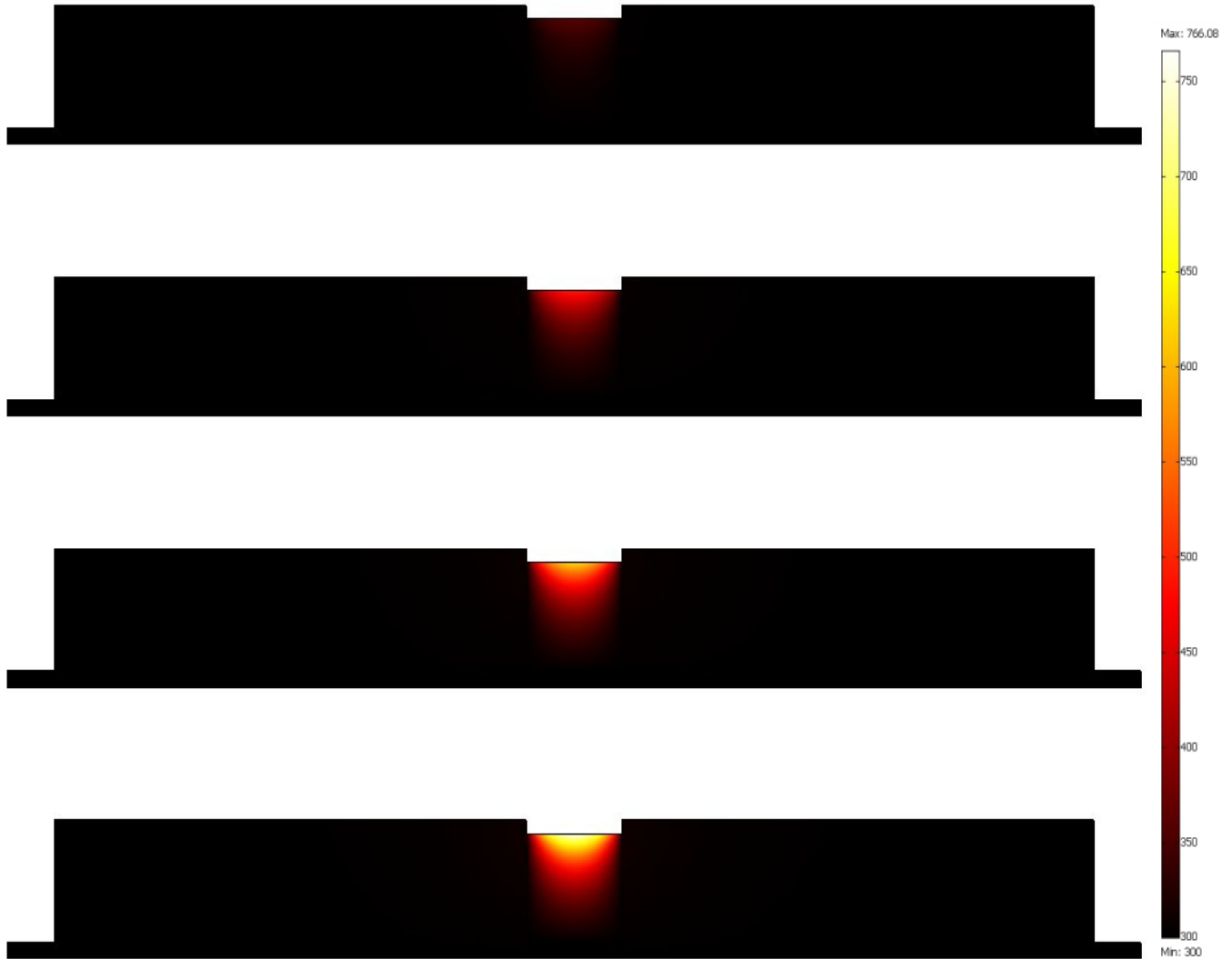


Figure 3-7 FEMLAB simulation of GST (center) being irradiated by (top to bottom) 0.2, 0.65, 1.1, and 1.55 mW/mm<sup>2</sup> of energy at steady state analysis, degrees in Kelvin.

To accurately determine the energy required for the time of a given pulse of light that is irradiated onto the GST, the simulation was modeled to reach the crystallization temperature range in the GST between 700 K and 800 K with pulse times of 3 sec, 30 sec, and 5 min. The respective input irradiance, assuming 100% absorption to achieve this temperature range was 500, 70, and 18 mW/mm<sup>2</sup> as is depicted in Figure 3-8.

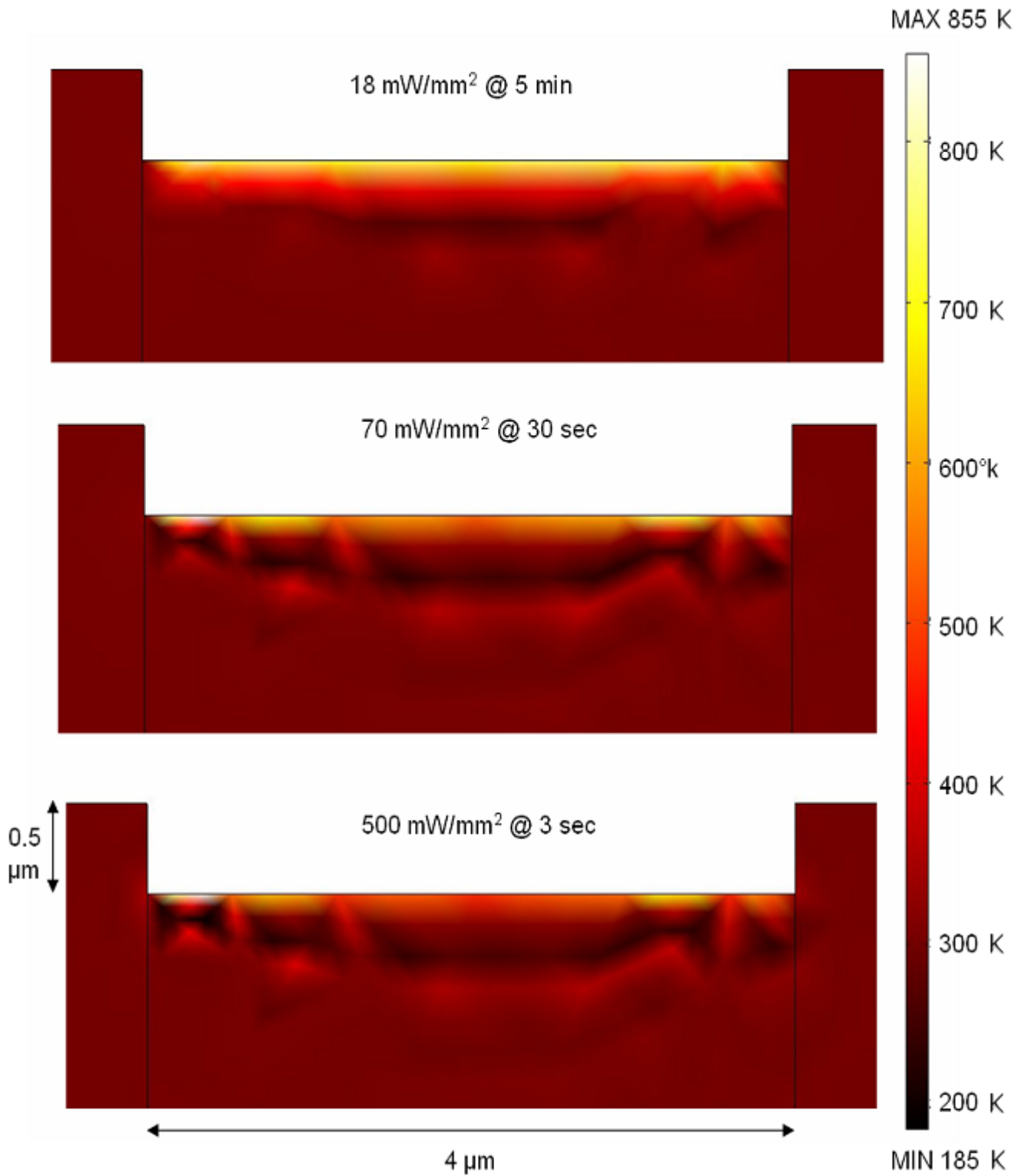


Figure 3-8 Transient thermal modeling of GST with different irradiance values and lengths of exposure to raise surface area to the crystallization temperature zone.

### 3.3.2 Scalability

Understanding the scalability of the GST is important to determine how the irradiance required to change states varies for different surface areas of GST. It is assumed the irradiance will be constant with respect to area as a function of light flux energy, wavelength, and the length of irradiance and will result in a change of temperature on the surface of GST. This temperature change is a function of absorptance (dependant on the wavelength), total time, and surface area. The equation for irradiance with respect to change in temperature is given by:

$$E_e(I_e, \lambda, t) \Rightarrow \Delta T(\alpha(\lambda), I_e, t, A) \quad (3-4)$$

where  $E_e$  is a given irradiance with photon energy flux,  $I_e$ , wavelength of light  $\lambda$ , and duration of light, pulsed onto the GST,  $t$ . This irradiant energy on the GST corresponds to a change in temperature,  $\Delta T$ , on the surface of the GST, where the temperature change is a function of the absorptance,  $\alpha$ , for a given wavelength, the photon energy flux, the time exposed to the light and the area,  $A$ , exposed by the light. The assumption is that, independent of the surface area of the GST test structure which is exposed to light, it will take the same amount of irradiance to change the states of the GST. Figure 3-9 shows a general representation of how different surface areas with equivalent irradiance changes the states of the GST, independent of the surface area of the GST test structure.

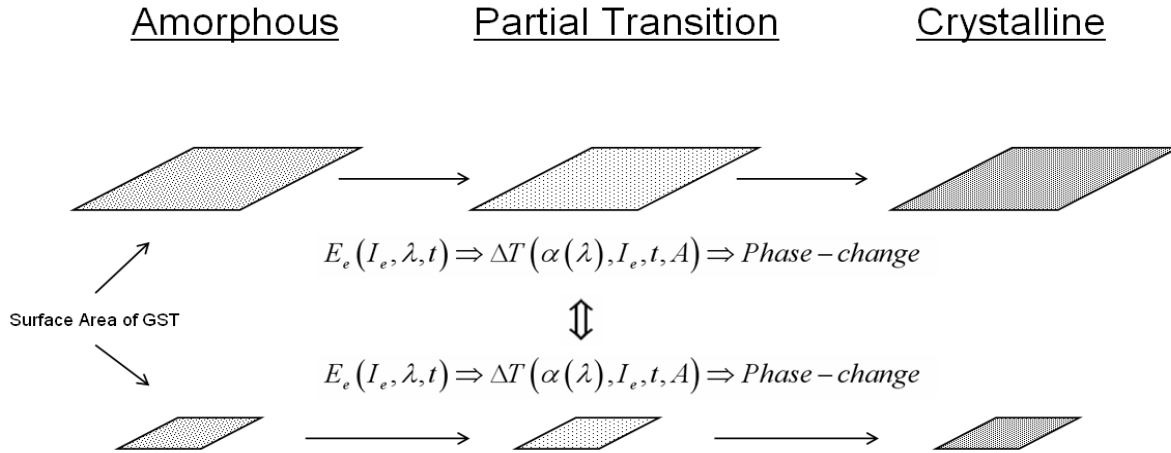


Figure 3-9 Irradiance to phase-change model, assumes constant irradiance required to change states independent of surface area (linear scaling of required total power).

In order to assess the validity of the assumption that GST should scale linearly with respect to the total energy required to change the states of the material, GST will be tested experimentally. The test data will provide a better understanding of how GST scales and help to determine an optimal device geometry and size. Since irradiance is in units of watts per area, scaling the area should result in the same change of temperature given a constant irradiance. This assumption is indicated by:

$$E_e \Rightarrow \Delta T(A_1) = \Delta T(A_2) \quad (3-5)$$

where  $A_1$  and  $A_2$  are different size areas.

### 3.4 Summary

After better understanding that the mechanism in creating the phase-change in GST is a thermal mechanism, which is independent of the energy source (optical or

electrical), modeling of this thermal mechanism for phase-change in GST was simulated using FEMLAB finite element analysis software. The modeling indicated the amount of thermal energy flux into the GST needed to raise the temperature into the crystallization region for phase shift from amorphous to crystalline states. This model was fairly primitive with respect to optical manipulation of the material. Optical energy into the GST would not only be absorbed at the surface, but through the GST by using its coefficient of absorption,  $\alpha$ , where the absorption into the GST relative to the distance from the surface,  $x$ , of the GST would be related by  $e^{-\alpha x}$ .

Although the model presented in this research is simpler than, and not as accurate as, using a model that incorporates  $e^{-\alpha x}$  for absorption into the GST, this model does provide an adequate understanding of the optical energy required to shift the states in GST. It also provides an understanding of the relationship between the length of the pulse of optical energy and the required optical power density to actuate the phase-change in the GST. The scaling factor versus energy required is considered to be linear for the range of device geometries considered in this research. For devices much smaller than what is designed in this experiment, thermal density would not dissipate as quickly due to surface area effects, and is not considered in the scaling assumption made in this chapter. Ultimately, for research into GST-DNA hybrid devices, whether or not the temperature range to activate the phase-change in GST is suitable for the salmon DNA needs to be addressed.

## *4. Design and Fabrication*

### *4.1 Introduction*

In any research that involves experimental testing, a test device needs to be manufactured; optimizations for test parameters, time and availability of resources, and benefit and cost analysis are all factors that are important and need to be carefully considered when designing a test device. This chapter covers these areas, including a brief outline of the design objective and some background into the interest of this research. The resources, cost, and benefits of possible fabrication methods are outlined. The solution, using AFIT's MEMS lab L-Edit design layout software and the PolyMUMPs fabrication process, is discussed in detail. Post processing procedures of the fabricated devices before the GST is grown is explained. Finally, the University of Utah's GST growth process is discussed, and the GST that is received back is imaged under an SEM and analyzed.

### *4.2 Design Objectives*

The design of a test circuit and selection of an appropriate fabrication method for this test circuit were driven by a few factors. One of the factors that needed to be considered when testing the GST material was scalability for ideal size integration in future chalcogenide devices. AFRL wanted a test circuit at sizes comparable to integrated circuit devices, i.e. in the micron and submicron levels. A design process was

needed that could meet this requirement, while also a compatible surface and test structure was needed for the deposition of the GST from a third party. This design needed to allow for direct analysis from the surface of the test structure to an external circuit, i.e. a design that would contain the test electrodes on the surface of the chip.

First, a design was needed to feasibly test the material with optical energy through an external circuit. The most common method is to drive the circuit with an external current via an applied voltage across the test material and detect the additional current (photocurrent) generated by the optical excitation incident on the GST. The test device needed a surface area with GST exposable to the light and to be connected to the external circuit with as little noise (external light) as possible. The design of the test circuit must have electrodes that connect to the GST in a way to test the material and also provide other benefits such as redundancy for any damage that could possibly happen to the test chips, allow for external noise reduction, test other desired factors such as scalability, and be simple in design for modeling, calculations, and feasibility of acquisition, i.e. low cost and readily available manufacturing resources.

### ***4.3 Resources, Cost, and Availability***

There are various avenues that could be taken for fabricating the test circuits. Fabrication processes, either at AFIT or AFRL, or hiring a commercial company were all available options. Not only did fabrication costs need to be considered, the timeline and quality of production were important as well. At AFIT, the clean room would suffice for fabrication purposes, but the materials that could be deposited with the current

equipment are limited, and there was no easy way to fabricate and acquire masks for the designs quickly enough to complete the thesis given the AFIT master's program timeline.

Before looking elsewhere, the availability of a fabrication process funded by AFIT/ENG for the Introduction to Microelectromechanical Systems (MEMS) course was determined to be a fast, reliable, and economical route to produce the design and fabricate the desired test circuits. AFIT has been using this commercial fabrication process, it is well established, and multiple copies of the design are fabricated which is ideal for protection against mishaps which could happen during the experiment. L-Edit by EAD Tanner is a software package used to layout MEMS structures at AFIT. In addition, bimonthly fabrication runs are available which can be useful to optimize the test circuit. This foundry process saved considerable time and possible unforeseen costs that could occur by fabricating the test circuit at AFRL, which would require obtaining custom designed masks and the appropriate materials to fabricate a working test structure.

#### ***4.4 L-Edit Design Layout***

L-Edit was used to create the test circuit designs for fabrication. L-Edit allows for a fast and simple way to design two-dimensional test circuits. Using L-Edit simplified the design process by allowing the user to setup each individual layer, to view the layer(s) together or individually, and to analyze the layout for possible design errors. A key benefit of L-Edit is that one can design a simple structure in a cell, then, this cell can be copied and arrayed within the master cell to accelerate the circuit layout. If



changes to the master cell are necessary, the original cell can be modified and thus all instanced cells will be changed, updated simultaneously, therefore allowing quick and efficient design modifications. These specific aspects of L-Edit were used in the design of the array of test electrodes for this experiment. See Figure 4-1, a top view of the complete test circuit design created in L-Edit. The gold squares are bond-pads which allow for the chip to be connected to an external circuit, the thinner gold rectangles are

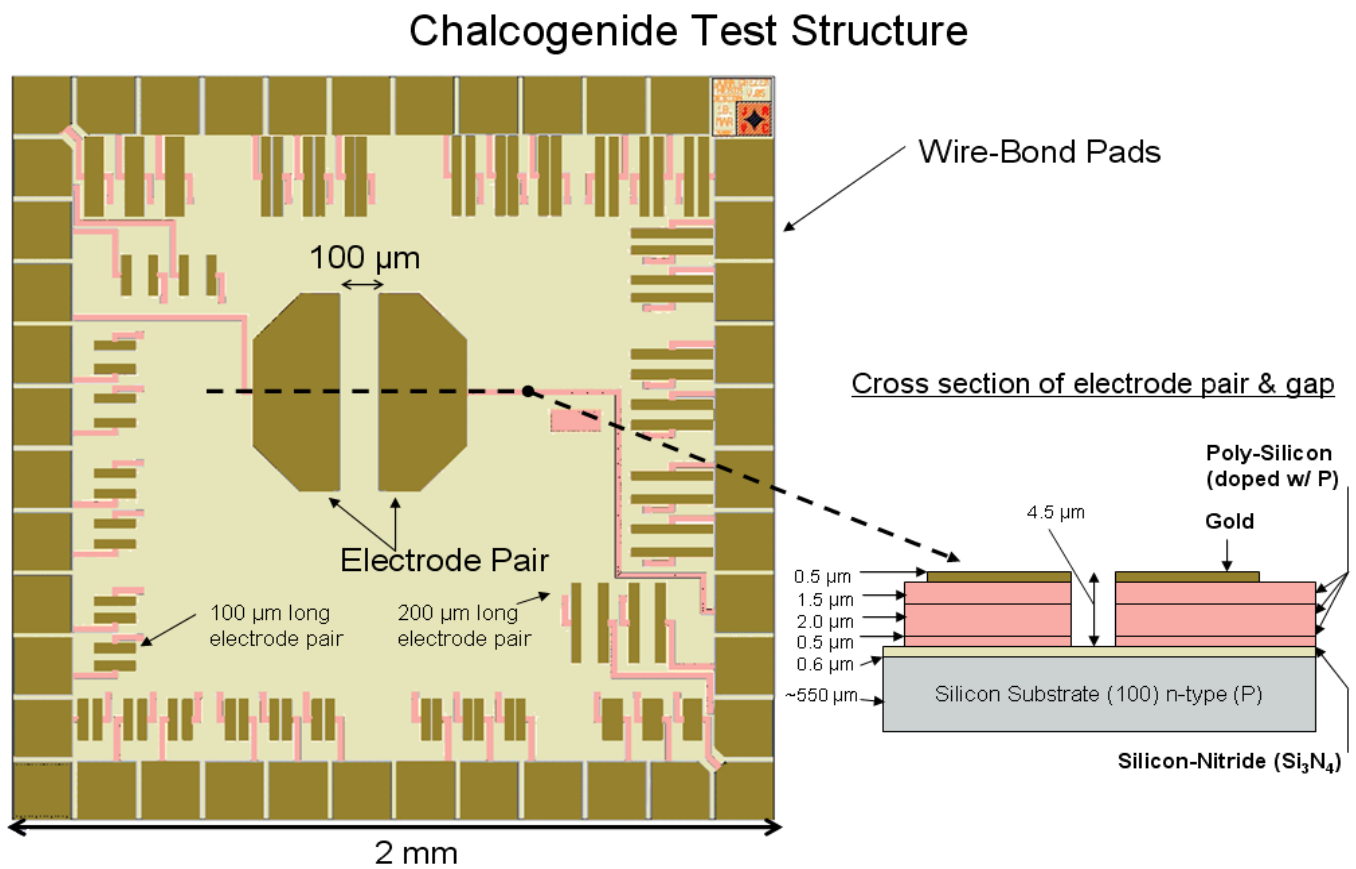


Figure 4-1 Top view of chalcogenide test chip designed in L-Edit.






the arrays of electrode pairs to test the GST material in this experiment, and the pink lines are the polysilicon conducting surface wires.

#### 4.5 *Fabrication Process*

The three layer PolyMUMPs process begins with a 100-mm n-type (100) silicon wafer of 1-2  $\Omega$ -cm resistivity. Using  $\text{POCl}_3$  as a dopant source the surface of the wafers are heavily doped with phosphorus using a standard diffusion furnace to help reduce and prevent charge feedthrough to the substrate from electrostatic devices on the surface (MEMS electrostatic devices that are being fabricated alongside the test devices). A 600-nm layer of silicon nitride ( $\text{Si}_3\text{N}_4$ ) is deposited by low-stress LPCVD (Low Pressure Chemical Vapor Deposition) on the silicon surface to act as an insulating layer between the substrate and the conducting polysilicon layers. Next the first of three polysilicon layers is deposited at 500-nm thick by LPCVD and patterned using standard semiconductor photolithography techniques with an accompanying reactive ion etch (RIE) process. The polysilicon layer is followed by a 2- $\mu\text{m}$  sacrificial oxide, polysilicon-glass (PSG), deposited by LPCVD and annealed at 1050°C for one hour; the PSG is patterned by RIE as well [36]. Figure 4-2 illustrates the possible combinations and patterning of the layers available in the PolyMUMPs fabrication process.

**MEMSCAP -- The Polysilicon Multi-User  
MEMS Processes, or polyMUMPs®**

- Started in 1992
- [www.memscap.com/memrus/](http://www.memscap.com/memrus/)
- 15 copies of a 1 cm × 1 cm die, \$3,200.00

-  Metal (gold)
-  Polycrystalline Silicon (doped with P)
-  Oxide (PSG: SiO<sub>2</sub> doped with P)
-  Nitride (Si<sub>3</sub>N<sub>4</sub>)
-  Crystalline Silicon

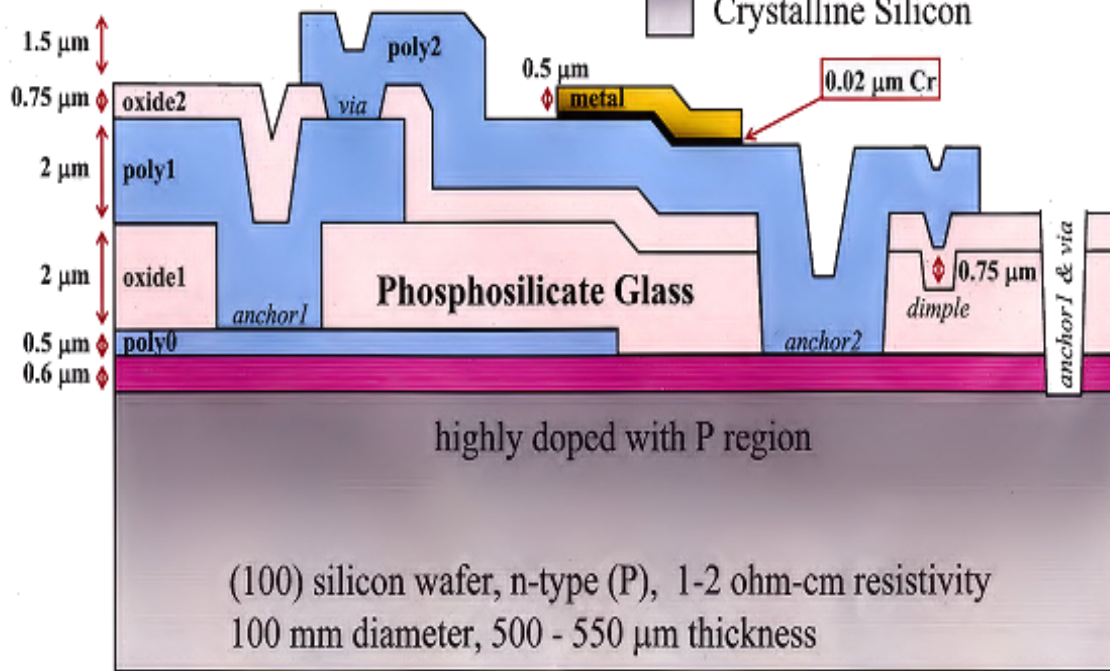


Figure 4-2 Cross section view of the three-layer PolyMUMPs process outlining the possible combinations of layer configurations [37].

After the first PSG layer, a second 2-μm polysilicon layer is deposited using the same process as the first polysilicon layer. A second 750-nm oxide layer is deposited next, using the same process as the first, followed by the final 1.5-μm layer of polysilicon. This oxide layer can be selectively patterned in two ways by creating either a via between the second and third polysilicon layers, or, where there is no second polysilicon

layer, the etch depth will reach the first polysilicon layer or  $\text{Si}_3\text{N}_4$  in the absence of the initial polysilicon layer. Following this etch, the final 1.5- $\mu\text{m}$  layer of polysilicon is deposited and etched with RIE. Lastly, the final layer in this fabrication process is a 500-nm gold layer with a 20-nm chromium layer acting as an adhesive connecting the gold to the polysilicon. The gold layer is patterned using a standard lift-off method [36].

#### ***4.5.1 MEMSCAP PolyMUMPs Fabrication Process***

The MEMSCAP company provides commercial polysilicon MEMS fabrication services for industry, university, and government research as a cost effective, proof of concept fabrication process. Their process, known as Multi-User MEMS Process (MUMPs), offers three different design and fabrication capabilities which are PolyMUMPs (a three layer polysilicon surface micromachined process), MetalMUMPs (a five layer electroplated nickel process), and SOIMUMPS (a four layer silicon on insulator micromachined process). Through the MEMS program at AFIT the PolyMUMPs process is used as an integral part of the course, by allowing students to not only learn the concepts of MEMS, but also to create their own designs.

Although this fabrication process is designed for MEMS device fabrication; accurate two-dimensional circuit wiring layouts can also be fabricated on a small-scale surface (2- $\mu\text{m}$  minimum feature size) chip to test the GST in this experiment. Another benefit to this fabrication process is that multiple layers of polysilicon are available to create different structures which enable the design of the trench between the electrodes. Figure 4-3 shows a pair of electrodes (6- $\mu\text{m}$  gap) fabricated in the PolyMUMPs process.

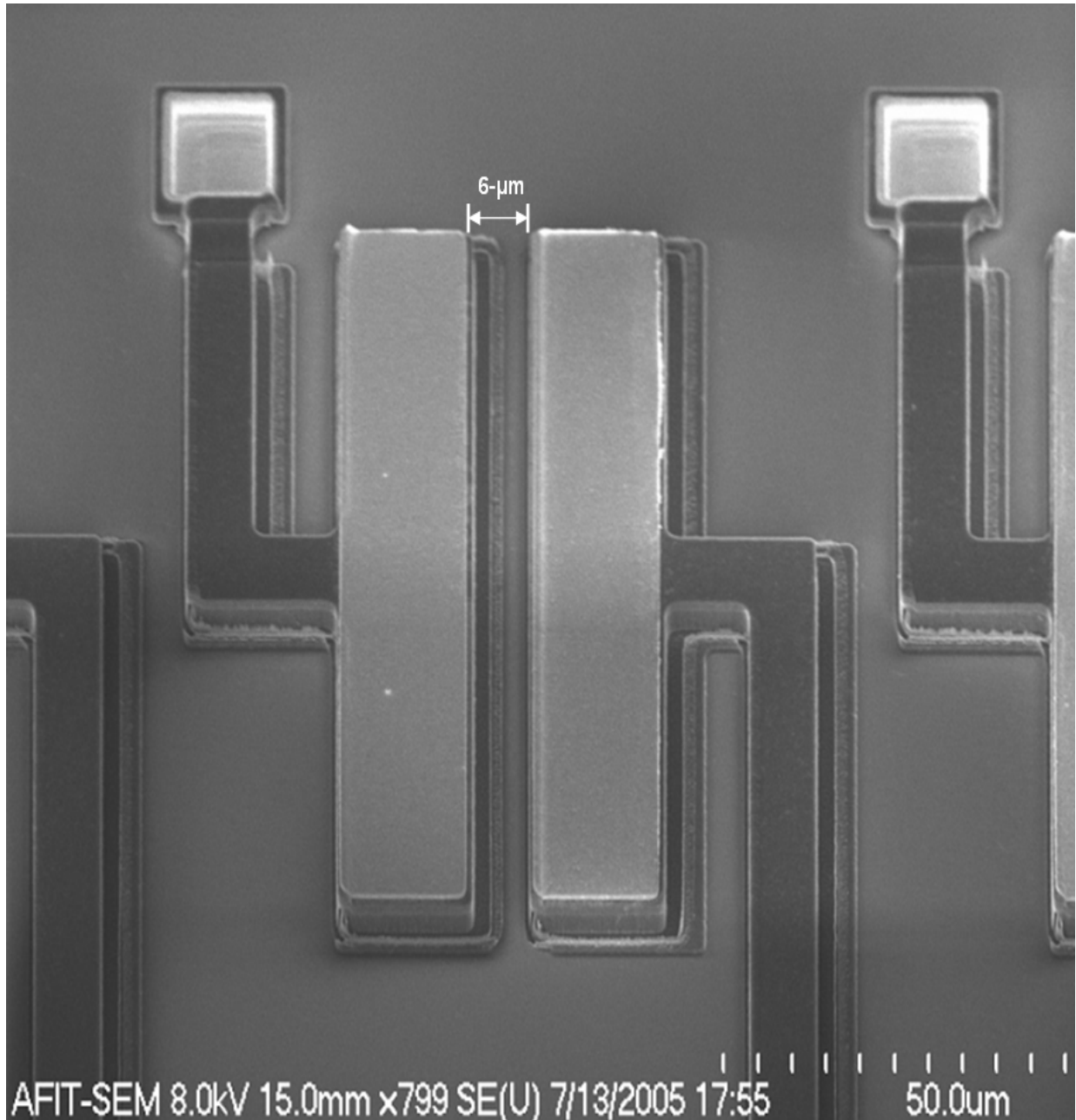


Figure 4-3 SEM top view of 6- $\mu\text{m}$  electrode pair with a 4.5- $\mu\text{m}$  trench.

The electrode height consists of all three polysilicon layers and one gold layer available in the PolyMUMPs process. This maximized the electrode height, which resulted in a trench depth between the electrodes of 4.5- $\mu\text{m}$ . Since the chalcogenide is

deposited everywhere on the surface of the test chip, the relatively deeper trench depth to feature size was ideal for better electrical isolation and less fringing effects. Using a design on the surface of the test chip is beneficial to this experiment, when compared to other efforts [21, 34, 38] which required the use of a heater element and electrodes beneath the chalcogenide to set, reset, and read the GST. This experimental design is optimized for light detection on the surface of the GST material.

#### ***4.5.2 Safety Procedure and Post Processing***

When the 1-cm by 1-cm chips are returned from MEMSCAP, there is an array of 25 different chips processed together on a single die. The chips are sent out to Micro Dicing Corp. to be sub-diced down to their 2-mm by 2-mm size. After the fabrication and subdicing processes are completed, some post processing needs to be completed at AFIT prior to the chips being shipped for chalcogenide deposition. The chips are received from the MUMPS foundry with all sacrificial oxide layers intact and a top photoresist layer for general protection of the MEMS parts. In order for the chips to function properly, these protective layers need to be removed by chemical etching. Prior to release, all equipment (tweezers, dish, etc.) needs to be cleaned using the following cleaning procedure: blow dry with  $N_2$  gas, rinse with acetone, then methanol, and finally with de-ionized water (DIW). Lastly, dry with  $N_2$  gas [39].

To release the oxide on the PolyMUMPs chips, they first need to be cleaned thoroughly. The chips were placed in a petri dish with acetone for 10 minutes to remove the bulk of photoresist and silicon dust from the subdicing process. This is followed by

placing the chips in fresh acetone for another 5 minutes to remove residual photoresist. The chips are then placed in methanol for 5 minutes to remove residue from the acetone cleaning steps. Finally the chips were placed in DIW until the HF setup was ready [39].

The sacrificial oxide release of the chips was done using 48% HF for 3 and a half minutes. The chips are then immediately placed in DIW for 5 minutes to stop the HF reaction. Normally the chips are dried using a supercritical point CO<sub>2</sub> drier to prevent stiction. However, these steps were omitted in this experiment due to no moving parts on the designed chips. Having no concern regarding stiction effects, the chips were dried on a hot plate at 90°C for 10 minutes. The chips were then placed in a gel-pack container to hold the chips securely. Once the chips were ready for chalcogenide deposition they were shipped to the University of Utah for the deposition process.

#### ***4.6 Deposition of Chalcogenide (University of Utah)***

The University of Utah processed and deposited Ge<sub>2</sub>Sb<sub>2</sub>Te<sub>5</sub> onto the test circuits designed for this experiment. University of Utah's growth process was examined using dispersive x-ray spectroscopy and secondary ion mass spectrometry, where their GST was found to be within  $\pm 2$  atomic % of the original sputtering targets. The electrical and optical characteristics of the GST layer were also analyzed using electron spin resonance (ESR) and photothermal deflection spectroscopy (PDS). The GST had an ESR signal when not illuminated implying a large defect density around  $10^{19}$  cm<sup>-3</sup> within the bandgap, indicating higher resistance in amorphous state, and the PDS tests showed that

the absorption edge in the GST was much broader than in standard ( $\text{GeSe}_2$ ,  $\text{As}_2\text{Se}_3$ ) chalcogenide glasses [40] indicating more efficient photo absorption.

Using RF sputtering, the GST was grown to 4- $\mu\text{m}$  at 6 $\text{\AA}/\text{s}$ , creating a low oxygen ( $3 \times 10^{19} \text{ cm}^{-3}$ ) impurity concentration, and 3 $\text{\AA}/\text{s}$  creating a medium oxygen ( $8 \times 10^{19} \text{ cm}^{-3}$ ) impurity concentration [40]. The GST was grown to 4- $\mu\text{m}$ , given the design of the electrode heights of 4.5- $\mu\text{m}$  to fill but not over fill the trenches between the electrodes.

Later, the decision to grow the GST at 6 $\text{\AA}/\text{s}$  for 500-nm was made for two reasons. First, the faster growth rate yielded a lower oxygen impurity concentration and as depicted in Figure 4-4 for GST, the faster growth rate (lower oxygen impurity concentration) yields a higher absorbance. A higher absorbance would require less irradiance energy to phase-shift the material. This is ideal for efficient operation of the devices. Second, the choice of depositing 500-nm of chalcogenide rather than 4- $\mu\text{m}$  follows other current research on GST for use as a phase-change memory device. Others [34, 38] have shown that working with GST layers (180-nm to 220-nm) are ideal rather than working with larger layers of GST due to faster switching speeds and less energy required for a phase-change because the energy required is a function of the total volume of GST that is changed. Growing 500-nm was determined more functional as opposed to [34, 38] due to the unique design used in this experiment.



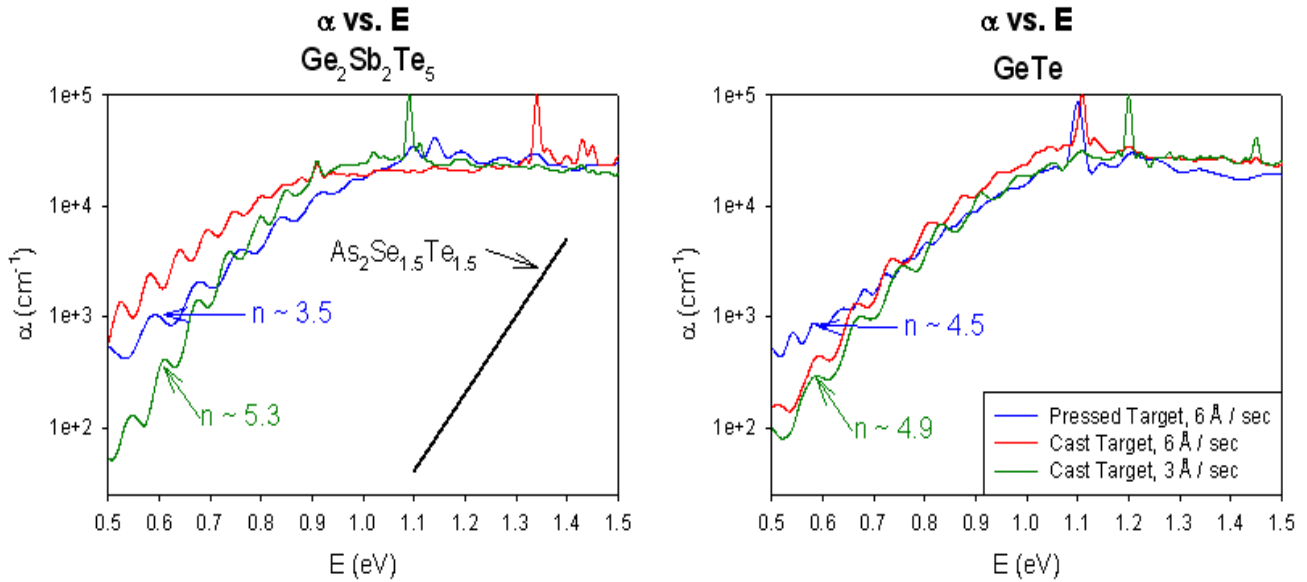


Figure 4-4 Absorption vs. photon energy in electron-volts (left) for  $G_2S_2T_5$  and GeTe (right) at different growth rates reflects the effects of higher oxygen impurities at lower growth rates [41].

After receiving the samples back from the University of Utah, before any experimental tests were performed, images of the devices were taken using both SEM and optical instruments. One of the concerns regarding the process of GST deposition was whether or not the surface contours of the devices would still be identifiable or whether the surface would all look the same (making device testing vary). Figure 4-5 shows an SEM image of one test chip that indicates that the device structure is still identifiable which is desirable for locating and testing individual devices on the chip. A closer look at the edges of the devices indicates that the deposition was conformal growth, as indicated in Figure 4-6 where 4- $\mu\text{m}$  of chalcogenide was deposited.

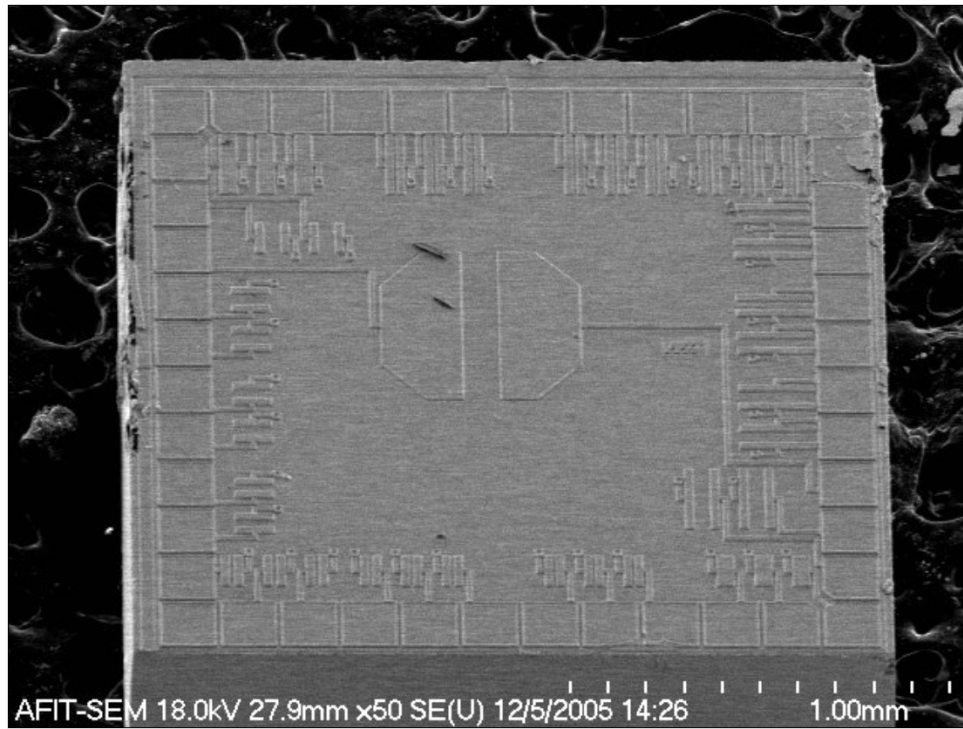


Figure 4-5 SEM image of test chip array with GST deposition at 4- $\mu\text{m}$ , low oxygen impurity concentration, coating entire chip surface.

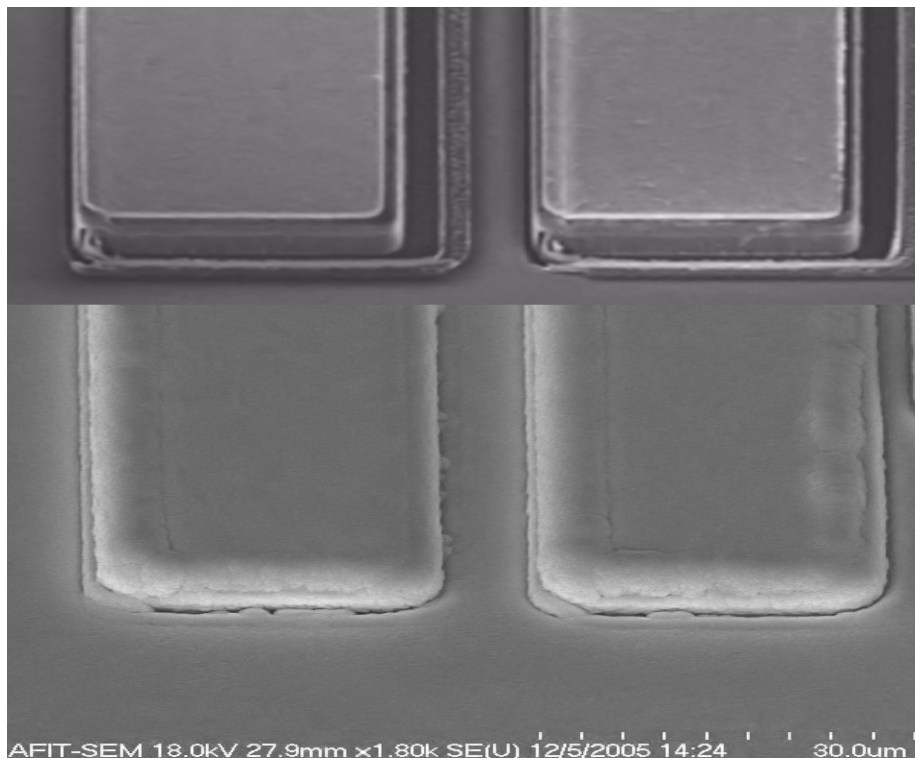


Figure 4-6 Electrode Pair (top) before GST deposition, (bottom) with 4- $\mu\text{m}$  of GST.

Looking closer at the chalcogenide material that the University of Utah deposited, the amorphous structure is apparent as shown in Figure 4-7 where random disordered pyramids about the size of 100-nm make up the structure on the surface of the GST.

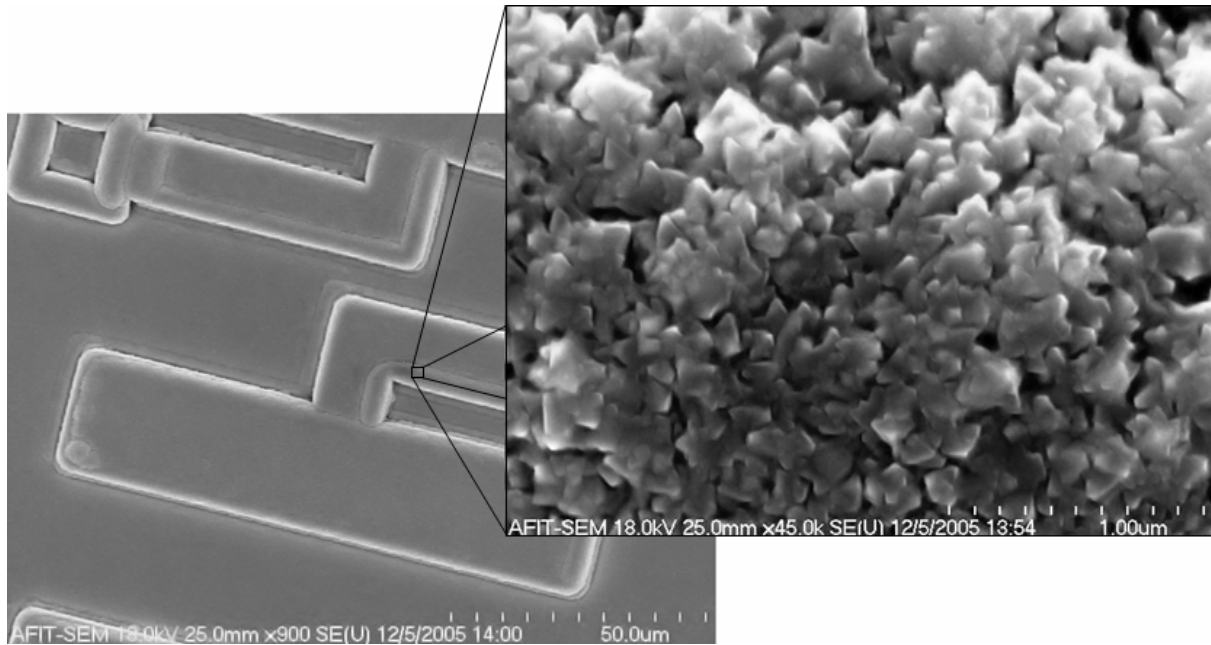


Figure 4-7 Chalcogenide material in amorphous state as grown through sputtering by the University of Utah; images from first batch of samples received in December.

It was important for the material to be grown in amorphous state because, as indicated by Figure 3-1 and Figure 3-2, varying states occur from amorphous to crystalline due to a longer set time and are more identifiable (further separated in resistance levels), as opposed to the change from crystalline to amorphous where most of the different states occur relatively close in resistance values.

#### 4.7 *Summary*

After considering the possible avenues for the fabricating of a test structure to analyze GST in this experiment, the PolyMUMP's commercial fabrication process was chosen for its reliability, ease of use, cost, quick turnaround, and well established connection with AFIT. The AFIT MEMS program already had funding for the use of this commercial process, so using this process was done at no additional cost. The University of Utah was chosen to grow the GST for this experiment; they had already been growing GST for AFRL/VSSE in Kirtland and because of this established venture the University of Utah agreed to grow GST on the test devices in this experiment at no cost. Ultimately, these two avenues were chosen because of their ready availability, quick attainability, and lack of additional costs. After the test samples were designed and fabricated, the preparatory release processes were performed before GST deposition, and then the test samples were sent to the University of Utah and had GST grown on them. The University of Utah provided several options of growth parameters, which were: oxygen impurity level ( $3 \times 10^{19}$ ,  $8 \times 10^{19}$ , and  $8 \times 10^{20} \text{ cm}^{-3}$ ), growth depth, and grown in either crystalline or amorphous form. For experiment procedures, test device layout, and optimal absorption ability, most of the GST was grown in amorphous form, with  $3 \times 10^{19} \text{ cm}^{-3}$  oxygen impurity level (the lowest possible from their growth process), and a film thickness of 4- $\mu\text{m}$ . Finally, before any testing was done, the GST was examined using an SEM to take images of the GST material structure.

## *5. Experiment and Setup*

### *5.1 Introduction*

The importance of experimental research is not only collecting the data and analyzing it. It is also important to identify and outline a clear methodology of the data recording procedures. Documenting the procedures that are performed in an experiment can help to explain inconsistencies or unexpected data, and they allow other research to more accurately reproduce the same experiment or identify possible errors in the experimental procedures. This chapter covers the steps taken in measuring the results in chapter six. The test setup and equipment parameters are given and the methodology for the different measurements is explained (responsivity vs. wavelength, resistance vs. intensity, and scalability). Table 5-1 outlines the general test matrix of the data that is desired.

Table 5-1 Test Matrix

<b>GST</b>	<b>Growth Depth</b>	<b>Oxygen Content</b>	<b>Responsivity vs. Wavelength</b>	<b>Resistance vs. Intensity</b>	<b>Scalability</b>
<b>4-<math>\mu\text{m}</math></b>	<b>Medium <math>8 \times 10^{-19}</math></b>	$\checkmark$	$\checkmark$	$\checkmark$	$\checkmark$
<b>4-<math>\mu\text{m}</math></b>	<b>Low <math>3 \times 10^{-19}</math></b>	$\checkmark$	$\checkmark$	$\checkmark$	$\checkmark$
<b>0.5-<math>\mu\text{m}</math></b>	<b>Low <math>3 \times 10^{-19}</math></b>	$\checkmark$	$\checkmark$	$\checkmark$	$\checkmark$

## *5.2 Lab Equipment and Test Setup*

In order to measure the resistance change of GST as a function of irradiance, accurate equipment is needed to not only capture the change in resistance of the material, but also to measure the intensity of light incident on the material. Two of the devices used in measuring the signal from the material were a Stanford Research Labs (SR) Lock-in Amplifier (SR530) and a SR Low Noise Current Preamplifier (SR570), where the noise level, using the equipment manuals specification sheet, was calculated to be at  $5 \times 10^{-11}$  amps rms. This level of accuracy was determined to be more than sufficient without using a Wheatstone bridge. Originally it was planned that there would be a Wheatstone bridge circuit setup to amplify the resistance change in the material in order to mitigate noise in the circuit and to cancel out ambient light noise by using two chips in the Wheatstone bridge where one was illuminated and the other was covered. Since the activating switch in the material is thermal, the major noise factor was determined to be from ambient light which was adequately removed using a cloth shroud to cover the probe station from most of the ambient light. Because of low noise level in the measurement instrumentation and adequate ambient light shielding, no Wheatstone bridge circuit was implemented.

The light source that was setup for this experiment was a tungsten 1500 W halogen bulb. Using a standard magnifying lens the light was focused through an optical chopper and into an Arc Spectra Pro-150 monochromator. The chopper was regulated by an HP3325A synthesizer/function generator where both the chopper and the

monochromator were controlled by a PC using a USB to IEEE488 bus converter with a visual basic (VB) macro programmed into an excel spreadsheet. The light was channeled through a fiber optic cable from the monochromator into the microscope on the probe station. Using an objective of 50x, the light was reduced to a 100- $\mu\text{m}$  spot size, illuminating only one pair of electrodes.

To measure the reaction from the light source, two probes on the probe station were connected to the low noise current preamplifier which applied the bias voltage. The current was swept across the device and amplifying the return signal by  $1 \times 10^4$ , then passing the signal to the lock-in amplifier the signal at the frequency of the AC signal generated from the chopped light source was measured. The applied bias from the preamplifier was also controlled through the VB macro, and the return signal from the lock-in amplifier was sent back to the VB macro to be recorded. Originally, the VB macro program was not completed when testing began so an HP4156A Precision Semiconductor Parameter Analyzer was connected to the probes for initial testing of the devices, applying the bias voltage and measuring the return signal from the devices. During this test phase the monochromator was controlled manually through an older PC (386). The equipment setup is depicted in Figure 5-1 using wavelengths ranging from 300-nm to 1100-nm in steps of 20-nm.

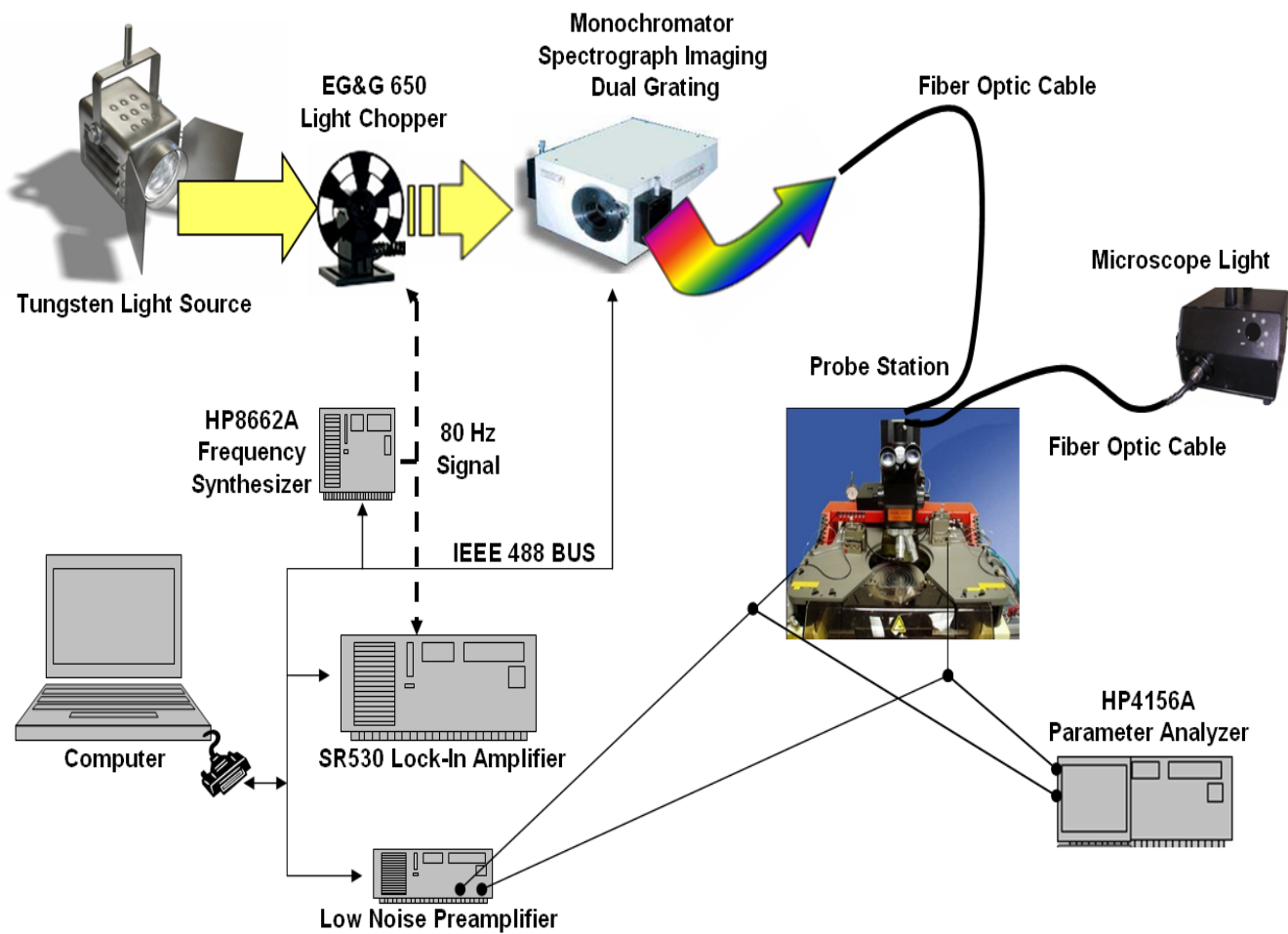


Figure 5-1 Experiment equipment configuration.

### 5.3 Experiment

The basis for the experimental methods in each of the three areas of the experiment (for responsivity vs. wavelength, resistance vs. intensity, and scalability) were very similar; the procedure was done by applying the light source to the surface of the device irradiating the material and recording the change in resistance in the GST through the change in current generated and voltage supplied. Originally, the responsivity versus wavelength measurements were going to be taken first, determining



the optimal wavelength for the other tests at the peak responsivity in the GST. Since the VB macro (control program) was still being developed and there were delays in the monochromator working properly, some preliminary resistance versus intensity measurements were taken first.

### ***5.3.1 Resistance vs. Intensity***

Using the parameter analyzer and the microscope's variable white light source, darkcurrent and photocurrent at variable intensities were measured. The light intensities were measured by removing the test devices from the probe station and placing a DP series photodetector PIN-10DP under the microscope, then measuring the current and voltage output on the photodetector with the preamplifier and lock-in amplifier. The irradiant energy was calculated using:

$$E_e = I \times V / A \quad (5-1)$$

where  $E_e$  is irradiance in  $\text{mW}/\text{mm}^2$  and  $I$  is current in amps,  $V$  is electric potential in volts, and  $A$  is area (spot size of light on the photodetector) in  $\text{mm}^2$ . The same technique was used with the monochromator to determine the irradiance output at individual wavelengths. Measuring the darkcurrent and various intensities of photocurrent using the parameter analyzer was performed using applied voltage ranges from  $-1.0\text{ V}$  to  $1.0\text{ V}$  on some devices and then  $-0.5\text{ V}$  to  $0.5\text{ V}$  on the rest of the devices because there was some concern that using the  $-1.0\text{ V}$  to  $1.0\text{ V}$  range might actually modify the states in the GST electrically [3].

Once initial testing was performed and the control program was operational for using the tungsten light source with the monochromator, resistance versus intensity at particular wavelengths was measured. To measure the photocurrent generated from the light source the function generator was set to 800 Hz which resulted in a chopping frequency of 80 Hz. This frequency was determined to be desirable because an 80 Hz signal will help mitigate noise coming from the ambient 60 Hz light.

### ***5.3.2 Responsivity vs. Wavelength***

There are many different figures of merit that give insight into the performance of photodetectors. Not only can photodetectors be characterized or quantified in this fashion, any optically reactive material can be classified similarly. The general equation for current responsivity is given by [13]:

$$\mathfrak{R}_i(\lambda, f) = \frac{\eta \lambda q}{hc \sqrt{1 + (2\pi f \tau)^2}} G \quad (5-2)$$

where  $\mathfrak{R}_i$  indicates responsivity in terms of current as a function of wavelength  $\lambda$  and electrical chopping frequency  $f$ ,  $\eta$  is the quantum efficiency,  $q$  is electron charge,  $h$  is Plank's constant,  $c$  is the speed of light,  $G$  is the photoconductive gain, and  $\tau$  is the time constant. Using the chopped light and monochromator this model of responsivity will be used. The responsivity data is collected by using the control program to automate the process of measuring the photoconductive gain over the range of wavelengths (between 300-nm and 1100-nm). For simplicity the efficiency is set to 100%

and the responsivity is calculated from the measured data. If it is found that the GST exhibits no photocurrent properties a more reasonable bolometric responsivity model (in W/V) will be used given by [42]:

$$\mathfrak{R}_i = I_b \left( \frac{dR_D}{dP_L} \right) \quad (5-3)$$

where  $I_b$  is the DC bias current through the detector, and  $\frac{dR_D}{dP_L}$  is the change in resistance due to the power absorption in the GST. Since this experiment relies on thermal actuation, not quantum effects, the responsivity of the devices are assumed to be fairly constant.

### **5.3.3 Scalability**

To determine effects of scaling on the GST devices in relation to the required irradiance power required to change the state of the GST, different geometries were tested. The gap between the electrodes where the GST was deposited ranges from 2- $\mu\text{m}$  to 30- $\mu\text{m}$  in increments of 4- $\mu\text{m}$ , and the lengths of the electrodes for each of these gaps are either 100- $\mu\text{m}$  or 200- $\mu\text{m}$ . By measuring the required irradiance that changes the state of the GST at different geometries, a relationship of scalability can be determined. This relationship will provide insight in determining what benefits, in power consumption and speed of operation, are gained from scaling the devices. The electrode pairs were tested individually with varying intensities of light. Using the same setup as described in section 5.2.1, chopped light from the monochromator irradiated the GST, the

preamplifier applied the bias voltage and the measured signal was sent to the lock-in amplifier to record the measured photocurrent. The photocurrent was recorded as a function of light intensity and gap distance, and data was grouped by gap size, then by intensity of light.

#### **5.4 *Electrical Testing***

Following the optical testing of the devices, electrical testing of the phase-change properties in the GST was performed. Other research [3, 21] presented effective testing methods by applying a current sweep across the electrode through the GST. The parameters that were desired were: the voltage threshold  $V_{th}$  required at the point where the GST shifts from amorphous to crystalline, the current level  $I_c$  where the GST is fully set to a crystalline state, and what effects scaling the gap size had on both  $V_{th}$  and  $I_c$ . The electrical testing was done using the parameter analyzer to apply the current sweep and measure the resulting voltage levels.

#### **5.5 *Summary***

Initially, the experimental procedures were planned to be only in the nature of optical testing the GST as explained in this chapter. Because of the modeling in chapter three (completed during the middle of the experimental testing) and the results from the optical testing, another form for testing the thermal phase-change mechanism in the GST was determined to be necessary. So, electrical testing and analysis of the GST was then performed to analyze its phase-change properties.

## ***6. Results and Analysis***

### ***6.1 Introduction***

This chapter presents the steps taken and the results from the optical experiments, as well as the results and analysis from the data collected through electrical testing of the chalcogenide samples. Although the experiment as described in chapter 1 and in section 5.2 posed a problem in collecting the desired optical data (due to available equipment), the overall results from the experiment were successful in testing the electrical properties of the GST samples and provided beneficial information for future research. Initial optical testing of the chalcogenide was performed before accurate modeling of the material was completed. Using the modeling data from FEMLAB and measuring the output power from the available optical power sources, it was later clear there was not enough optical power to change the state of the GST. This finding also agreed with the results collected from the optically tested data. The chalcogenide could still be coupled with the salmon DNA electrically using other optically sensitive devices, and so testing the electrical properties of the material was also a feasible solution. Thus, it was important to test the GST samples from the University of Utah and compare their GST to the literature for reliability in future research and device fabrication.

## 6.2 Photo Analysis

The initial photo testing data of the chalcogenide seemed to indicate that these GST samples did in fact exhibit photocurrent properties as well as the ability to change and hold multiple states within the material through photo actuation as shown in Figure 6-1.

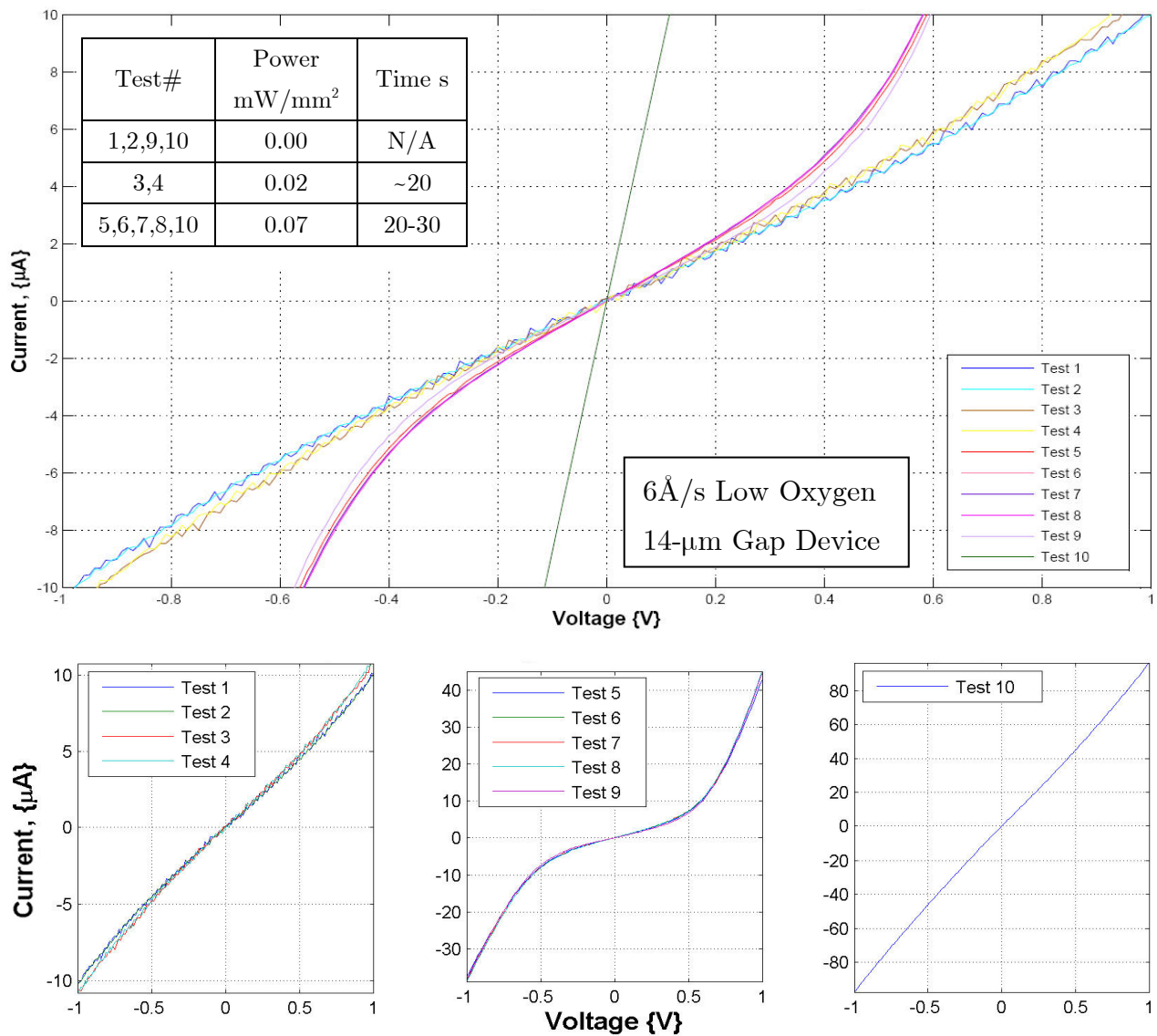


Figure 6-1 Current vs. Voltage plot of initial photo testing data, 6 Å/s Low Oxygen GST with gap of 14-μm, indicating three possible states.

Figure 6-1 represents the data taken by using the microscope light to illuminate the material as described in section 5.2. Initial photo testing of the chalcogenide samples was done via the microscope light source using the parameter analyzer due to delays in completing the control program for the monochromator. This initial data (resistance vs. intensity) of the GST was thought to be ideal for two reasons. First, the data indicated that GST had multiple states, as depicted in the three lower plots in Figure 6-1, where each subplot represents a different state in the GST. As more light were irradiated onto the samples, the material exhibited changes in resistance which were measured using a -1 to 1 voltage sweep and extracting the resistance from the recorded current.

The second reason the data appeared ideal was because the results support a photocurrent phenomena. Tests one and two were done as dark current with no light except the ambient room light on the material. Then test three and four were done with the microscope light set to the lowest setting, measured to be  $0.02 \text{ mW/mm}^2$ , using a 10DP series photodetector to measure the power output assuming the reflectance and absorbance of the detector was equivalent to that of the GST samples. The drop in the resistance between tests one and two and tests three and four was believed to be a photocurrent effect. The next test that was performed as the data was presenting ideal results was setting the light source to 50% of the maximum power the microscope light provided. The voltage sweep was again applied -1 to 1 volt and measured as tests five through eight. Note, with each illuminated test the light source was incident on the GST approximately 20 s for low levels and between 15 to 30 s when at 50% power.

Using the same procedures as before, with the photodetector, the output power of the microscope light at 50% was measured as 0.07 mW/mm<sup>2</sup>.

The next measurements, tests five to eight, presented data that showed a significant change (four times less) in resistance as compared to the previous results (tests one to four). It was thought that the material had changed to a new state between crystalline and completely amorphous. To see if the material had changed to a new fixed state, the light source was turned off and the data was recorded as test nine in Figure 6-1. The results showed a slight increase in resistance, which is represented by the drop in current (test nine, Figure 6-1). This indicated there could possibly be photocurrent in the GST. The microscope light source was turned back on to low power (50% power was not used due to concern of changing the state of the material again) to see if the material would drop in resistance and exhibit an I-V curve similar to tests five to eight. The data measured presented no change, being identical to test nine. Next, it was desired to test the GST to determine if the material could change to a new state again. The total irradiance time was added, the time each of the light pulse was incident on the device for tests three to eight, which came to about three minutes, and was used for the next desired irradiance time. The GST was intended to be irradiated for three minutes to induce a second phase-change, but actually ended up being irradiated a little over five minutes before test ten data was measured while the light source was still at 50% power. It appeared that the GST sample had changed states again by the dramatic decrease in resistance. This was confirmed by removing the light source and testing the



sample again and measuring the same data as in test ten. Other electrodes on the same sample were then tested and all tested appeared to exhibit the same data as in test ten. Since the entire sample was irradiated by the light source it was believed that the light source was the cause of the change between states in the material, and the slight variations in resistance levels such as between tests two and three, indicated a dark current photocurrent relationship in the GST.

A -1 to 1 volt sweep was determined to be a safe voltage range due to current research being done using that voltage range. Although other research used this voltage range to actually change the states of their GST [3, 21], the samples in this experiment were on the order of ten times or larger (the path the current must take between electrodes) of those using a -1 to 1 V range to change the states of the material, and thus it was determined that this voltage range would not change the states in the GST samples. To verify that using this voltage range was not effecting the change in the GST samples, the next chip test was identical to the first, a 4- $\mu\text{m}$  layer of GST deposited over the test structure at 6  $\text{\AA}/\text{s}$  for low oxygen content (the low oxygen content as discussed in section 4.5 increases the absorbance of photoenergy as depicted in Figure 4-4).

Using a -0.5 to 0.5 voltage range, which is below the threshold voltage to change the GST from amorphous to crystalline even with GST layers as small as 90-nm [21], was determined very safe in not effecting the material states. Unfortunately, all the measurements taken from the second chip tests produced results similar to test ten shown in Figure 6-1; subsequent testing of this sample produced the same results. Either

through fabrication or other unknown means, the data from this sample indicated that it was already in a crystalline state.

Although chalcogenide material can be reset back to an amorphous state, there were some concerns about the process of resetting the GST in this experiment due to the eutectic temperature of gold and polysilicon being 636 K (a known phenomenon regarding gold and polysilicon in the PolyMUMPs process). Because the electrodes were gold on polysilicon, it was uncertain what effect this would have on the GST during transition between states. Using a microscope light or a chopped light source through a monochromator was thought to be too small of a power source to raise the surface of the GST to the needed temperatures for crystallization at 750 K. If the first sample was changed to crystalline due to the microscope light, it would be impossible to change these devices back electrically such as many other researchers have done because the unmasked device layout was entirely exposed during the GST deposition, and consequently each chip was entirely covered with the GST. Because the light source irradiated the GST on the entire chip, and if this did cause the GST to become crystalline, the entire sample would be covered with a conductive layer of material. This prevented further testing of the particular sample. Electrically resting the state of the material across the electrodes was not possible because of the conductive layer of GST coating the entire chip resulting in the current flow not being guided through designed layout. The only way conceivable way to recover and reset the GST, if this was the case, would be to some how reset the GST on the entire sample optically.

At this point in the experiment the control program was completed and ready to operate the monochromator. Since the initial testing indicated that the GST exhibited photocurrent properties, which was ideal for using the chopped light source and measuring an AC signal (photocurrent generated) on the lock-in-amplifier as described in sections 5.1 and 5.2, fine spectrum light source testing of the other samples was performed using the monochromator setup. The spectrum of 300-nm to 1100-nm was swept in increments of 20-nm on the other four samples, two samples with 4- $\mu\text{m}$  GST grown at 3  $\text{\AA}/\text{s}$  (medium oxygen concentration) and two samples with 0.5- $\mu\text{m}$  GST grown at 6  $\text{\AA}/\text{s}$  (low oxygen concentration). Both sample types exhibited no AC signal from these wavelengths with a noise level of  $5 \times 10^{-11}$  A-rms, implying the signal was less than the noise level from the instrumentation or there was no signal present and the material was not exhibiting photocurrent properties.

If the GST was actually capable of generating a photocurrent, a possible reason why these samples were not exhibiting this behavior was concluded to be that for the 3  $\text{\AA}/\text{s}$  (medium oxygen concentration) samples, the absorbance would be lower as the oxygen impurity concentration increased as described in section 4.5. Thus these samples might not allow enough photoenergy to be absorbed to generate any significant signal. One conclusion for the other samples that had the same material properties as the first two samples, 6  $\text{\AA}/\text{s}$  (low oxygen concentration), except that the chalcogenide layers were 0.5- $\mu\text{m}$  versus 4.0- $\mu\text{m}$ , was that the thickness of the GST layer affected the absorbance ability. That is, as the unabsorbed photons passed further into the material, more

photons would be absorbed and generate a greater photocurrent. For the 0.5- $\mu\text{m}$  layer GST samples, it was concluded that the thickness was not adequate for optical absorption, thereby being the possible cause for the results measured.

The next step was to use the microscope light which was on the order of ten times more irradiance than the monochromator, which measured  $9.2 \mu\text{W}/\text{mm}^2$ . Unfortunately, since the microscope light is unfiltered white light (all wavelengths), measuring for responsivity versus wavelength (individual wavelengths) could not be done, but measurements using this light source could yield data that indicated the power required to shift the GST material between states. The other disadvantage of using the microscope light was that the spot size was 3.5-mm on the surface of the probe-stage, versus the light from the monochromator via fiber optic which had a spot size of 60- $\mu\text{m}$  on the probe-stage. Since the data from the first chip indicated that testing the samples via the microscope light yielded reasonable data, using this method again on the next chip was the next logical step.

Measuring the resistance change using the parameter analyzer, sweeping the voltage from either -0.5 to 0.5 V or later -1 to 1 V with the GST both shielded from light and being illuminated, presented no change in the resistance of either test sample, the 3  $\text{\AA}/\text{s}$  growth GST with layer thickness of 4- $\mu\text{m}$  or the 6  $\text{\AA}/\text{s}$  growth GST with layer thickness of 0.5- $\mu\text{m}$ . These results implied that there were no photocurrent effects occurring. Because all available samples were tested, it was concluded that the light sources available were not powerful enough to manipulate the current GST samples

thermally and that these samples were not photoconductive. More data was needed, so a second batch of seven chips was fabricated to test if they would be photoconductive. Five were fabricated with the same conditions as the first sample tested, and two with a growth rate of  $9 \text{ \AA/s}$  to  $4\text{-}\mu\text{m}$ . These two samples were hoped to have an even lower oxygen content due to the faster growth rate and thus have a higher photo absorbance. This growth process had never been done before by the growers and unfortunately the growth process failed to come out as desired. One of the resulting samples is shown in Figure 6-2, where the test structures have been completely covered and are unrecognizable. The other five samples grown to the specification of the first sample tested were fabricated without any problems.



Figure 6-2 Test Chip with growth of GST at  $9 \text{ \AA/s}$  to  $4\text{-}\mu\text{m}$  thick (no usable devices).

While the new samples were being fabricated the modeling was completed using FEMLAB as discussed in section 3.2.1. The modeling results agreed with the conclusions that the light sources available did not produce enough power to heat the GST to the point of changing from an amorphous to a crystalline state. Although this conclusion did not agree with the results from the first sample, more testing was needed to confirm whether or not GST shifted states optically or through the applied voltage bias when measuring the devices. This modeling did not rule out the light sources to be used to generate photocurrent if these new samples were able to do so. Because the first sample of  $6\text{\AA}/\text{s}$  (low oxygen content) with layer thickness of  $4\text{-}\mu\text{m}$  seemed to produce photocurrent effects, although all other samples did not, it could not be concluded whether the GST that the University of Utah produced was capable of producing photocurrent effects or not.

After extensively testing the new batch of samples using both the monochromator setup with the lock-in-amplifier and the microscope light setup with the parameter analyzer, the data measured using either test method, with the GST being both shielded from light or illuminated, produced the same results. This indicated that the new samples of GST did not produce any photocurrent effects. It would have been concluded that this chalcogenide material was not photoconductive, but there was some inconclusive evidence due to structural differences in the two batches that was found using the SEM. Figure 6-3 compares SEM images of samples (taken before testing), from both batches showing (left) the second batch, and (right) the first batch, both

grown at the same parameters of  $6\text{\AA}/\text{s}$  grown to  $4\text{-}\mu\text{m}$  thick; indicating the two batches of GST were not the same material or material structure.

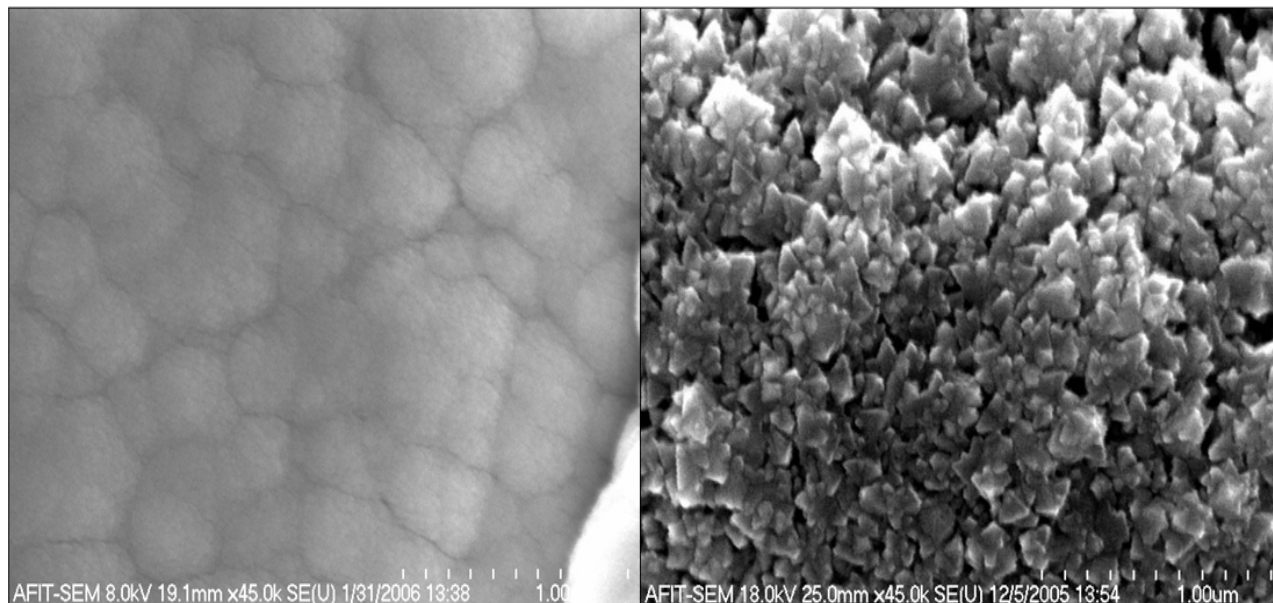


Figure 6-3 GST material structure both at 45k magnification, batch one (right), batch two (left), both grown at  $6\text{\AA}/\text{s}$  (low oxygen content) to  $4\text{-}\mu\text{m}$  thick.

These new samples produced no photoreaction; SEM images before and after optical testing showed identical material structure. Because of the difference in the material structure between the two batches, the measured data could not be conclusive in ruling out that the first sample in batch one did not exhibit photocurrent. The next step was to determine if this GST behaved electrically like those in other research articles.

### **6.3 Electrical Analysis**

Following test procedures for electrically testing the GST similar to [3] and [21], the parameter analyzer was used to sweep a current across the devices to test their

ability to change states between amorphous and crystalline. By applying current sweeps of 0 to 0.5 mA and then 0 to 1 mA, the voltages were measured for dark and illuminated samples showing no change in the state of the GST. A change in the state of the GST is indicated when, while sweeping a voltage across the device, the voltage rises quickly (in amorphous state) and when reaching the voltage threshold  $V_{th}$  of the GST a sharp drop in voltage is seen as the current is steadily increased.

The current sweeps were increased gradually until noticeable effects, reaching  $V_{th}$ , in the GST occurred. Although other researchers used current sweeps around 0.5 and 1 mA, the tests in this experiment used current sweeps upwards to 100 mA to produce changes in the GST states. Figures 6-4 through 6-6 represent the data collected in these tests with electrode gaps of 2- $\mu\text{m}$ , 6- $\mu\text{m}$ , and 10- $\mu\text{m}$  respectively. Other data was collected on similar tests with wider electrode gaps but these results indicated that larger electrode gaps were not likely (14 to 20- $\mu\text{m}$  gaps) to change states, or no state changes occurred at all (24 – 100- $\mu\text{m}$  gaps) due to the available current generated by the testing equipment. This was believed to be caused by larger gaps having a larger volume of GST and thus more GST acting as a heatsink, requiring more current to heat up the GST to the needed crystallization zone temperature to change the states reliably. Comparing these results to those other researchers have collected, see Figure 2-9; there are both similarities and differences between the data.



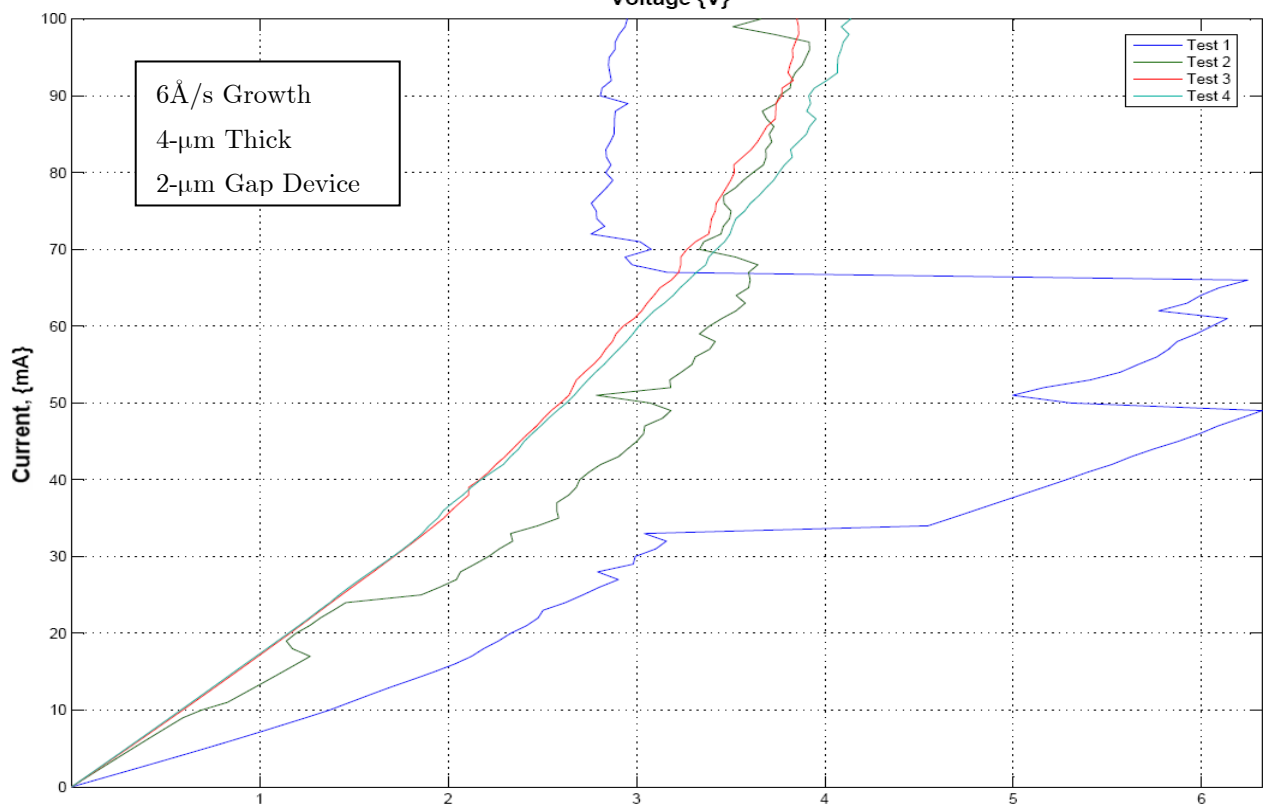
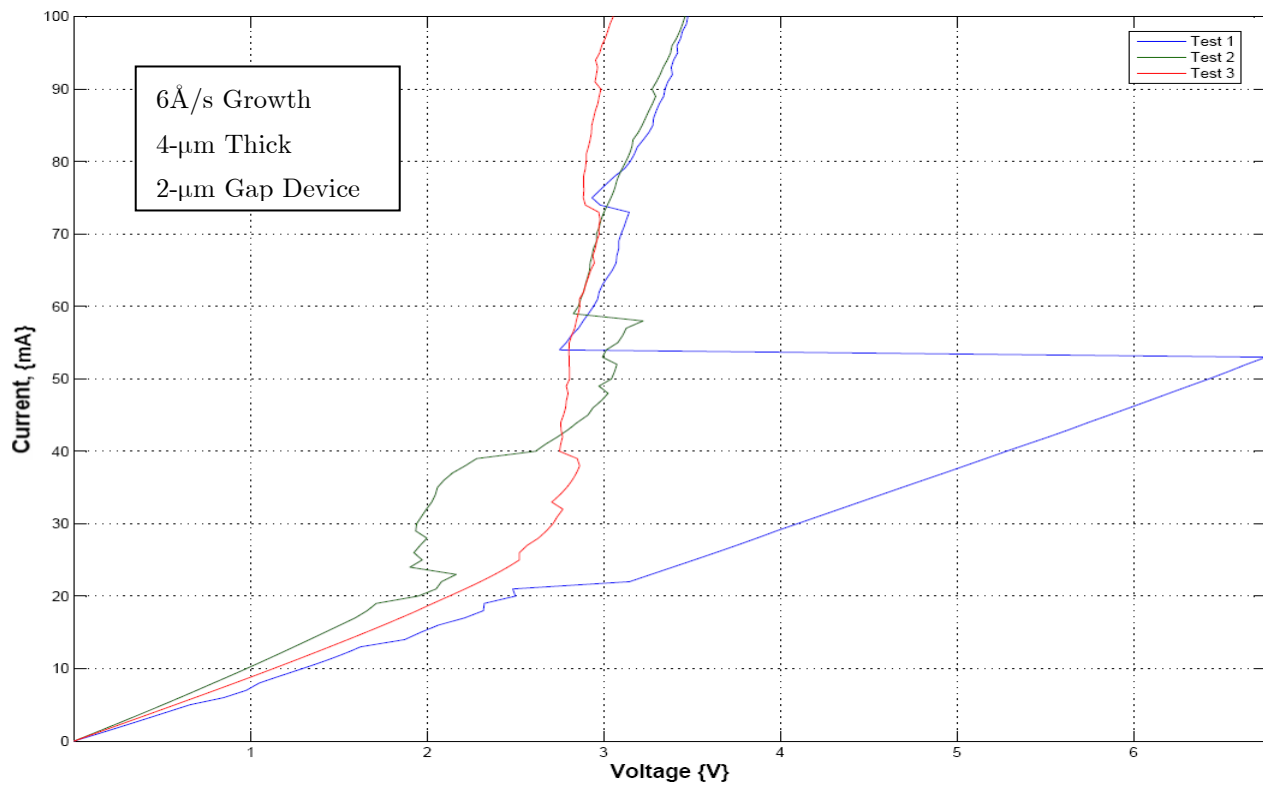


Figure 6-4 GST current sweep test of two separate devices with electrode gap of 2-μm.

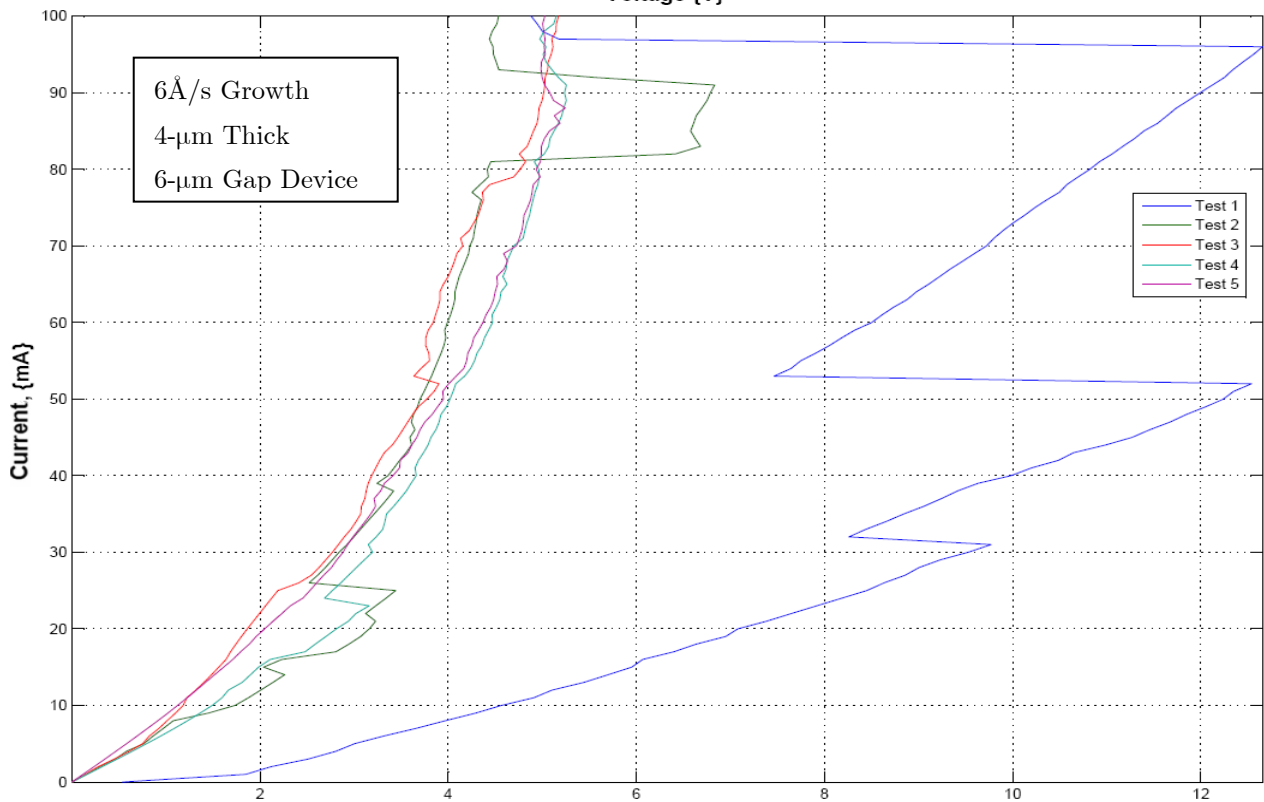
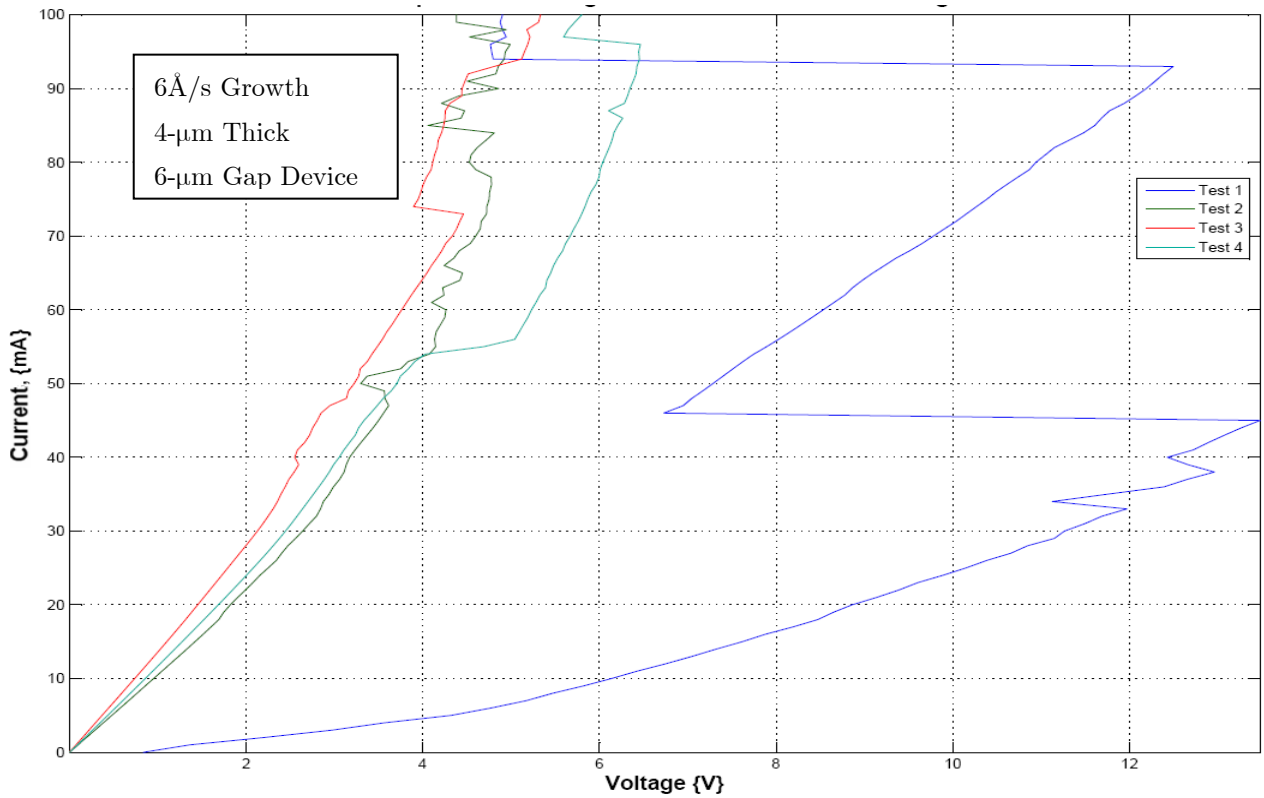


Figure 6-5 GST current sweep test of two separate devices with electrode gap of 6-μm.

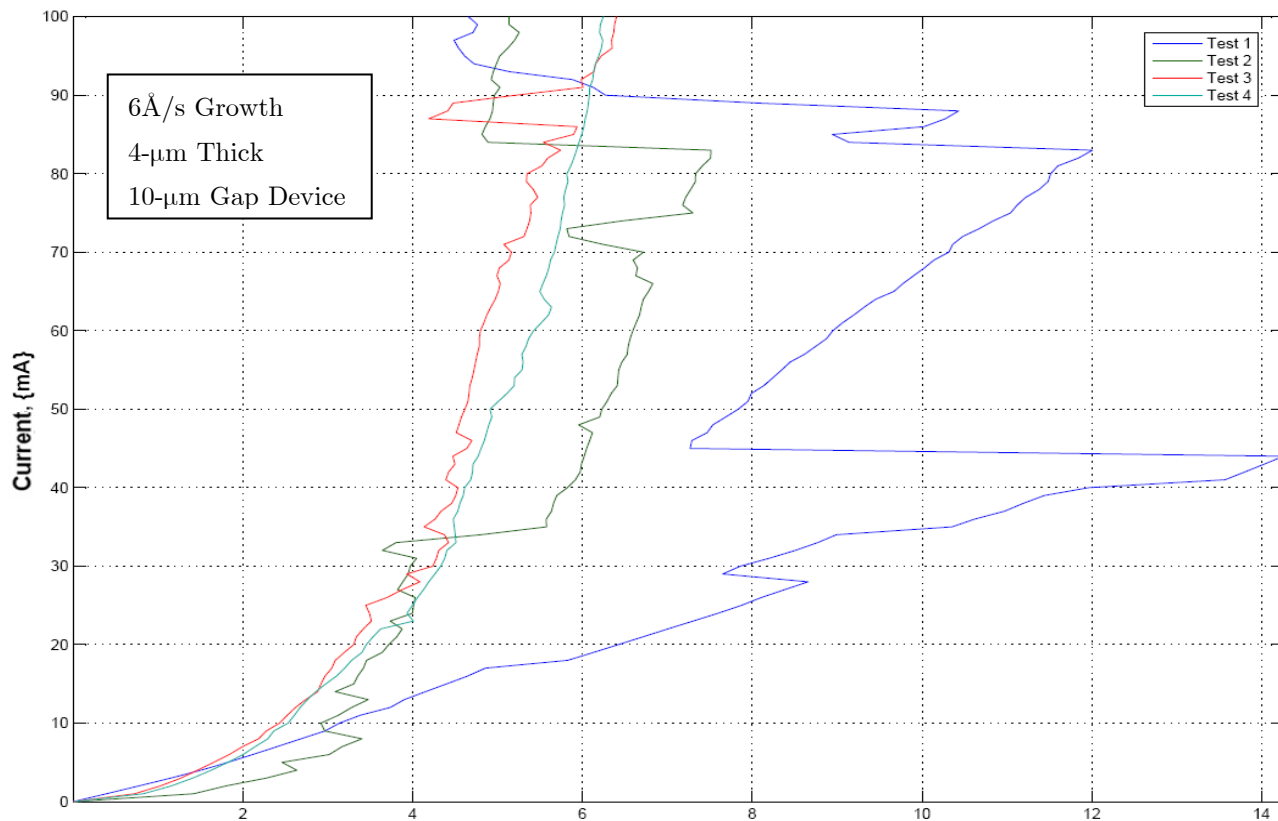
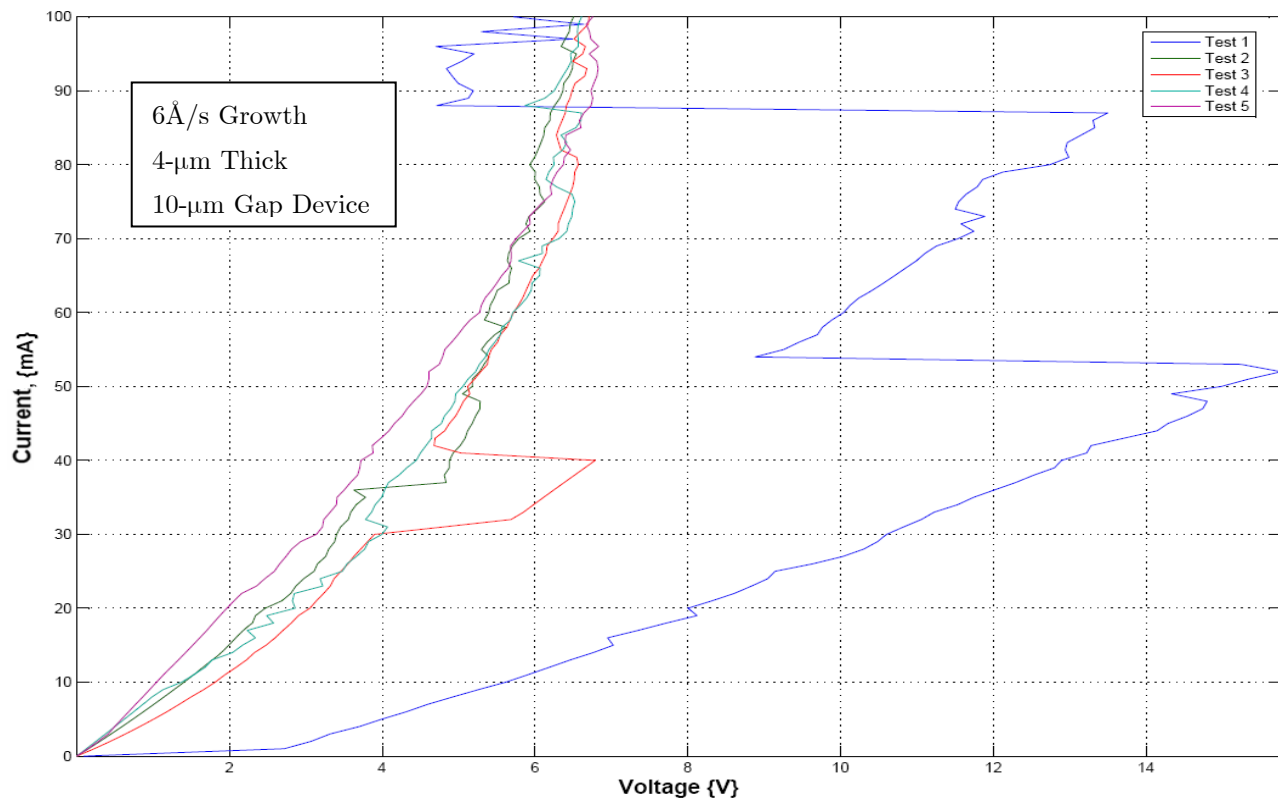


Figure 6-6 GST current sweep test of two separate devices with electrode gap of 10-μm.

It was concluded that to reach  $V_{th}$  and change the state in the GST for these tests required more energy, as compared to other research, even for the smallest geometries of 2- $\mu\text{m}$ . This was because these geometries were not only much larger, as compared to [21], which used an electrode gap filled with the GST of 90-nm, the design in [21] was also much better insulated from heat dissipation effects in contrast to the design used in this experiment having large areas of GST between the electrodes making contact with the surface of the chip. One interesting detail about the data collected and presented in Figures 6-4 through 6-6 in contrast to Figure 2-9 is that in Figure 2-9 there is only one voltage threshold where the chalcogenide shifts from amorphous to crystalline. In Figures 6-4 through 6-6 there is a pattern of two major points where the material reaches a voltage threshold in amorphous state (higher resistance) then abruptly drops resistance, i.e. changing to a more crystalline form. After the second drop in resistance (around 60 mA for a 2- $\mu\text{m}$  gap and 80-90 mA for larger gaps) the state is believed to be changed to fully crystalline. This conclusion was supported by subsequent current sweeps, where the plots were characterized by an exponential line at a much lower resistance level than the initial test. The data represented in these figures is important because it indicates where the voltage threshold,  $V_{th}$ , for the given geometries in this experiment and shows the trend of how  $V_{th}$  changes with respect to the change in geometry of the test structure.

The jaggedness from the current sweeps in the changes in voltage indicates how, because of the open geometry preventing a guided current path, the current has dynamic

and unpredictable paths across the GST between the electrodes. New current paths are sporadically created, where spots in the GST across the electrodes cools and forms crystalline, or heats up quickly then cools quickly creating amorphous regions and forcing the current in a new direction where lower resistance is. This dynamic change in the path of the current flow is the cause of the jaggedness and sporadic changes in the voltage being measured. The reason the subsequent current sweeps appear exponential is because when the initial current sweep set the material to crystalline, a complete path between the electrodes of GST may be crystalline, but this path could also be very narrow. As the current increases, the crystalline path of GST heats up the surrounding amorphous GST, lowering the equivalent resistance, but not reaching  $V_{th}$  to cause growth of more permanent crystalline in the GST.

### ***6.3.1 Phase-change Results Comparison to Other Research***

There are a couple of theories why the phenomenon of two major  $V_{th}$  is occurring in contrast to other research data having only one  $V_{th}$ . One theory is due to scalability and the other, which seems to be the more significant theory likely to explain this effect, is the eutectic temperature between gold and polysilicon. To change the states within GST a temperature of about 760 K is needed. The design of the electrodes, having both polysilicon and gold (where the eutectic temperature is 636 K), adjacent to the GST being tested, this lower (eutectic) temperature is reached before the GST reaches the temperature to crystallize fully. Because the eutectic bonding of the gold and polysilicon creates a new material with a higher resistance, the crystalline path of GST between the

electrodes is cut off by the higher resistance. Thus, this is believed to be the reason behind this partial shift in phase, before the GST fully shifts to crystalline form, where the second shift leading up to the  $V_{th}$  at a greater current is caused by the current making a new crystallized path through the GST.

Figure 6-4 presents the data collected over a 2- $\mu\text{m}$  gap which indicates only one shift to a crystallization form, or a minor second shift as depicted in the bottom plot of Figure 6-4 at 50 mA which is where the other 2- $\mu\text{m}$  gap test completely changed to crystalline. It was concluded that because the gap is much smaller, the GST can heat up and crystallize, then cool down before generating enough heat to affect the surrounding gold and polysilicon to induce the eutectic phenomenon. However, as shown in the bottom plot of Figure 6-4, this is not necessarily true, but more likely than test devices with larger gaps. Figure 6-7 shows the before and after effects of a 6- $\mu\text{m}$  gap electrode pair and GST from applying a current sweep of 0 to 100 mA and inducing crystallization in the GST. Looking at the tested electrode pair in Figure 6-7 under a microscope reveals coloring (lighter grayish-purple) changes in the electrodes that match those commonly found after the eutectic phenomenon during testing of other MEMS devices using the same fabrication process.

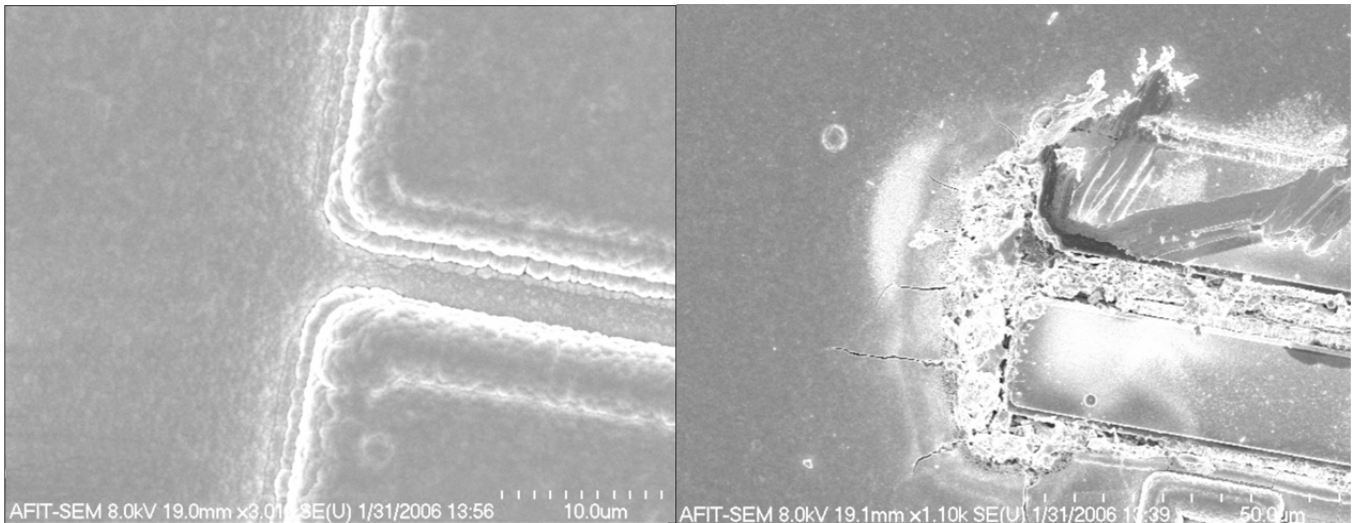


Figure 6-7 Electrical test of GST before (left) amorphous, and after (right) current sweep 0 to 100 mA, transitioning GST around electrodes to crystalline form.

### ***6.3.2 Scalability Analysis***

Looking at the scalability electrically is much different than optically; the original design was laid out to support a large exposed surface area where light could irradiate the test device. Electrically, the large geometries prove ineffective in changing the material states and appear unreliable. Figures 6-4 through 6-6 not only indicate in the initial current sweep the voltage thresholds and shifts from amorphous to crystalline, and in the subsequent current sweeps a crystalline state, they also have other, smaller, random and abrupt changes in the resistance of the GST both in the initial sweep and subsequent sweeps of current. Looking at this data and other data measured from larger electrode gaps indicates a trend that as the gap between the electrodes increases so does the frequency and unpredictability of these random shifts in resistance occur. Since the current flow will take the path of least resistance, larger gaps present problems in

providing a single current path between the electrodes. Areas where the material began to heat up and crystallized begin to cool down and not form a completely crystallized path between the electrodes, while other areas begin to heat up and form a crystallized path between the electrodes. This randomness and less isolated control of the exact current flow between the electrode is understood to be the cause of these other minor and random changes in the resistance level within the GST.

One useful part in comparing the data for scalability in the tests depicted in Figures 6-4 through 6-6, as suspected, is that as the gap between the electrodes increases so does the required  $V_{th}$  needed to shift the GST to a crystalline state. For the 2- $\mu\text{m}$  gap, the trend to reach  $V_{th}$  was 6-7 V. At 6- $\mu\text{m}$   $V_{th}$  increased to 12 V on average and sometime a little higher, and at 10- $\mu\text{m}$   $V_{th}$  is over 14 V. This is due in part because of more energy needed from a larger surface area of GST that is being cooled by the substrate between the electrodes. Also, since there is more material (a longer path for the current to flow through the GST) the resistance will be higher and the needed voltage to attain the same amperage across the electrodes will increase. This indicates that as the devices scale down, the threshold voltage required scales at a magnitude greater than the scaling factor alone, meaning that smaller devices sizes would be more efficient from benefits other than the geometry alone.

#### **6.4 Summary**

The initial results, from optically testing the first GST sample (growth parameters of 6 $\text{\AA}$ /s and a layer thickness of 4- $\mu\text{m}$ ), indicated ideal characteristics that this GST



sample responded to light, generating a photocurrent and showing permanent changes in resistance due to phase-change in the GST. This sample was tested, optically, until it was believed to have transitioned to a crystalline state, which due to the test chip design was no longer testable. The only other sample with identical growth parameters indicated, from its initial test results, that it was already in a crystalline form (cause unknown). The other four samples, with growth parameters of  $3\text{\AA}/\text{s}$  and a layer thickness of  $4\text{-}\mu\text{m}$ , and of  $6\text{\AA}/\text{s}$  and a layer thickness of  $0.5\text{-}\mu\text{m}$ , had test results which indicated no photoresponse for either photocurrent generation, or ability to change states with the applied optical power density (equal to that irradiated on the first sample). It was concluded that the growth parameters from the first sample were optimal and for further optical testing, new samples with these growth parameters were needed.

A new batch of test chips had GST grown on them identical to the growth parameters of the first sample test, which produced ideal results. Following the same experimental procedures, none of the new samples provided any optical response. It was concluded that a higher optical power density, then that which was available, was needed to shift the GST from amorphous to crystalline, and it was uncertain why the first sample reacted to the low optical power density. SEM imaging of the GST samples comparing the two batches revealed that the two batches had a very different structure, further leading to inconclusive findings from the test data between the two batches.

Electrical testing of the GST was also performed to analyze the phase-change capabilities, provide insight in scalability based on the design geometries used in this

experiment, and to identify the voltage threshold,  $V_{th}$ . The  $V_{th}$  value measured, which is the required voltage level to shift the GST from amorphous to crystalline, indicated unique results as compared to other research using similar test procedures. The uniqueness in the results measured in this experiment presented a second rise in voltage and a second  $V_{th}$  before a fully crystallized path between the electrodes was created. It was concluded that this was the result of the eutectic phenomenon occurring between the gold and polysilicon in the electrodes. Other than this unique second  $V_{th}$ , at a higher current level, these test results presented data very similar to other research, indicating a predictable  $V_{th}$  in the GST when the material changed from amorphous to crystalline. Subsequent current sweeps confirmed the change to a crystalline state in the GST by a predictable lower resistance level in the GST, indicated by the lower voltage as the current was increased (as compared to that of the initial, amorphous state current sweep).

The electrical manipulation of the phase-change in the GST also indicated a trend in the scalability with relation to the device geometry, that as the device size was reduced, the scaling factor of energy required to shift the state in the GST was reduced by a factor greater than that of the size scaling factor alone. It was concluded that these results, for the power scaling factor, were affected not only by the size of the device, but of the surface area ratio as well. The smaller device sizes reduce the percent of surface area, leading to less heat loss in the GST and allowing for more efficient operation for the required power to shift the GST from amorphous to crystalline.

## *7. Conclusion and Future Recommendations*

### *7.1 Research Summary*

This research examined the phase-change capabilities of GST for novel photonic applications, determining the feasibility of coupling GST with light sensitive DNA for new volumetric memory applications. Although the experimental data desired (resistance vs. intensity, and responsivity vs. wavelength) was not attained, the modeling and data that was gathered provided useful results for analysis of GST. The unique properties of chalcogenides were researched and ones applicable to this study explained in the literature review. GST's thermal behavior, due to interaction of photo absorption, was modeled using finite element analysis software (FEMLAB) in steady state and suitable pulse times of 3 sec, 30 sec, and 5 min for the experiments performed in this research.

The theoretical data calculated the photon energy required to change the state within the GST assuming 100% absorption of photon energy. Methods and designs of the test device used in this experiment were considered and an analysis of benefits, costs, and time were applied to the fabricated samples. Details of the fabrication processes used were explained and SEM images of the final samples obtained. Optical and electrical testing of the GST samples for phase-change capabilities were performed and

the results analyzed. The results from the electrical testing of the GST samples were also compared and contrasted to other similar research.

## ***7.2 GST for Multistate and Hybrid Applications***

Applications using GST as a phase-change semiconductor are still developing and the understanding of its unique properties is incomplete. Both electrical and optical applications have been developed and fine tuned, but these applications are very specific. The ability to combine these two applications of optically changing the material, and electrically reading the state of the material, has not been developed yet.

### ***7.2.1 Optical Manipulation of GST***

Optical applications using GST material have been implemented in the use of DVD-RAM discs where GST is the writable material with 18% and 30% reflectivities. Phase-change implementation for this application is effective, because when a 20 to 30 mW laser [43] modifies the GST with a spot size diameter around 600-nm, the process of reading back the recorded data is also done optically by the reflectiveness on the surface of the GST. Simulations done in this research indicate that only a very thin layer near the surface of the GST is effected by light energy at short pulses, even for higher energy levels than necessary to change the material adequately between states. Only by applying the optical energy for long periods, such as the steady state analysis done in chapter three, does the GST further from the surface react as well. Long pulse times are ineffective because not only is the GST heated, but also the surrounding material,

adversely affecting the ability to quench the material during a reset back to an amorphous state. Therefore, longer pulse times would only be suitable for set times, such as the five minutes test done in this experiment. Short pulse times are adequate for optically reading back the reflectivity of the surface of the GST, but electrically; measuring the resistance level (the state of the GST) with an applied voltage and current across the GST could require more crystallized GST than a thin layer on the surface. Otherwise negative effects can occur, such as when current density increases, unwanted heating effects would occur, that could alter and degrade the reliability of the device; this could be mitigated by reducing the read voltage and current, but further research is needed.

One point to note that emerged during the optical testing of the GST was that Dr. Fritz Schuermeyer (photonics and chalcogenide specialist assisting with the experiment) believed the chalcogenide to be a photoconductive material, having properties beyond thermal effects with optical energy. Photoconductivity was also an important property in producing responsivity versus wavelength plots to determine the most effective wavelength to use for optical manipulation of the GST. Using the experimental setup as described in chapter five with the chopped light and the monochromator, the lab equipment was setup to detect signals above a noise level of  $5 \times 10^{-11}$  A-rms. No photocurrent was detected in the second batch, indicating that GST does not possess photoconductive properties (at least not these test samples). The first batch was found inconclusive because of mixed results between the first sample and the

others tested. Finally, the results from the second batch could not provide conclusive evidence about the photoconductive properties in the first batch because there were significant differences in the GST structure between the two batches of samples. Further research is needed to solidify these conclusions about the photoconductiveness in GST.

For thermal activation using optical testing, the GST samples indicated that the photo energy needed was greater than available light sources produced. Ultimately, it was concluded that optical manipulation of GST in a design where the GST state is read electrically is ineffective and could cause reliability issues. Other concerns dealing with coupling this type of application with the marine DNA discussed in chapter three needs to be investigated further, such as comparison of the needed temperatures of the DNA polymer to the temperature of the GST to reset to an amorphous state.

### ***7.2.2 Electrical Manipulation of GST***

Current research in the electrical manipulation of GST and other phase-change materials is of high interest. GST offers great benefits compared to current flash memories due to its high program to failure rate of  $10^{13}$  as compared to flash memory having  $10^5$  read/writes before failure [34]. Also, it is much more resilient to radiation effects due to storing information in the material state as compared to flash memory that stores information through capacitance, which is more easily affected by radiation.

The electrical testing of GST in this experiment mostly provided insight for optimizations in future research, and showed how unexpected factors can occur (in the sense of the design used). The geometry, size, and other materials coupled in testing the

GST in this investigation were all factors that can be improved for future research. It is not completely unexpected that the design used yielded good, but not optimal data for an electrical test of the GST since the design was developed for optical testing. Some conclusions for more optimal designs were: minimizing the possible paths the current flow can take, reducing excessive heatsink loss through insulation layers such as described in [22], and optimizing device design to reduce additional unknown and/or unwanted effects (such as with the eutectic phenomenon between gold and polysilicon that occurred in this experiment).

Applications using GST as a data storage material by reading the state of the material electrically seem most effective through electrical manipulation of the states within the GST. This research showed theoretically how optical energy can change the states within the GST, but the implementation of electrical manipulation has been determined to be more effective and reliable due to a more complete change of the state of the GST between the electrodes. Electrical testing of the GST samples was analyzed, showing that the phase-change properties in the GST through I-V curves matched (with some differences) other research [21] that indicate how GST shifts between states. The differences between the data collected in this research and others [3, 21] were concluded to be effects caused from two things: the larger scale of the test structures in this experiment, and the eutectic temperature between gold and polysilicon, which the electrodes in this design were made of both gold and polysilicon. The eutectic temperature of polysilicon and gold is lower than the crystallization and melting points

of the GST. The electrical testing results also indicated a nonlinear effect in power consumption to drive the devices (changing the state of the GST), where smaller scale devices improve by a factor greater than scaling size alone. Note that the scaling factor, for power required to changes states, is only relevant to the geometry and design presented in this experiment. Overall the capability of GST in applications using electrical manipulation of the material state either for binary or multistate functions appears to be reliable for future research, and other research [3, 21, 22], supports this with results that are very reliable and predictable through electrical manipulation of the phase-change within the GST.

### **7.2.3 Reliability**

One of the key factors in any research is knowing the test parameters. This means ensuring all the variables are the same for each test, or accounting for and understanding the difference in the parameters between tests, and mitigating other unwanted, unknown, effects through tightly controlled experimentation. Part of this research dealt directly with some unexpected differences in the test samples, which is a concern in the reliability of the GST grown by the University of Utah. As shown in Figure 6-3 the material structure of the GST from the first test batch and the second are considerably different. Feedback from the grower indicated there were no significant differences in the sputtering of the two batches, only that the basic vacuum pressure (the pressure before argon is put into the system) was different. The pressure during the first batch of samples was  $6\sim 7 \times 10^{-7}$  mTorr, while the second batch pressure was only  $4 \times 10^{-6}$



mTorr. When the pressure goes below  $10^{-5}$  mTorr, the growers consider this vacuum level good to sputter. The grower noted that the vacuum system didn't work during the second batch. Other than these factors it is unknown why the two batches of GST samples are different. It is essential that the reliability of the GST is constant for each of the tests in order to produce reliable data. Unfortunately, because of the unknown difference in the GST, additional testing is needed to provide more conclusive results.

#### *7.2.4 Design and Fabrication*

Another important part of measuring accurate and successful results is setting up the experimental conditions for optimal data collection. In the case of this experiment, part of this was the fabrication of the test structure on which the GST was deposited and tested. Knowing all the test parameters beforehand is a vital key to accomplishing a successful design for the test structure. For the most part the conditions in this experiment and design parameters for the test structure corresponded well with the procedures of testing the optical properties of the GST. Due to the timeline of this research, an understanding of the GST was still being researched while design of the test structures was created. This led to a design that placed gold on the polysilicon electrodes to allow better conductivity to the GST, and consequently caused the problem with the gold and polysilicon fusing together at their eutectic temperature of 636 K which is below the transition temperature of the GST. Fusing together the gold and polysilicon created a new material with a higher resistance and added more unknown and unwanted effects to the results of the experiment.

Although the data collected was adequate and provided insight to the electrical phase-change properties of GST, conditions would have been more favorable if these additional effects could have been removed by a better understanding of all the parameters involved with the experiment. Having to deal with this additional phenomenon only reinforces the necessity of understanding the whole picture of the experiment as much as possible before design and testing begin to insure accurate and desired data collection.

### ***7.2.5 Summary of Conclusions***

Even though this research theoretically models GST using optical actuation to modify the state within the material, the results of short pulse times equating to only a very shallow surface of the GST being manipulated indicated that for reading the GST electrically, optical control of the phase-change is ineffective. Electrical manipulation (through the same mechanism of Joule heating – ohmic losses) of the phase-change in the GST appears to be more effective, reliable, and predictable. Although the design used in this experiment was not optimal for electrical testing of the GST, the results indicated areas where improvements in the test design could be made. Specifically, smaller geometries are desired to mitigate random and less specific paths for the current to flow across the electrode through the GST as seen in section 6.3. Smaller geometries using thin layers of GST and fabricating the electrodes as thin layers both above and below the GST would also help improve efficiency at a greater than linear rate, help reduce unwanted heat loss, and allow for faster device operations (set and reset times).

Accuracy and reliability for the experiment are always important. This experiment found that more research is needed to determine the quality of the GST and why there is a difference between the first and second batch of samples. Fabrication and test structure material uses in this research caused additional undesired effects which need to be considered in future testing.

### ***7.3 Lessons Learned***

Unknown and unwanted factors are always issues to cause problems in an experiment. Not all of these factors can be found ahead of time and dealt with appropriately, but planning ahead as much as possible and knowing the experiment clearly before design and setup will greatly reduce these problems.

#### ***7.3.1 Test Equipment***

It always takes longer than planned to learn how to use the equipment, configure appropriately, and verify the condition when sharing resources with others. Relying on others for assistance is acceptable when learning the equipment; otherwise it is better to know how to use the equipment appropriately and thoroughly for the experiment. Most of the difficulties in the experiment, causing a lot of the extra time, were related to the crucial other 10% of the equipment procedures that had to be learned independently.

### ***7.3.2 Design***

A design should only be created after the experiment is clearly and fully understood. This will help reduce the many possible undesirable difficulties that can arise within the experiment because of premature planning and design implementation.

### ***7.3.3 Experience***

One of the most important lessons that came about because of this research was the understanding of the experience gained, and the experience itself. Future research may be similar or different, but the experience gained has given insight to experimental research that will greatly help to prevent problems like overlooking the eutectic phenomenon of gold and polysilicon with respect to the heating of the GST. This experience has also helped in instilling the importance of finishing the modeling beforehand for accurate testing and appropriate use of equipment, such as knowing the power requirements to optically change the GST. Acquiring higher power and smaller spot size optical sources such as lasers would have enabled more effective testing of the GST.

## ***7.4 Recommendations for Future Research***

Using GST to store the information from the DNA as needed in a multistate application could be possible. Direct coupling and optical manipulation appears impractical due the high temperature required to changes states and lower temperatures needed for the DNA, 300 to 400°C max (as indicated by AFRL). Since the DNA

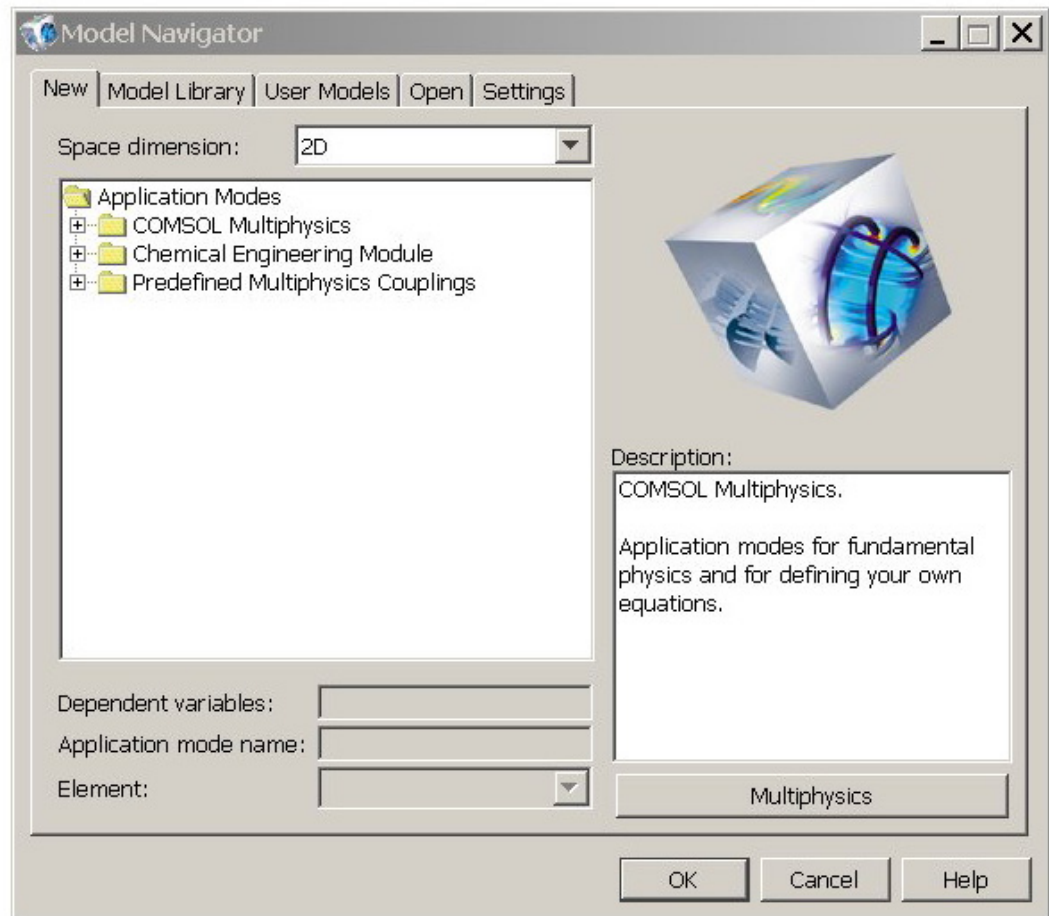
operates optically, other interface devices are needed to capture the DNA information, such as current photonic photodetectors, holographic imaging, etc., that can operate at lower temperatures. Then, electrically the information could be stored in the GST. Dr. Ovshinsky's research [33] indicates there are actually more transitional states when transitioning from crystalline to amorphous than when transitioning from amorphous to crystalline; see Figure 3-1, which indicated that GST has multistate capabilities and could be useful for use as data storage for the DNA, although this research found results indicating more of a binary state in the GST. If it is found in future research that GST does exhibit photocurrent properties, looking at the responsivity vs. wavelength of the material would be something that would allow for a characteristic transfer function of the GST to be derived for large scale modeling in SPICE of GST devices.

For future research in coupling the DNA with GST, other avenues, such as more optically sensitive devices coupled with the DNA which can transfer a signal to be amplified and stored in a GST memory array, are suggested for providing an interface from the DNA to the GST or other electrical devices. Research on GST seems very promising in its phase-change properties through electrical manipulation. Since there are some definite benefits to GST in regards to its lifetime and its durability in harsh environments, developing applications using GST as an electrically actuated phase-change memory cell appears desirable. Future research would benefit this type of application by researching more optimal geometries, less interactive materials surrounding the GST, and accurately growing quality GST material. Another issue to

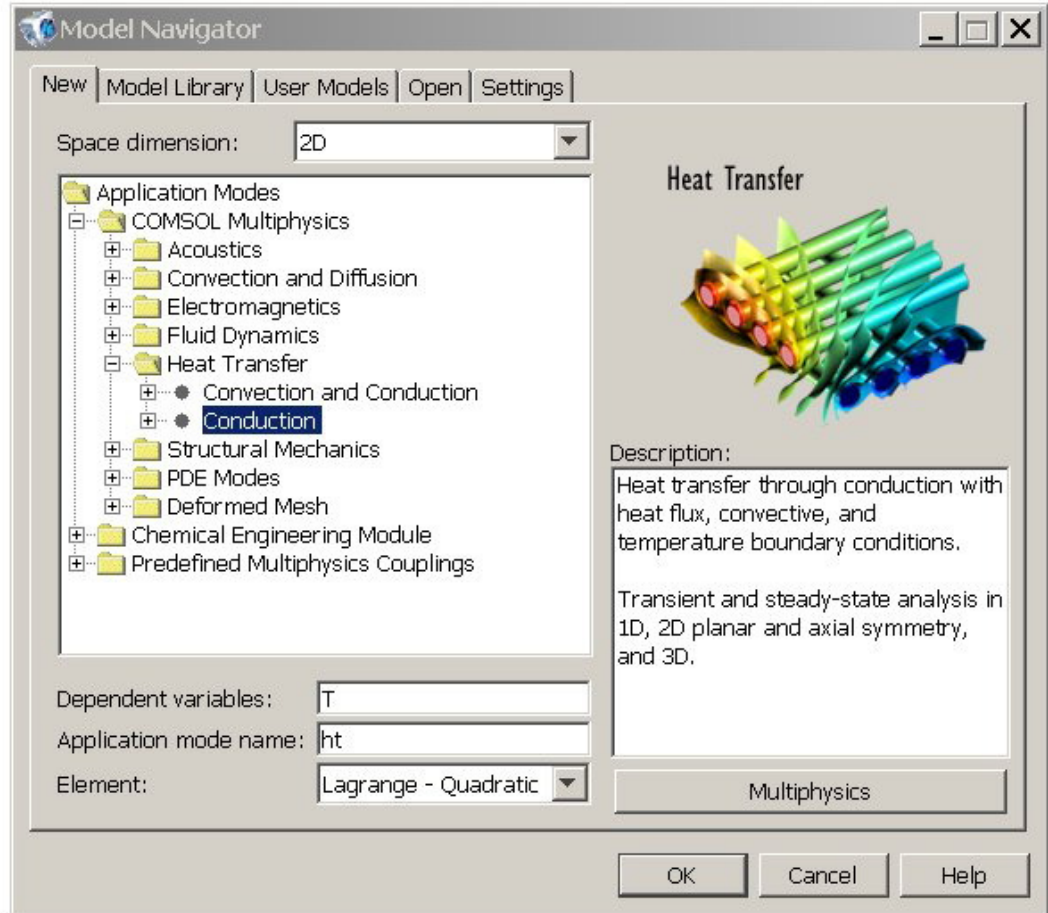
look at when designing a test circuit that is exposed completely to the deposition of the GST is proper masking of probe pads to remove GST from those areas. This is important because it will reduce such things as buildup of material on the probes causing variation in the measurements due to inadequate contact between the probes and the probe pads.

## *Appendix A – FEMLAB Procedures*

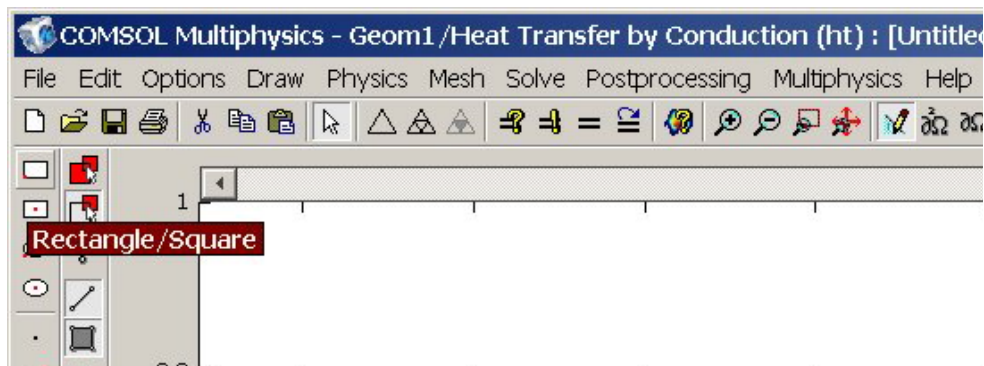
STEP 1: Run COMSOL Multiphysics v3.2. The first window you will see is the Model Navigator window.



STEP 2: Choose 2D for space dimensions, and under Application Modes choose COMSOL Multiphysics, then Heat Transfer, then Conduction. Finally, click OK.

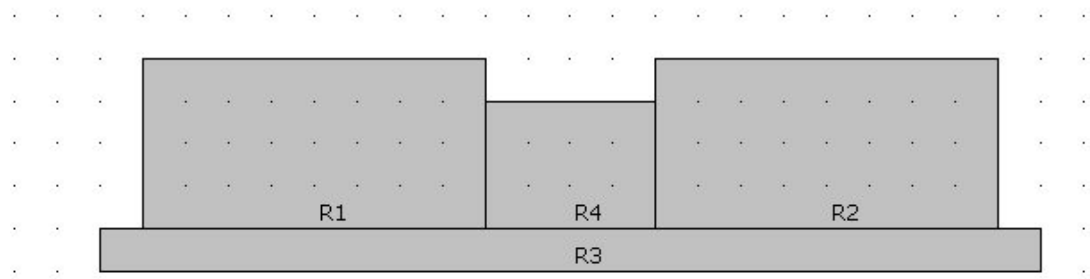


STEP 3: The COMSOL Multiphysics general layout window will open up. Select the rectangle/square button from the toolbar on the left. This will allow you to draw rectangular objects that can later be modified for material properties to apply boundary or internal thermal effects and more.

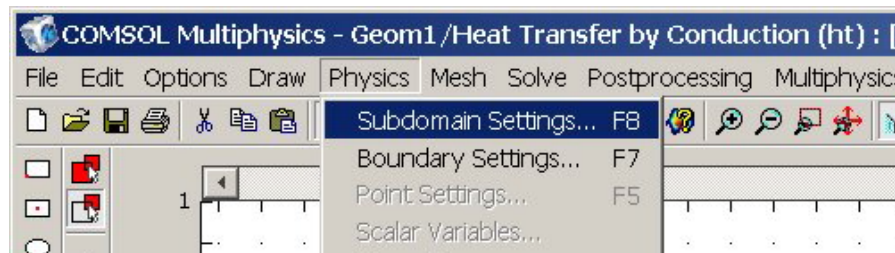




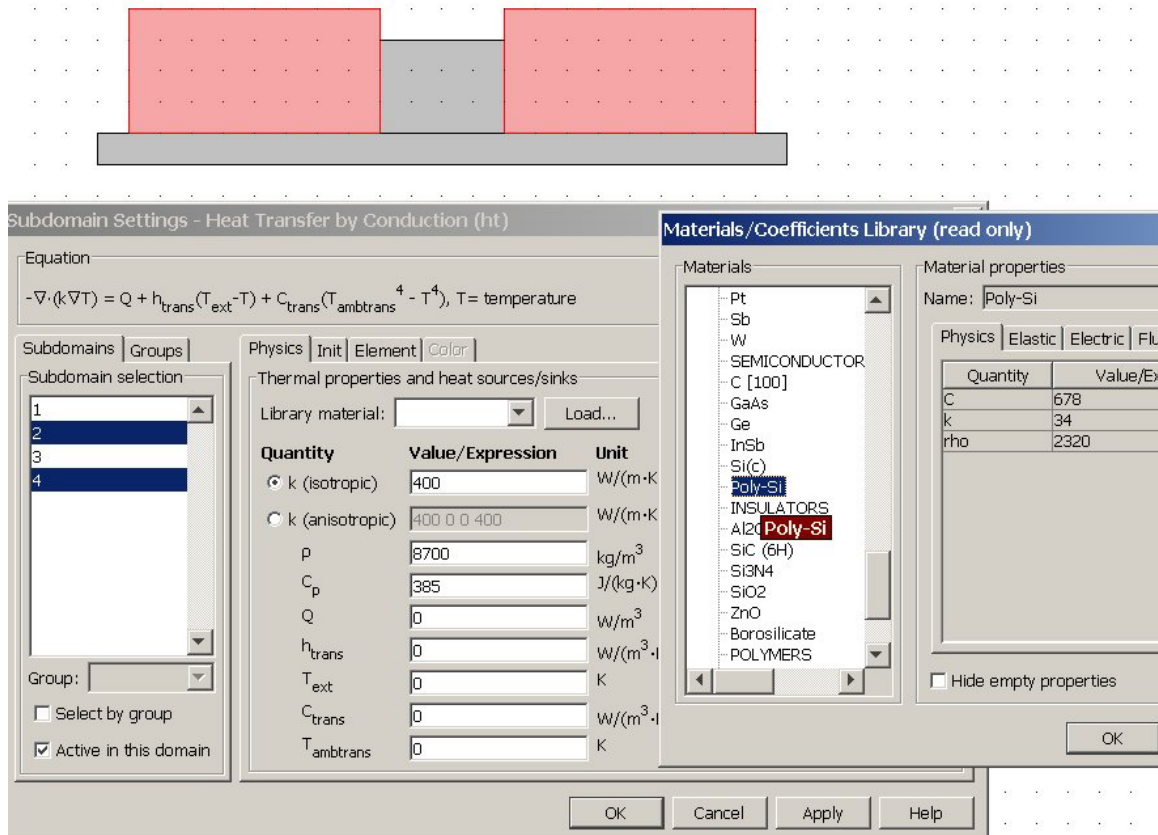
STEP 4: Using the rectangle/square button from the toolbar on the left, the model from chapter three is created. Four rectangles are drawn as shown.



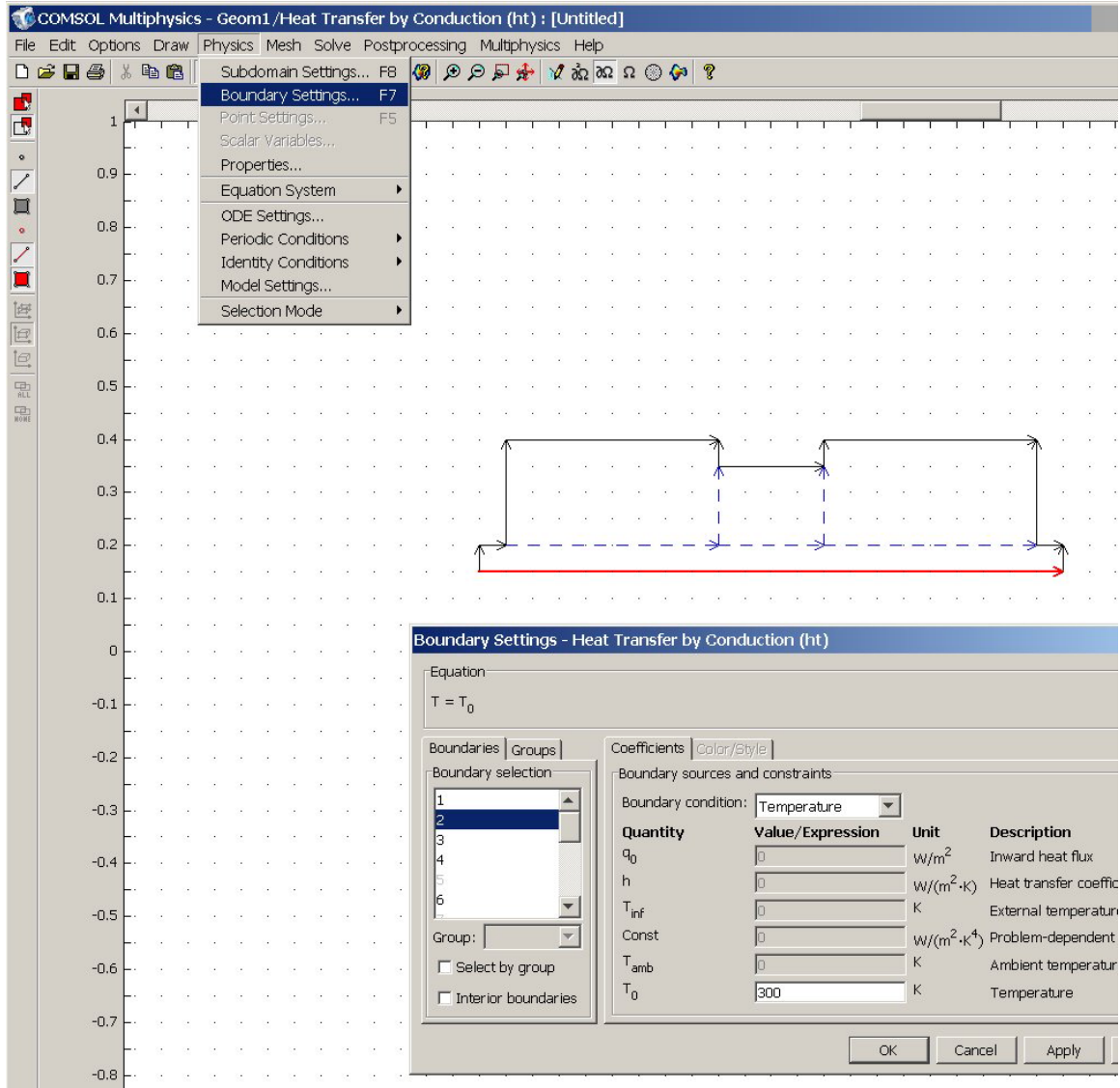
STEP 5: In this step the material properties of each of the rectangles will be set. Go up to Physics menu at the top and choose Subdomain Settings...



Select the two regions next to the GST in the subdomain selection window, then click on Load button for Library Material, and choose Poly-Si. Follow the same procedures for selecting the bottom thin rectangle, set it to Si<sub>3</sub>N<sub>4</sub>. Then, manually input the material properties from Table 3-1 for GST as the center square. Before this step is complete, make sure all subdomains have the ambient and internal temperature set to 300 K.

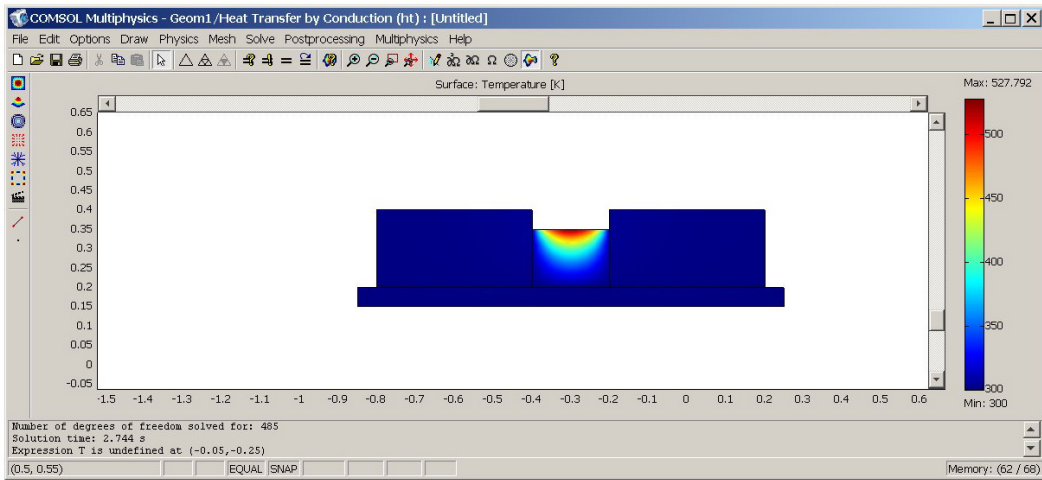
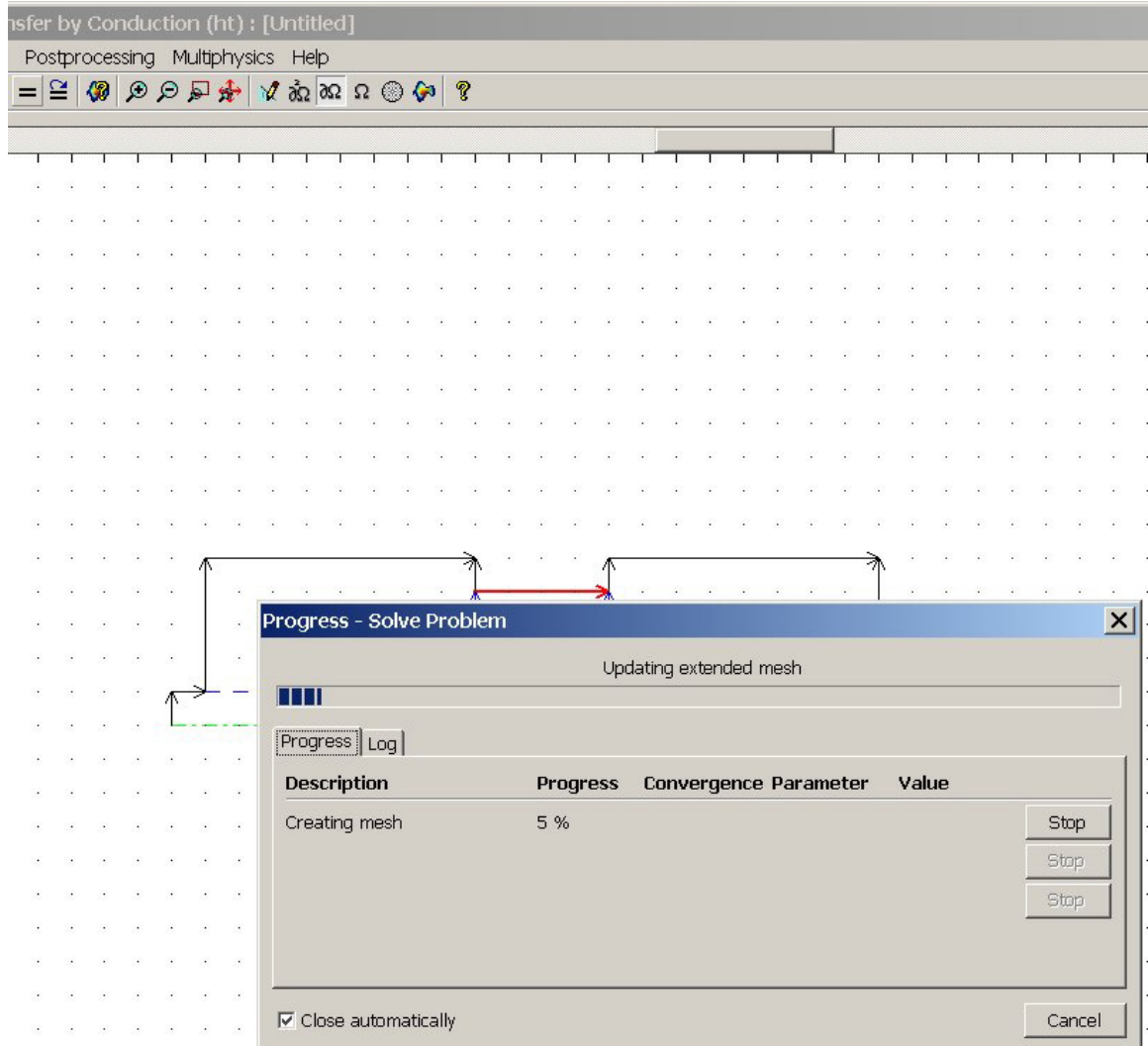


STEP 6: In this step the boundary settings will be configured for the desired simulation. Go to the Physics menu again and choose Boundary Settings... By default all external boundaries are set to thermal insulators. Select the number in the boundary selection window that corresponds to the bottom of the  $\text{Si}_3\text{N}_4$  layer, and choose temperature from the boundary condition dialogue box. Set the temperature,  $T_0$ , to 300 K.

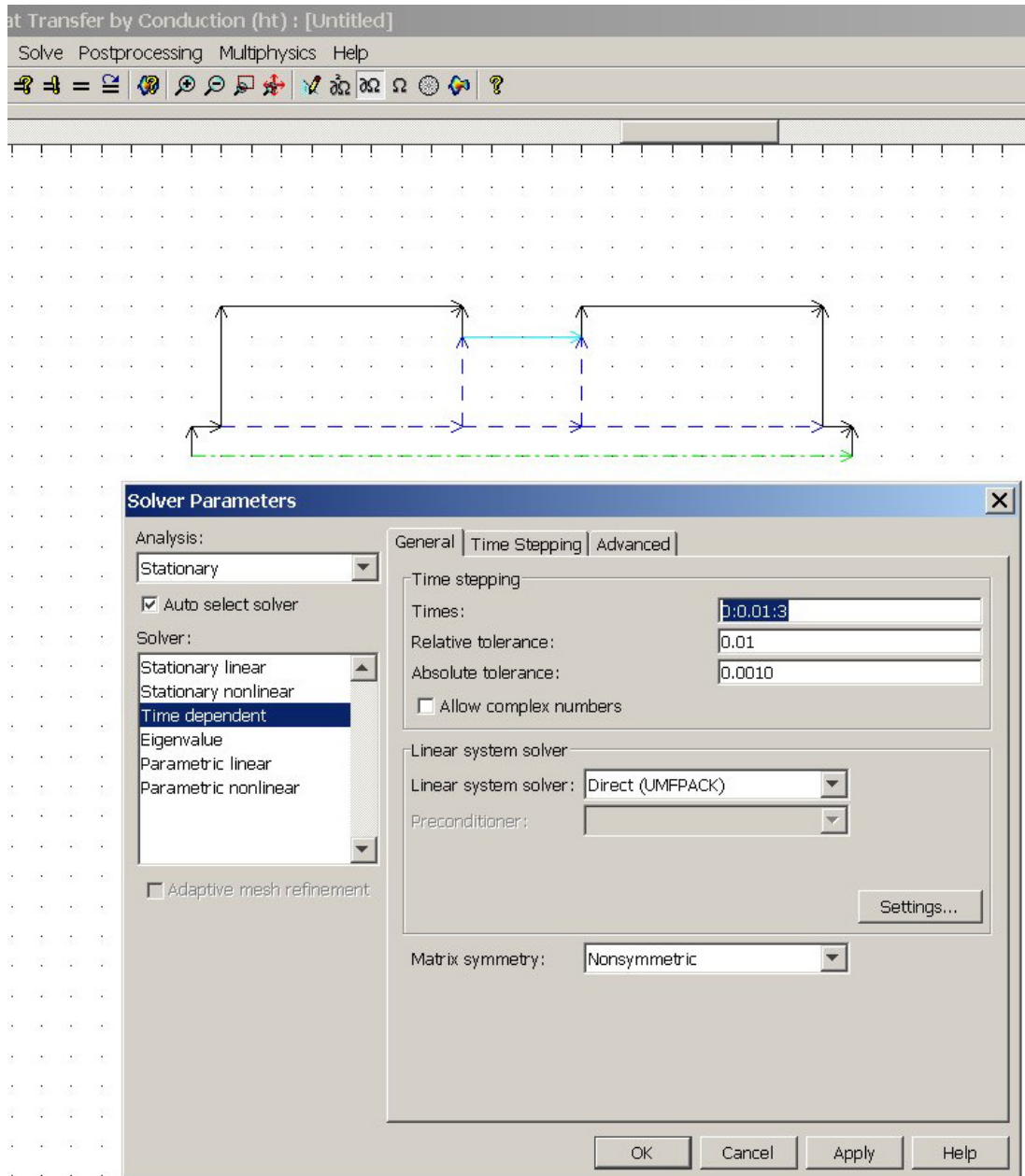


Select (by clicking on the line) the top surface of the GST and choose heat flux from the boundary condition dialogue box and set the inward heat flux,  $q_0$ , to  $1550 \text{ W}/\text{m}^2$ .

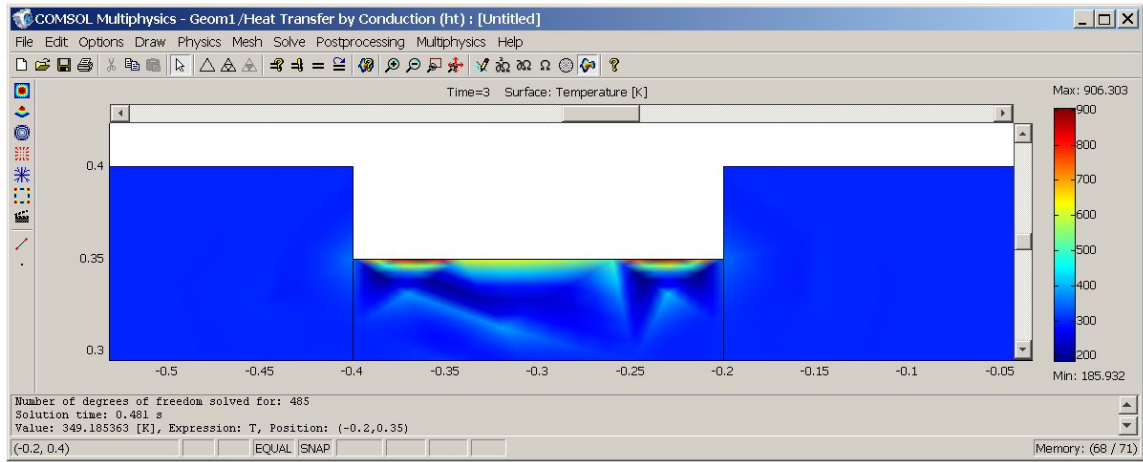
STEP 7: Run the simulation with the current settings by clicking on the Solve button on the top toolbar (an equal sign). This solution (default settings) runs a steady state analysis given the set parameters.



STEP 8: Configure the simulation for transient analysis. First the inward heat flux will be raised for the shorter time being irradiated. Using the procedures in step six, set the top surface of the GST to an inward heat flux of 500,000 W/m<sup>2</sup>. Next, click on the Solve Parameters button from the top toolbar (an equal sign with a question mark over it). Change the option in the Solver window from stationary nonlinear to time dependant, and set the time stepping settings (time option) to 0:0.01:3.



STEP 9: Run the simulation again for transient analysis.



## Appendix B – GST SEM Images

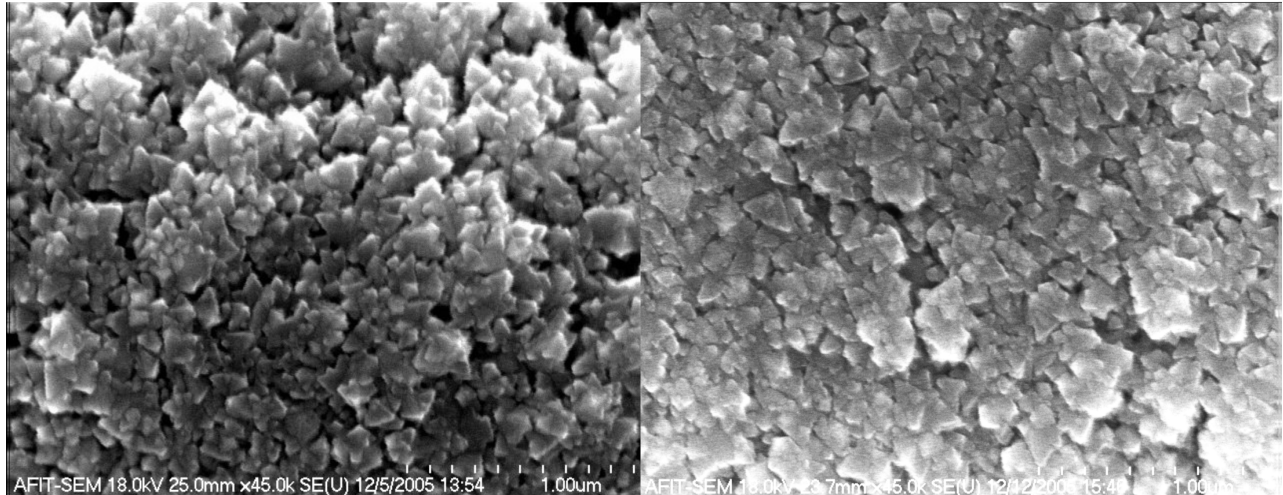


Figure B-1 GST material from batch one, test sample one (left) before any testing was performed in amorphous state, and (right) after optical testing was performed and the data from Figure 6-1 was recorded, now believed to be in a crystalline state.

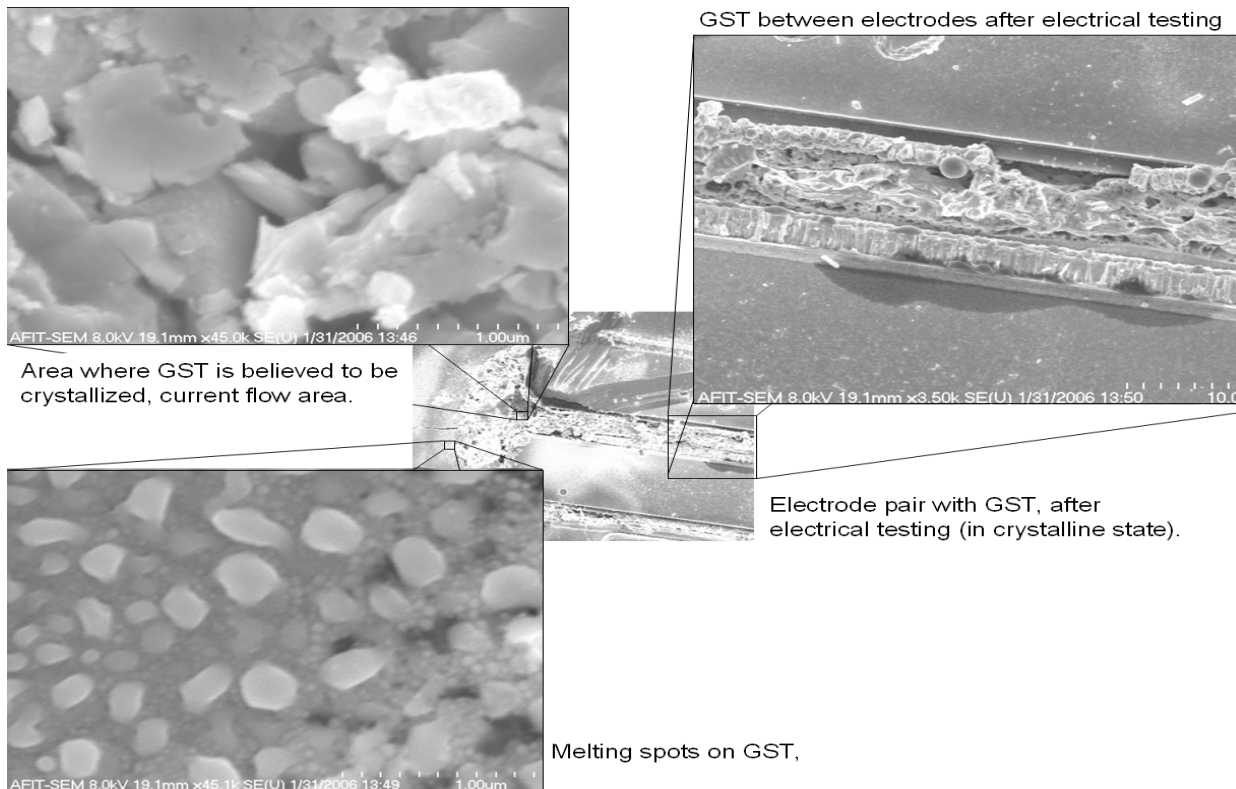


Figure B-2 GST batch two after electrical testing where GST is in a crystalline state.

## Appendix C – Test Matrix Data

Table C-1 GST Test Matrix Data

Growth Parameters	Trench Gap	Sample Batch	Responsivity vs. Wavelength	Resistance vs. Intensity	Electrical Testing	Scalability	Comments
6Å/s, 4-µm	14-µm	1	Did not test, equipment not setup yet	Dark ⇒ 100kΩ .02 mW/mm <sup>2</sup> ⇒ 90kΩ .07mW/mm <sup>2</sup> ⇒ 24kΩ, (state changes) .07mW/mm <sup>2</sup> (5 min) ⇒ 11kΩ (state change)	Did not test.	Did not test, sample reacted as crystallized before this test.	This sample (only sample) indicated that the GST could produce photoconductive and could change states (ideal sample).
3Å/s, 4-µm	2-µm to 30-µm	1	Produced no photocurrent response, nor state changes.	Produced no photocurrent response, nor state changes.	Did not test.	Did not test, due to no optical response.	No photoresponse, was believed to be caused from higher oxygen content ⇒ lower absorption.
6Å/s, 0.5-µm	2-µm to 30-µm	1	Produced no photocurrent response, nor state changes.	Produced no photocurrent response, nor state changes.	Did not test.	Did not test, due to no optical response.	No photoresponse, was believed that the material needed to be thicker to absorb sufficient light.
6Å/s, 4-µm	Photo-tested 2-µm to 30-µm Electric al- tested 2-µm to 100-µm	2	Produced no photocurrent response, nor state changes	Produced no photocurrent response, nor state changes.	Electrical testing matched other research with minor differences, indicating $V_{th}$ and current value relating to the gap size of the devices	Geometry and device design indicated a visible scaling factor with respect to the size of the electrode gap and the power required to shift states in the material.	Electrical testing of the GST proved most reliable; optical testing needed higher power light sources to conduct conclusive research about the optical response of the GST. The difference in material between batches needs to be investigated more thoroughly.



## References

1. *The Human Brain*, in *Scientific American*. 2004. p. 58.
2. J.H. Yi', Y.H.H., J.H. Park, B.J. Kuh, H. Horii, Y.T. Kimt, S.O. Park, Y.N. Hwang', S.H.Lee',S.J. Ahn', S.Y. Lee', J.S. Hong', K.H. Leet, N.I. Lee\*, H.K. Kang', U-In Chug and J.T. Moon. *Novel Cell Structure of PRAM with thin metal layer inserted GeSbTe*. in *IDEM*. 2003: IEEE.
3. Pirovano, A., A.L.L., Augusto Benvenuti, Fabio Pellizzer, and Roberto Bez, *Electronic Switching in Phase-Change Memories*. IEEE TRANSACTIONS ON ELECTRON DEVICES, 2004. **51**(3): p. 452-459.
4. Stuchlik, M., P.K., S.R. Elliott, *OPTO-MECHANICAL EFFECT IN CHALCOGENIDE GLASSES*. Journal of Optoelectronics and Advanced Materials, 2001. **3**(2): p. 361 - 366.
5. Stuchlik, M., P.K., and S. R. Elliott. *Micro-Nano Actuators Driven by Polarized Light*. in *Sci. Meas. Technol*. 2004: IEEE.
6. Kolobov, A.V., and Kazunobu Tanaka., *Photoinduced Phenomena in Amorphous Chalcogenides: From Phenomenology to Nanoscale*, in *Handbook of Advanced Electronic and Photonic Materials and Devices Volume 5: Chalcogenide Glasses and Sol-Gel Materials*, H.S. Nalwa, Editor. 2001, Academic Press: San Diego. p. 47-85.
7. Krecmer, P., et al, *Reversible Nanocontraction and Dilation in a Solid Induced by Polarized Light*. Science, 1997. **277**: p. 1799-1802.
8. Li, J., and D. A. Drabold, *Direct Calculation of Light-Induced Structural Change and Diffusive Motion in Glassy As<sub>2</sub>Se<sub>3</sub>*. Physical Review Letters, 2000. **85**(13): p. 2785-88.
9. Tanaka, K., *Photoinduced Structural Changes in Amorphous Semiconductors*. Semiconductors, 1998. **32**(8): p. 861-66.
10. Pirovano, A., e.a., *Electronic Switching Effect in Phase-Change Memory Cell*. IEDM Tech. Dig., 2002: p. 923-926.
11. Ovshinsky, S.R., *Reversible Electrical Switching Phenomena in Disordered Structures*. Phys. Rev. Lett., 1968. **21**(20): p. 1450-1453.

12. Microsoft. *Encarta Encyclopedia 2004*. History of Photography [CD-ROM] 2003 [cited].
13. Dereniak, E.L., and G. D. Boreman *Infrared Detectors and Systems*. 1996, New York: Wiley-Interscience.
14. Marciniak, M., *Optical Radiometry OENG650 Course Lecture Notes*. Spring Quarter, 2005, Air Force Institute of Technology.
15. IUPAC, *International Union of Pure and Applied Chemistry Compendium of Chemical Terminology*, in *2nd Edition*, A.D. McNaught, and Andrew Wilkinson, Editor. 1997, Royal Society of Chemistry, Cambridge, UK.
16. Sze, S.M., *Semiconductor Devices: Physics and Technology*. 2 ed. 2002, New Jersey: Hoboken: Wiley.
17. Blake, T.F., *Investigation of Ge<sub>2</sub>Te<sub>2</sub>Sb<sub>5</sub> Chalcogenide Films for Use As An Analog Memory*, in *Air Force Institute of Technology*. 2000: Ohio, Dayton.
18. Ovshinsky, S.R., *An Introduction to Ovonic Research*. *Journal of Non-Crystalline Solids*, 1970. **2**: p. 99-106.
19. Sato, K. *Introduction to Optoelectronics Optical Storage*. [Course Presentation] 2004 [cited; Available from: [www.tuat.ac.jp/~katsuaki/STEP/STEP041214OHP.ppt](http://www.tuat.ac.jp/~katsuaki/STEP/STEP041214OHP.ppt)].
20. G.F. Zhou., e.a. *Crystallization Behavior of Phase Change Materials: Comparison Between Nucleation and Growth-Dominated Crystallization*. in *Proceedings of SPIE*. 2000: SPIE.
21. Ielmini, D., et al., *Analysis of Phase Distribution in Phase-Change Nonvolatile Memories*. *IEEE Electronic Device Letters*, July 2004. **25**(7): p. 507-509.
22. Small, E., S. M. Sadeghipour, and M. Asheghi. *Numerical Modelling of Heat Transfer and Phase Transition in Programming the Ovonic Unified Memory Cells*. in *Pacific Rim Technical Conference and Exhibition on Integration and Packaging of MEMS, NEMS, and Electronic Systems (IPACK2005)*. 2005. San Francisco, CA: ASME.
23. Rawson, H., *Inorganic Glass-Forming Systems*. 1967, London: Academic Press.
24. Lopez, C., et al, *Processing and Characterization of Bulk Chalcogenide Glasses Used for Waveguide Applications*. *Journal of the American Ceramic Society*, 2002. **85**: p. 1372-1376.

25. Saliminia, A., et al. *Efficient Bragg gratings in single mode planar waveguide of chalcogenide glasses*. in *Conference on Lasers and Electro-Optics*. 1963. Europe.
26. Green, M.A., *Crystalline and Thin-Film Silicon Solar Cells: State of the Art and Future Potential*. Solar Energy, 2003. **74**(3): p. 181.
27. Kellermann, K., et al., *Optically Pumped Lead Chalcogenide Infrared Emitters on Silicon Substrates*. Physica E: Low-Dimensional Systems and Nanostructures, 2004. **20**: p. 536-539.
28. Zolotarev, V.M., *FTIR Spectroscopy Employing Thermoplastic Glasses—A Nondestructive Method for Studying Solids*. Sov. J. Opt. Technol., 1988. **35**(8): p. 499–510.
29. Bormashenko, E., et al., *Optical Properties and Infrared Optics Applications of Composite Films Based on Polyethylene and Low-Melting-Point Chalcogenide Glass*. Society of Photo-Optical Instrumentation Engineers, 2002. **41**(2).
30. Ovshinsky, S.R., D. Adler, M. S. Shur, and M. Silver, *Threshold switching in chalcogenide-glass thin films*. J. Appl. Phys., 1980. **51**(6): p. 3289–3309.
31. Maurice, J., C. Lee. *Research Spawns New Advances in Optoelectronic Technology*. 2002 [cited; Nov - Dec 02:[Available from: [www.afosr.af.mil/pdfs/Dec02RH2.pdf](http://www.afosr.af.mil/pdfs/Dec02RH2.pdf)].
32. Wikipedia. *Discovering DNA*. [Encyclopedia] 3 Jan 06 [cited; Available from: [www.answers.com/topic/dna](http://www.answers.com/topic/dna)].
33. Ovshinsky, S.R., B. Pashmakov, *Innovation Providing New Multiple Functions in Phase-Change Materials to Achieve Cognitive Computing*. 2004, Energy Conversion Devices: Rochester Hills, MI.
34. Salamon, D., B. F. Cockburn. *An Electrical Simulation Model for the Chalcogenide Phase-change Memory Cell*. in *MTDT*. 2003: IEEE.
35. efunda. *Conduction: General Theory*. 2006 16 Jan 06 [cited; Available from: [www.efunda.com/formulae/heat\\_transfer/conduction/overview\\_cond.cfm](http://www.efunda.com/formulae/heat_transfer/conduction/overview_cond.cfm)].
36. Koester, D., Allen Cowen, Ramaswamy Mahadeven, Mark Stonefield, & Busbee Hardy, *PolyMUMPs Design Handbook*. 2003, MEMSCAP.
37. Kladitis, P., *Introduction to MEMS Course Notes*. Winter Quarter, 2005, Air Force Institute of Technology.

38. Chen, Y.C., H. P. Chen, Y. Y. Liao, H. T. Lin, L. H. Chou, J. S. Kuo, P. H. Chen, S. L. Lung, and R. Liu, *A High Performance 180nm Nonvolatile Memory Cell using Phase Change Sn-Doped  $Ge_2Sb_2Te_5$  Chalcogenide*. IEEE, 2003. **0-7803-7765-6(03)**: p. 32-35.
39. Denninghoff, D., *PolyMUMPs Sacrificial Oxide Release Procedures*. 2005, Air Force Institute of Technology. p. 1.
40. Olson, J.K., *Growth and Characterization of Thin Film Telluride Glasses*. 2004, University of Utah. p. iv.
41. Taylor, P.C., *Amorphous Chalcogenide Films for Reconfigurable Electronic Applications*. 2004, University of Utah. p. 5.
42. Lewis, J. *Factors Affecting Microbolometer Responsivity*. 1994 17 Feb 06 [cited; Available from:  
weewave.mer.utexas.edu/MED\_files/MED\_research/microbolometers/microblmt  
r\_anlys/bolo\_respnsvty.html.
43. Marken, A. *Double Layer DVD+R Media White Paper*. 2004 20 Feb 06 [cited; Available from: [www.cd-info.com/tech/media/dl.html](http://www.cd-info.com/tech/media/dl.html)].

## *Vita*

Lieutenant John R. V. Chezem was born 1978 in Stayton, Oregon. Actively involved with leadership and outdoor programs in the Boy Scouts of America, he earned the rank of Eagle Scout in 1996. He graduated with honors from Columbia River High School, Vancouver, Washington in 1997. In 1999 he achieved Black Belt in Kong Soo Do Karate and promoted to Second Degree Black Belt in 2001 after two years as an instructor. Upon accepting an Air Force ROTC scholarship, he attended the University of Portland, where he met his beloved wife and married in 2003. He graduated from the University of Portland, cum laude, with a Bachelor of Science in Electrical and Computer Engineering ABET accredited in May 2004. Upon graduation he was commissioned as a Second Lieutenant in the United States Air Force and was accepted direct accessions to attend the Air Force Institute of Technology (AFIT) and study for a Master of Science Degree in Electrical Engineering. He graduated from AFIT in March 2006, with the addition of two sons, one born in 2005, and one expected in 2006.

# REPORT DOCUMENTATION PAGE

*Form Approved*  
*OMB No. 074-0188*

The public reporting burden for this collection of information is estimated to average 1 hour per response, including the time for reviewing instructions, searching existing data sources, gathering and maintaining the data needed, and completing and reviewing the collection of information. Send comments regarding this burden estimate or any other aspect of the collection of information, including suggestions for reducing this burden to Department of Defense, Washington Headquarters Services, Directorate for Information Operations and Reports (0704-0188), 1215 Jefferson Davis Highway, Suite 1204, Arlington, VA 22202-4302. Respondents should be aware that notwithstanding any other provision of law, no person shall be subject to a penalty for failing to comply with a collection of information if it does not display a currently valid OMB control number.

**PLEASE DO NOT RETURN YOUR FORM TO THE ABOVE ADDRESS.**

<b>1. REPORT DATE</b> (DD-MM-YYYY) 23-03-2006		<b>2. REPORT TYPE</b> Master's Thesis		<b>3. DATES COVERED</b> (From - To) October 2004 - March 2006	
<b>4. TITLE AND SUBTITLE</b>  Analysis of Photoconductive Properties in Ge <sub>2</sub> Sb <sub>2</sub> Te <sub>5</sub> (GST) Chalcogenide Films for Applications in Novel Electronics			<b>5a. CONTRACT NUMBER</b>		
			<b>5b. GRANT NUMBER</b>		
			<b>5c. PROGRAM ELEMENT NUMBER</b>		
<b>6. AUTHOR(S)</b>  Chezem, John R.V., Second Lieutenant, USAF			<b>5d. PROJECT NUMBER</b>		
			<b>5e. TASK NUMBER</b>		
			<b>5f. WORK UNIT NUMBER</b>		
<b>7. PERFORMING ORGANIZATION NAMES(S) AND ADDRESS(S)</b>  Air Force Institute of Technology Graduate School of Engineering and Management (AFIT/EN) 2950 Hobson Way, Building 640 WPAFB OH 45433-8865			<b>8. PERFORMING ORGANIZATION REPORT NUMBER</b>  AFIT/GE/ENG/06-14		
<b>9. SPONSORING/MONITORING AGENCY NAME(S) AND ADDRESS(ES)</b>  AFRL/IF-TA (AFMC) Attn: Dr. Robert L. Ewing 2241 Avionics Circle, Bldg. 620 Wright-Patterson AFB, OH 45433-7334  robert.ewing@wpafb.af.mil (937) 255-6548 x3592			<b>10. SPONSOR/MONITOR'S ACRONYM(S)</b>		
			<b>11. SPONSOR/MONITOR'S REPORT NUMBER(S)</b>		
<b>12. DISTRIBUTION/AVAILABILITY STATEMENT</b>  APPROVED FOR PUBLIC RELEASE; DISTRIBUTION UNLIMITED.					
<b>13. SUPPLEMENTARY NOTES</b>					
<b>14. ABSTRACT</b> <p>This thesis investigated the thermal phase-change properties in Ge<sub>2</sub>Sb<sub>2</sub>Te<sub>5</sub> (GST) chalcogenide-based films and determined the feasibility of coupling the GST with photosensitive DNA material for novel optical device applications. Modeling and testing of GST were researched with the approach that GST would react as a resistive mechanism through thermal manipulation. A test structure was fabricated with a 2-μm MEMS fabrication process. GST material was deposited (by RF sputtering) on the surface of the test structures. The GST was analyzed primarily in the amorphous to crystalline transition states due to more distinct changes in the resistance between partial states. Using both filtered light (via a monochromator), and non-filtered white light, light was incident on the GST for photo response testing. A biased voltage was applied to the device and the current change was measured. The GST was tested electrically, applying a current sweep across the device and measuring change in resistance as the GST changed states. Data recorded on the thermal properties of GST leading to resistive changes from both optical and electrical sources was analyzed.</p> <p>The results of this research indicate how future optical and electrical testing of the GST can be improved. The data measured by testing the GST electrically was compared to other research data (following similar testing procedures), revealing that optimal designs need sub-micro layers of GST with electrodes placed above and below the GST. It was concluded that higher power light sources will be needed to continue exploring the optical reaction of GST in future research.</p>					
<b>15. SUBJECT TERMS</b> Amorphous semiconductor, Ge <sub>2</sub> Sb <sub>2</sub> Te <sub>5</sub> , phase-change nonvolatile memory, thermal mechanism, photocurrent, DVD-RAM					
<b>16. SECURITY CLASSIFICATION OF:</b>		<b>17. LIMITATION OF ABSTRACT</b>	<b>18. NUMBER OF PAGES</b>	<b>19a. NAME OF RESPONSIBLE PERSON</b> James A. Fellows, Lt Col, USAF (ENG)	
a. REPORT	b. ABSTRACT	c. THIS PAGE	UU	<b>19b. TELEPHONE NUMBER</b> (Include area code) (937) 255-3636, ext 7230 (james.fellows@afit.edu)	
U	U	U	141		